Enantioselective Alkynylation of Carbonyl Compounds Based on Cooperative Copper Catalysis

Takaoki Ishii

2015

Contents

General Introduction ---------- 1

Chapter 1 ---------- 18

Cooperative Catalysis of Metal and O–H···O/sp^3-C–H···O Two-point Hydrogen Bonds in Alcoholic Solvents: Copper-catalyzed Enantioselective Direct Alkynylation of Aldehydes with Terminal Alkynes

Chapter 2 ---------- 91

Enantioselective Alkynylation of α-Keto Ester Derivatives Catalyzed by Chiral Hydroxy Amino Phosphine Copper Complexes

Publication List ---------- 110

Acknowledgment ---------- 111

General Introduction

Biological systems often recognize a pair of enantiomers as different substances, and in many cases, different enantiomers exhibit different properties. For example, one may serve as a drug, while the other act as toxic. To obtain enantiomerically enriched compounds effectively, chemists continue to attract their interest to asymmetric catalysts.[1] Stereoselective synthesis based on asymmetric catalysis is superior in terms of both efficiency and economy. Many researchers have studied in this area, thus various enantioselective chemical transformations are now performed with only catalytic amount of chiral promoters.

Development of efficient, practical and environmentally benign catalytic system, for the synthesis of optically active compounds, represents a grand challenge in this area. Cooperative catalysts are one of the most prominent promoters. In the catalytic transformation, cooperative catalysts activate two or more compounds simultaneously in the overall reaction. Therefore, it has a great potential in enhancing reactivity and precise control of stereochemistry with high efficiency. Development of novel cooperative catalysis in asymmetric chemistry is discussed in this section.

1. Cooperative Catalysis

1.1. Biocatalysts

Enzymes are highly valuable tools for chemists to obtain enantiomerically pure molecules in highly efficient ways, even though they are often specific for certain substrates. Enzymes achieve efficient enantioselective molecular transformation through cooperative catalysis. For instance, the proposed transition state model of class II aldolase shows the simultaneous activation of substrates (Scheme 1). The asymmetric aldol reaction of dihydroxyacetone phosphate (DHAP) is catalyzed by aldolase under neutral conditions. According to a research on transition state conducted by Fessner and Schloss,[2] the Zn^{2+} activates carbonyl group and it increases the acidity of hydroxymethylene. The glutamate-73 facilitates abstraction of proton as a Brønsted base to effect enolization of DHAP. Simultaneously, the phenol of the tyrosine-113′ residue works as a Brønsted acid, which donates a proton to aldehyde. Oriented hydrogen bonds play critical roles in catalysis, stabilizing a transition state with stereocontrolled manner to give the product.

Scheme 1. Model of class II aldolase-promoted enantioselective aldol reaction.

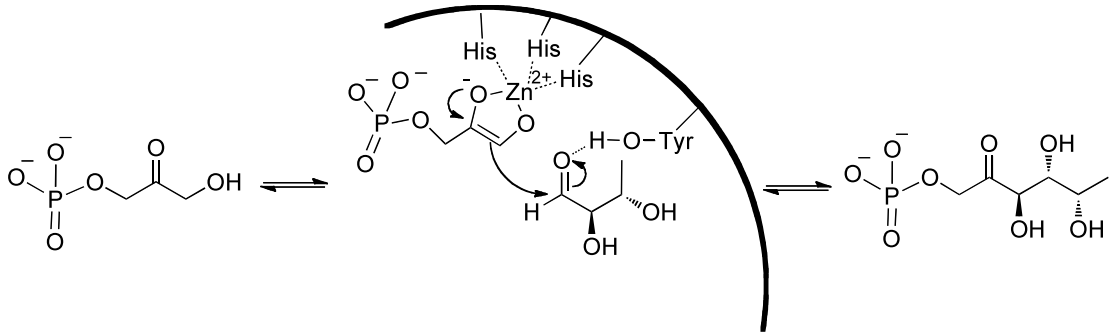

Chemists often use hydrogen bonds in designing artificial catalysts, having it in mind to mimic enzymatic catalysis. It is considered that by imitating nature, the principle of multifunctional catalysis could offer many advantages over existing strategies. In fact, various high-performing enantioselective artificial catalysts reminiscent of enzymes have been developed to date.

1.2. Lewis Acid–Brønsted Base Catalysts

The concept of cooperative catalysis, wherein both partners of a bimolecular reaction are simultaneously activated, is very powerful for designing efficient asymmetric catalysis. One of the earliest example of such catalysis was demonstrated in 1986 by Ito, Sawamura and Hayashi (Scheme 2).[3] They successfully accomplished an asymmetric aldol reaction of α-isocyanocarboxylates with aldehydes by employing a gold complex catalyst system containing chiral ferrocenylphosphine ligand **L1** bearing a tertiary amino group at the terminal position of pendant chain to obtain enantioenriched 5-alkyl-2-oxazoline-4-carboxylates with high yields and enantioselectivities. They proposed a hypothetical transition state model as shown in Scheme 2. The Au catalyst coordinates to the cyano groups to control the orientation of a prochiral enolate, while the terminal amino group abstracts one of α-methylene protons. Simultaneously, the Au complex activates aldehyde to produce corresponding chiral aldol adduct.

Scheme 2. Gold-catalyzed asymmetric aldol reaction of α-isocyanocarboxylates.

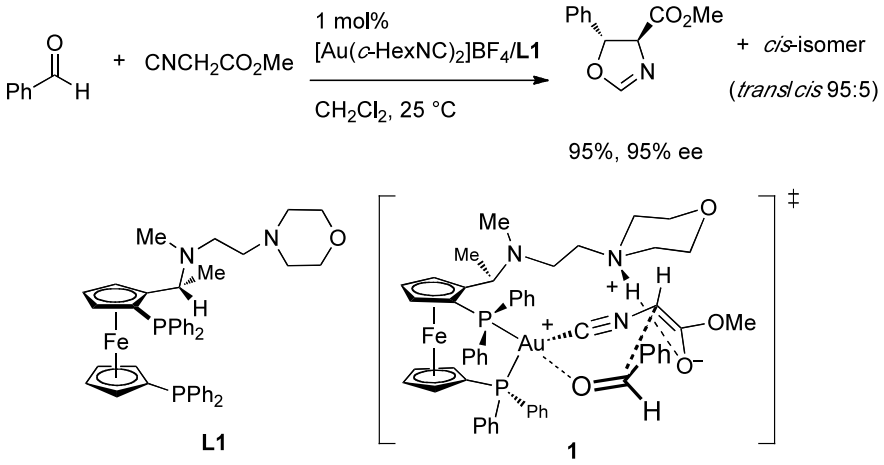

Shibasaki and co-workers developed the concept of heterobimetallic catalysis. These catalysts exhibited both Lewis acid and the Brønsted base. Since the first report of a catalytic asymmetric nitroaldol reaction using the rare earth-alkali metal BINOL (REMB) complexes in 1992, they developed various transformations that were difficult to achieve using the conventional monometallic catalysis.[4] The activation of substrates and nucleophiles occurs simultaneously at the Lewis acid and the Brønsted base moieties in the catalyst, giving high enantioselectivity in a products. For instance, direct catalytic asymmetric aldol reaction catalyzed by lanthanum-lithium-BINOL (LLB) complex, utilizing an unmodified ketone as a nucleophile is shown in Scheme 3.[5] Thus, KOH, prepared from KHMDS and H_2O, interacts with LLB. Ketone is deprotonated by KOH and the aldehyde is activated and fixed by the lanthanum metal at the same time to give enantiomerically enriched aldol adduct.

Scheme 3. Catalytic direct asymmetric aldol reaction promoted by LLB complex.

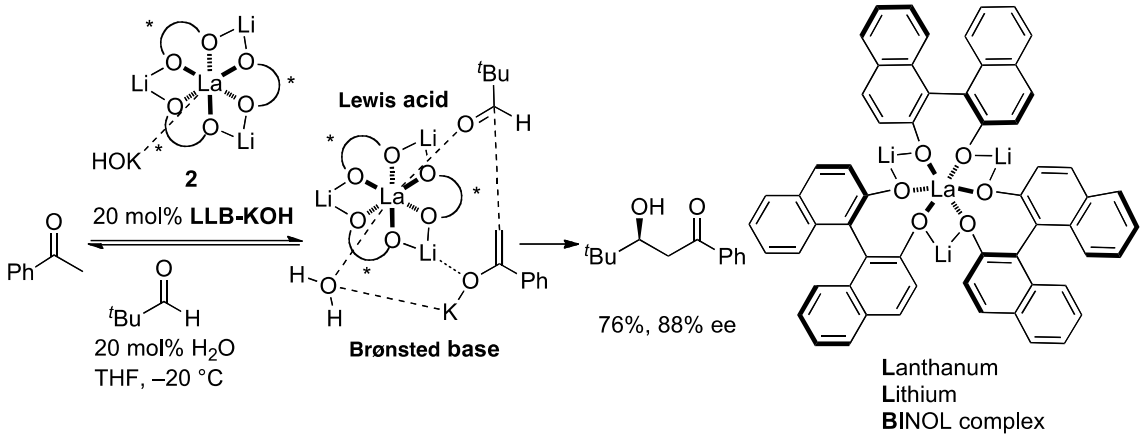

1.3. Cooperating Ligand in Catalysis

In 1995, Noyori and Ikariya reported asymmetric transfer hydrogenation of ketones catalyzed by an ethylene diamine coordinated ruthenium complex (Scheme 4).[6] This reaction proceeds through the interconversion of a 16-electron amide complex and a 18-electron amine hydride complex (Scheme 5). The amide complex **3** reacts with 2-propanol as a Brønsted base and gives the hydride amine complex **4**. On the other hand, one of the amine protons on the hydride amine complex activates the ketone as a Brønsted acid through six-membered transition state **5**. Then, chiral alcohol is produced and the hydride amine complex regenerates the amide complex. Mechanistic studies revealed that the amide protons work efficiently for binding the substrate. In the BINAP-diamine/Ru system, neither the ketone substrate nor the alcohol product interacted with the metallic center during the catalytic cycle. A Ru–H species was detected in a study using NMR spectroscopy. It was proposed that the molecular surface of the coordinatively saturated Ru–H intermediate. differentiate the enantiofaces of the prochiral ketones.

Scheme 4. Enantioselective hydrogenation of ketone by ruthenium complex.

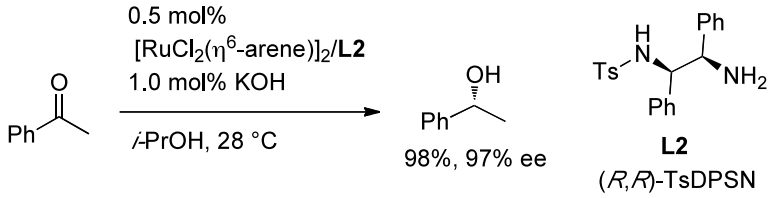

Scheme 5. Catalytic cycle for Ru-catalyzed asymmetric hydrogenation.

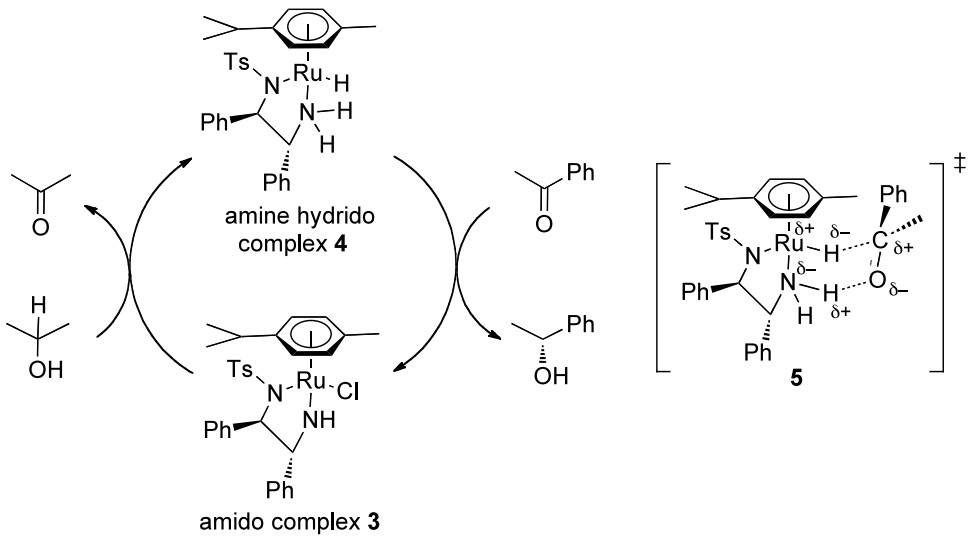

1.4. Metal-free Cooperative Catalysis

Metal-free cooperative catalysis has received much attention. Various efforts were devoted to the development of organocatalyst. The first examples of intramolecular aldol reactions catalyzed by proline were independently reported by Hajos and Pariish and Wiechert *et al* in the early 1970s (Scheme 6).[7,8] Despite early successes using the proline catalyst, prevalence of its use is relatively recent.

Scheme 6. Intramolecular Hajos-Parrish-Eiechert aldol reaction.

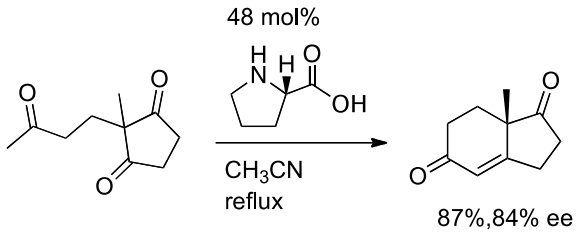

In 2000, effective proline-catalysed direct intermolecular reaction between ketones and aldehydes was disclosed by List and Barbas III (Scheme 7).[9] The reaction with a wide range of substrates provided the aldol products with high enantioselectivities.

Scheme 7. Proline-catalyzed enantioselective aldol reaction.

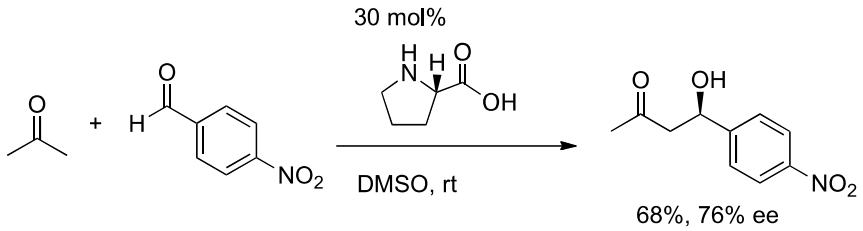

Houk carried out a detailed investigation of reaction mechanism by using quantum mechanical calculations (Scheme 8).[10] Thanks to its secondary amine functionality and relatively high pK_a value, the proline is a good nucleophile as well as Brønsted acid. The reaction is initiated by the formation of the enamine intermediate **A** from proline and ketone. Then, a carboxylic acid moiety in the intermediate **A** activates aldehyde via nine-membered transition state **B** to produce the chiral product.

Scheme 8. Proposed catalytic cycle of proline-catalyzed aldol reaction.

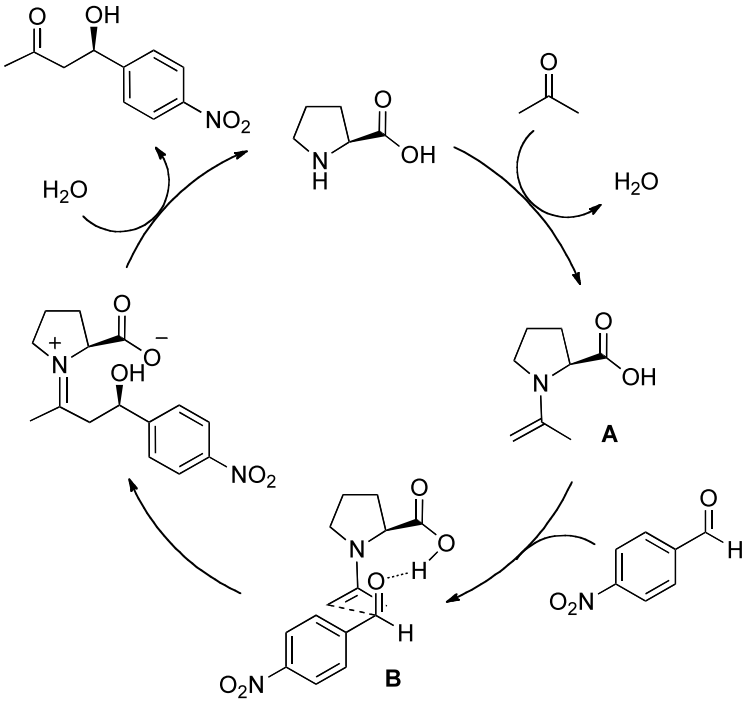

Increased numbers of metal-free cooperative catalysts were reported in recent years. Chiral phosphoric acid also represents one of the remarkable advances of asymmetric synthetic chemistry. BINOL-derived phosphoric acid esters provide sterically tunable chiral Brønsted acids. In 2004, Akiyama and Terada developed this type of catalysts independently and used them for a number of transformations. The phosphoryl oxygen on phosphoric acid acts as a Brønsted base (or Lewis base), while the hydroxy group serves as Brønsted acid cooperatively.[11,12] This organocatalyst enabled the formation of multiple hydrogen bonds and thus orientational control could be effective. The appropriate choice of the substituents at the 3,3'-position were also crucial for realizing of high enantioselectivity.

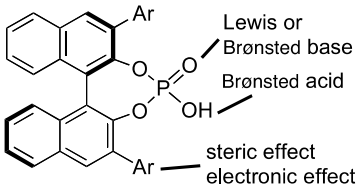

Akiyama and co-workers developed the enantioselective Mannich-type reaction of silyl enolates with aldimines (Scheme 9).[11] In the presence of organocatalyst **6**,

β-amino esters were obtained with high enantioselectivities. The introduction of a hydroxy group in the *ortho* position of the aryl group of the aldimine was essential for both reaction rate and enantioselectivity. On the basis of experimental results and DFT calculations, they proposed that the reaction proceeds through nine-membered zwitterionic cyclic transition state **7** consisting of the aldimine and the phosphoric acid.

Scheme 9. Enantioselective Mannich-type reaction catalyzed by chiral phosphates.

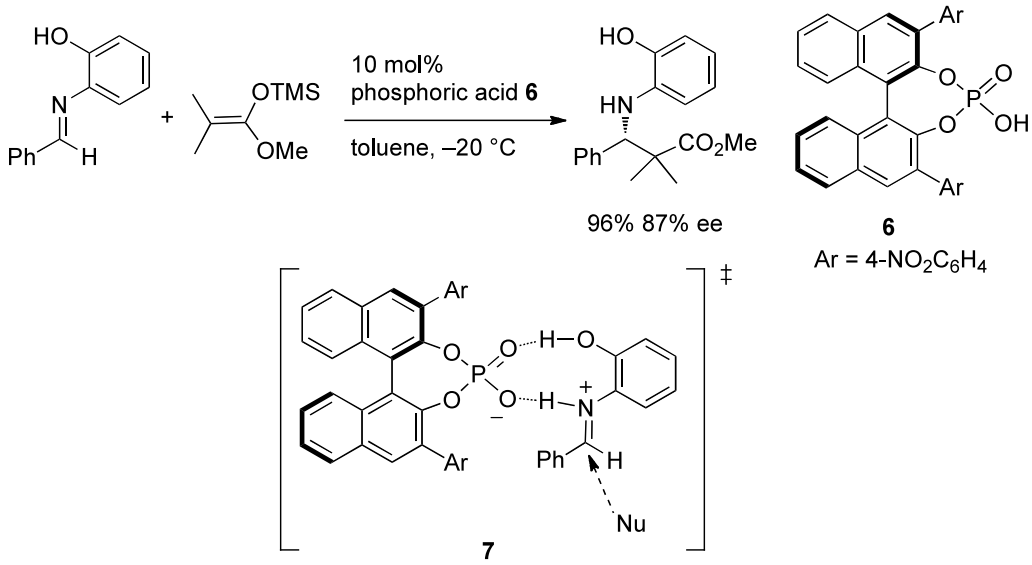

Many reactions based on activation of imines have been reported. Terada and co-workers developed aza-Friedel-Crafts alkylation of furan (Scheme 10).[13] Phosphoric acid **8** provides an atom-economical approach for synthesizing chiral nitrogen-containing compounds that are important in organic synthesis and biochemistry. They thought that the reaction proceeded through intermediate **9**, which was generated by the protonation of the imine.

Scheme 10. Chiral phosphate-catalyzed asymmetric aza-Friedel-Crafts alkylation.

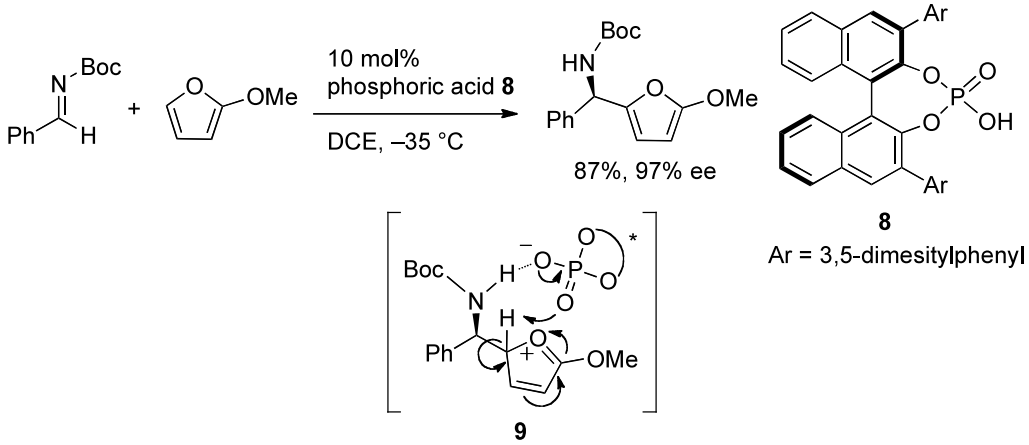

1.5. Outlook of Cooperative Catalysis

Cooperative catalysis has proven to be highly effective in a variety of reactions. They provided efficient methods to access a wide range of enantioenriched products through a number of interactions between catalyst and substrates. During last three decades, various remarkable reactions by means of chiral cooperative catalysts have been developed to expand their synthetic utilities. Despite such a remarkable progress, however, novel cooperative catalytic processes are still needed. In response to the rising demand of highly effective and environmentally friendly catalysts, it is expected that the area of cooperative catalysts will continue to be developed and have a broad application in asymmetric reactions.

2. Enantioselective Addition of Terminal Alkynes to Carbonyl Compounds

Increasing attention has been paid to the efficient synthesis of the propargylic alcohols. In particular, the enantioselective carbonyl addition of terminal alkynes to aldehydes is recognized as an important reaction to prepare chiral propargylic alcohols. Therefore, in fact, various metal salts and reaction conditions have been investigated to date.[14] This section overviews the progress of the direct asymmetric alkynylations of carbonyl compounds.

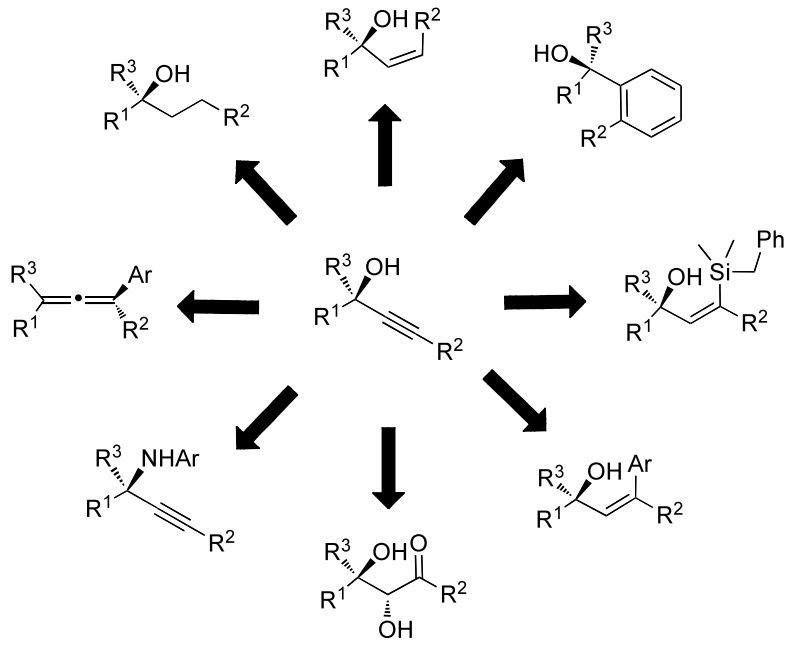

Figure 1. The broad utility of propargylic alcohol derivatives.

2.1. Zn-mediated Alkynylations

It has been known that zinc is an effective metal in the asymmetric addition of alkynes to carbonyl compounds. To date, various methods involving catalytic and stoichiometric reaction have been developed. Carreira reported the first example of catalytic asymmetric alkynylation of aldehyde with $Zn(OTf)_2$ and *N*-methyl ephedrine **L2** in 2001 (Scheme 11).[15] In the presence of **L2**, *in situ* generated catalytic amount of zinc acetylides underwent the reaction to afford the propargylic alcohols with excellent enantioselectivities. This system shows the broad generality toward the reaction of aliphatic aldehydes.

Scheme 11. Zn-catalyzed alkynylation.

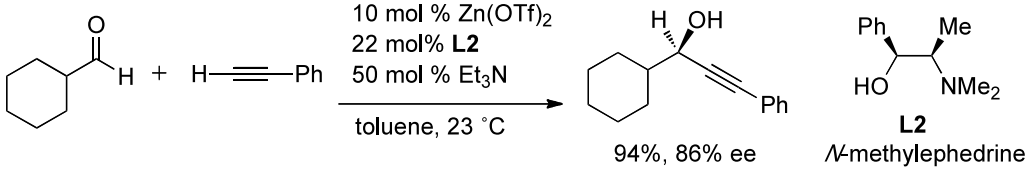

Wang and co-workers developed a new amino alcohol ligand **L3** (Scheme 12).[16] By use of amino alcohol ligand **L3**, β-amino alkoxyl zinc atom acts as a Lewis acid to

activate aldehyde, while the nitrogen atom of pyridyl group works as a Lewis base to activate the alkynyl zinc. Usually, Ti(O-*i*-Pr)$_4$ or other metal species were needed for the activation of aromatic aldehydes. However, they proved that some ligands could promote a reaction owing to the property of cooperative catalysts.

Scheme 12. Bifunctional zinc catalyzed asymmetric alkynylation of aldehydes.

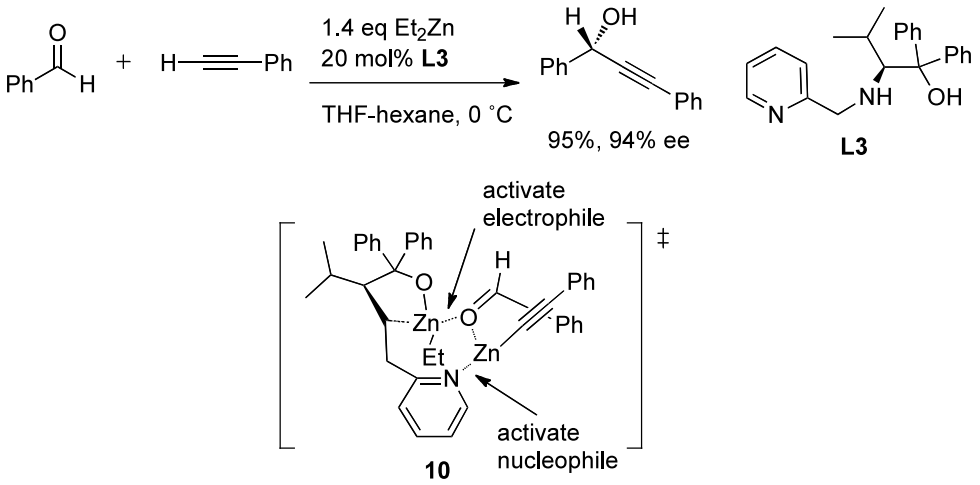

2.2. In-Catalyzed Alkynylation

Indium(III) are often used for a wide range of reactions as a Lewis acid while they are also known as effective activator of alkynyl groups. Shibasaki developed the In(III) catalyzed alkynylation of aldehydes by applying these properties (Scheme 13).[17] The effective activation of both substrates enabled the reaction to proceed in asymmetric manner by the use of BINOL **L4** and dicyclohexylmethyl amine. The reaction shows excellent enantioselectivities as well as broad scope with respect to both reacting species in mild conditions. On the basis of the observation of non-linear effect, they proposed bimetallic mechanism as shown in Scheme 14.

Scheme 13. Asymmetric alkynylation of aldehyde catalyzed by an In/BINOL complex.

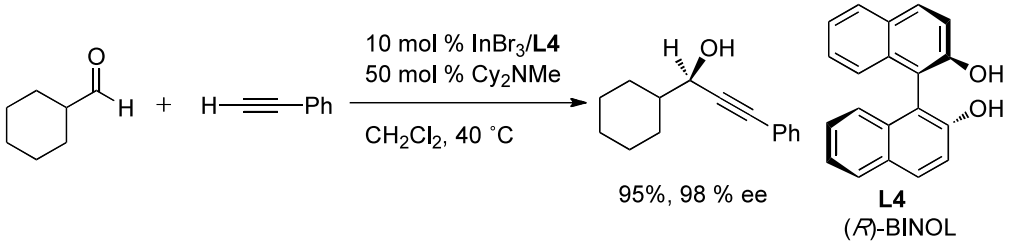

Scheme 14. Proposed bimetallic mechanism

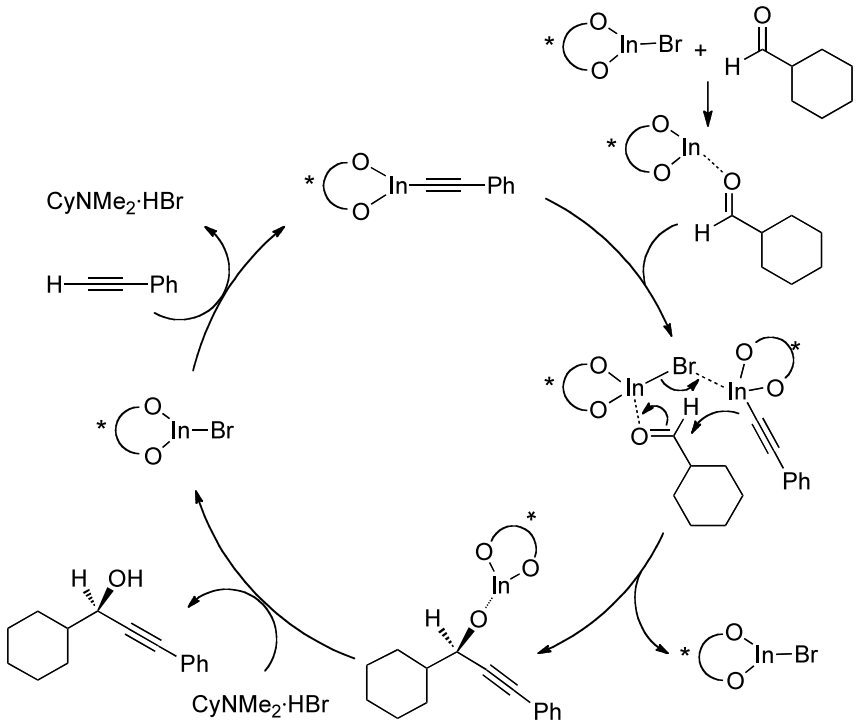

2.3. Ru-Catalyzed Alkynylation

A curious application of NCN pincer ligand was reported through the use of Ru-phebox complex **11** by Nishiyama, which afforded the chiral propargylic alcohols in high yields and enantioselectivities (Scheme 15).[18] However, substrates were limited to aromatic aldehydes and phenyl acetylene derivatives.

Scheme 15. Asymmetric alkynylation catalyzed by chiral Ru-phebox complex.

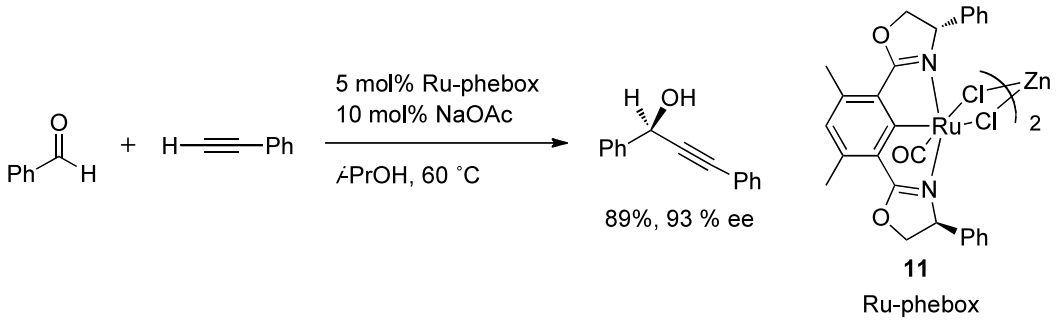

11
Ru-phebox

2.4. Cu-Catalyzed Alkynylations

2.4.1. Asymmetric Alkynylations of Imines

First copper-catalyzed enantioselective direct addition of terminal alkynes to imines was introduced by Li and co-workers using 1,3-bis(oxazolin-2-yl)pyridine ligand **L5** and copper salts (Scheme 16).[19, 20] In most cases, imines were formed from aldehydes in situ prior to the addition of phenylacetylene in one pot.

Scheme 16. Enantioselective direct addition of terminal alkynes to imines catalyzed by Cu-pybox complex.

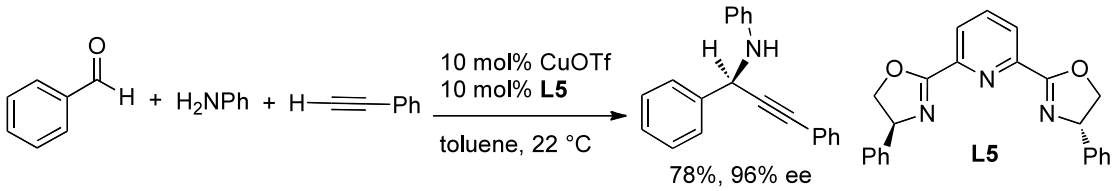

Recently, cooperative catalytic model involving α-amino acid as catalysts was reported by Arndtsen and co-workers (Scheme 17).[21] α-Amino acid is involved in the chiral H-bonding complex with the imine substrate. Combination of metal catalyst with the ability of amino acid, which formed hydrogen bond, provided an efficient way for inducing the enantioselectivity.

Another important point to note is its flexibility and practicality. By changing amino acids or phosphines, the suitable catalyst structure can be easily introduced. They examined lots of commercially available N-Boc protected α-amino acids and phosphines. This simplified ligand screening allowed N-Boc-proline **15** to be identified as the optical amino acid for the reaction. In addition to amino acid, as a result of phosphine screening, P(*o*-tolyl)$_3$ was selected as the optimal ligand for this reaction.

Scheme 17. Asymmetric alkynylations of imines by cooperative hydrogen bonding and Cu catalyst.

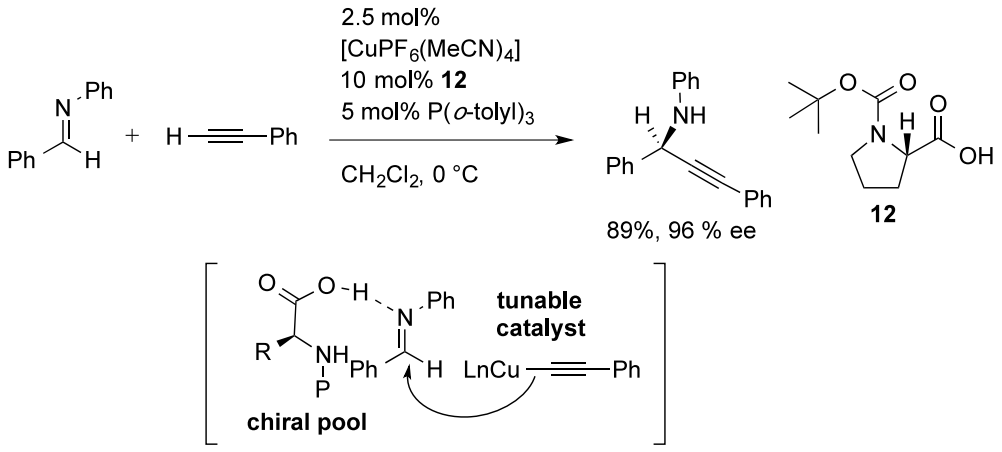

2.4.2. Asymmetric Alkynylations of Carbonyl Compounds

Although the addition reactions of copper acetylide to imines were widely explored, few studies on copper-catalyzed enantioselective alkynylation of carbonyl compounds were reported. For example, Shibasaki and co-workers disclosed the enantioselective alkynylation of activated trifluoromethyl ketones using copper catalyst in 2007 (Scheme 18).[22] Obtained chiral propargylic alcohols bearing a quaternary carbon center can be useful intermediates for Efavirenz (anti-HIV drug) and its related compounds. With copper-DTBM-SEGPHOS **L6** as a catalyst, chiral tertiary propargylic alcohols are obtained in high yields, albeit in moderate enantioselectivities.

Scheme 18. Cu-catalyzed enantioselective alkynylation of trifluoromethyl ketones.

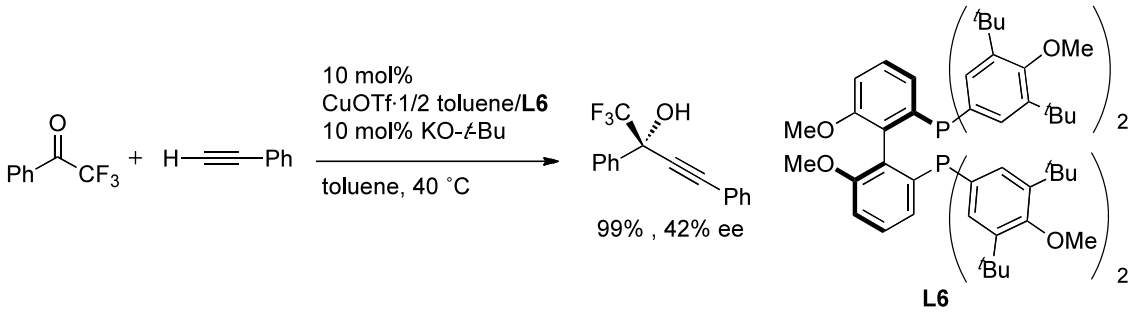

Copper-catalyzed direct alkylation of aromatic aldehydes using chiral bisphosphine TRAP **L7** was achieved by Sawamura.[23] Copper-TRAP complex showed high catalytic activity due to the large P–Cu–P bite angle that induces large distributions of active

monomeric species. Compared with other solvents, alcoholic solvents were more effective to enhance the rate of the reaction, as well as improved enantioselectivity. Based on this intriguing phenomenon, they proposed six-memberd transition state **13** involving alcohol solvent as shown Scheme 19. An alcohol solvent participates in the addition reaction through coordination to the copper center and simultaneously protonation of the carbonyl oxygen occurs. Consequently, the activated aldehyde is attacked by copper-acetylide with enantioselevtive manner. The products were obtained in high yields, but in moderate enantioselectivities. Problem about narrow range of substrates was also remained.

Scheme 19. Enantioselective addition of terminal alkynes to aldehydes catalyzed by a Cu–TRAP complex.

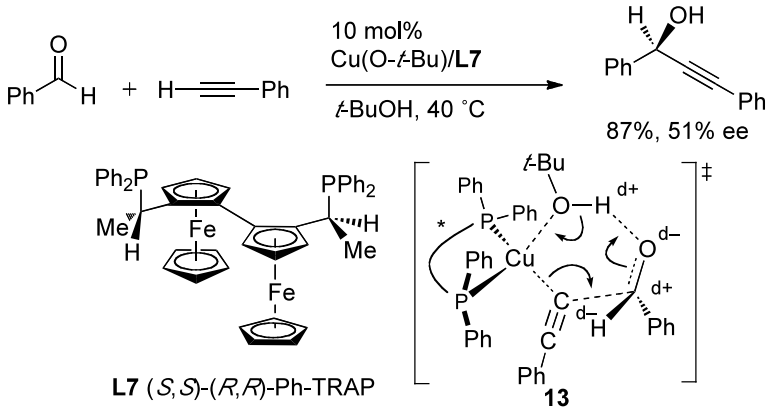

3. Overview of This Thesis

The work described in this thesis focused on the cooperative catalyst reactions based on copper-hydroxy amino phosphine ligands. In the course of catalyst design, the author focused on the previous observation of solvent effect of alcohols. In the alkynylation with TRAP ligands, alcoholic solvents were superior solvent to induce the high enantioselectivity. This observation implied the participation of an alcoholic solvent molecule in a cooperative mechanism as illustrated in Scheme 18. This curious experimental result in mind, the author designed and synthesized hydroxy amino phosphine ligands containing an alcoholic hydrogen-bonding site and applied them to copper-catalyzed asymmetric alkynylations of carbonyl compounds. This thesis is organized into two sections.

3.1. Cooperative Catalysis of Metal and O–H···O/sp^3-C–H···O Two-point Hydrogen Bonds in Alcoholic Solvents: Copper-catalyzed Enantioselective Direct Alkynylation of Aldehydes with Terminal Alkynes (Chapter 1).

A copper-catalyzed enantioselective alkynylation of aldehydes with terminal alkynes with prolinol-based hydoroxy amino phosphine chiral ligands was developed (Scheme 20). This reaction presents a case in which ligand–substrate hydrogen bonding interactions cooperate with a metal center in protic solvents. Quantum mechanical calculations show the occurrence of a non-classical sp^3-C–H···O hydrogen bond as a secondary interaction between the ligand and the carbonyl substrate, which results in highly directional catalyst–substrate two-point hydrogen-bonding (see a transition state **14**). The enantioselective catalysis is applicable for both aliphatic and aromatic aldehydes in combination with various alkynes with different terminal substituents, thus providing a useful method for preparing enantioenriched propargylic alcohols, which eliminates problems of existing systems such as a limited substrate range or use of precious metals and organic bases in large quantities.

Scheme 20. Cu-hydroxy amino phosphine complex catalyzed enantioselective direct alkynylation of aldehydes with terminal alkynes.

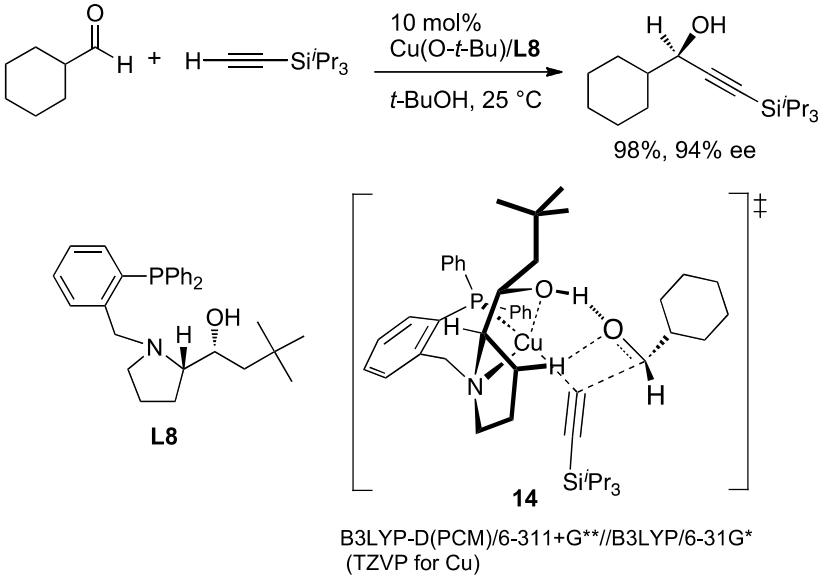

3.2. Enantioselective Alkynylation of α-Keto Esrer Derivatives Catalyzed by Chiral Hydroxy Amino Phosphine Copper Complexes (Chapter 2)

The author found that the chiral hydroxyl amino phosphine ligands are applicable to copper(I)-catalyzed enantioselective alkynylations of α-keto esters with terminal alkynes (Scheme 21). This copper catalysis provides an efficient method for accessing a wide range of enantioenriched chiral tertiary propargylic alcohols with high enantioselectivities. The hydrogen-bonding interactions between chiral catalysts and substrates in alcoholic solvents are proposed.

Scheme 21. Enantioselective alkynylation of α-keto ester derivatives catalyzed by chiral hydroxy amino phosphine copper complex.

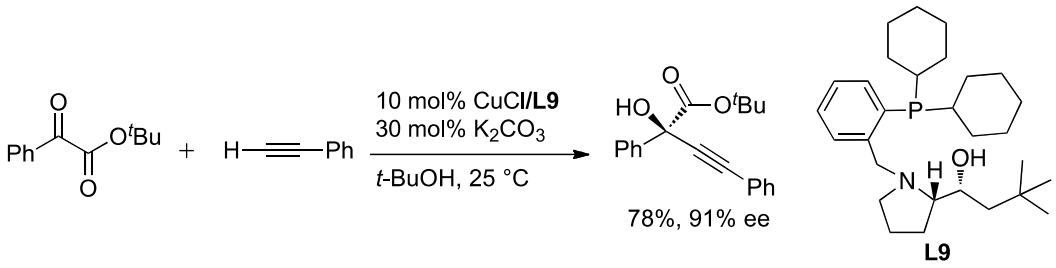

References

[1] *Catalytic Asymmetric Synthesis third edition*, (Ed. Ojima, I), John wiley and sons, New Jersey, **2010**.

[2] Fessner, W.-D.; Schneider, A.; Held, H.; Sinerius, G.; Walter, C.; Hixon, M.; Schloss, J. V. *Angew. Chem. Int. Ed.* **1996**, *35*, 2219.

[3] (a) Ito, Y.; Sawamura, M.; Hayashi, T. *J. Am. Chem. Soc.* **1986**, *108*, 6405. (b) Sawamura, M.; Nakayama, Y.; Kato, T.; Ito, Y. *J. Org. Chem*, **1995**, *60*, 1727. For a review on the catalytic asymmetric synthesis by means of secondary interaction between chiral ligands and Substrates, see: (c) Sawamura, M.; Ito, Y. *Chem. Rev.* **1992**, *92*, 857.

[4] (a) Sasai, H.; Suzuki, T.; Arai, S.; Shibasaki, M. *J. Am. Chem. Soc.* **1992**, *114*, 4418. For reviews on the earth-alkali metal BINOL complexes and their applications, see: (b) Shibasaki, M.; Yoshikawa, N. *Chem. Rev.* **2002**, *102*, 2187. (c) Shibasaki, M.; Kanai, M.; Matsunaga, S.; Kumagai, N. *Acc. Chem. Res.* **2009**, *42*, 1117.

[5] (a) Yamada, Y. M. A.; Yoshikawa, N.; Sasai, H.; Shibasaki, M. *Angew. Chem. Int. Ed. Engl.* **1997**, *36*, 1871. (b) Yoshikawa, N.; Yamada, Y. M. A.; Das, J.; Sasai, H.; Shibasaki, M. *J. Am. Chem. Soc.* **1999**, *121*, 4168.

[6] (a) Ohkuma, T.; Ooka, H.; Hashiguchi, T.; Ikariya, T.; Noyori, R. *J. Am. Chem. Soc.* **1995**, *117*, 10417. (b) Haack, K.-J.; Hashiguchi, S.; Fujii, A.; Ikariya, T.; Noyori, R. *Angew. Chem. Int. Ed. Engl.* **1997**, *36*, 285.

[7] Hajos, Z. G.; Parrish, D. R. *J. Org. Chem.* **1974**, *39*, 1615.

[8] Eder, U.; Sauer, G.; Wiechert, R. *Angew. Chem. Int. Ed. Engl.* **1971**, *10*, 496.

[9] (a) List, B; Lerner, R.A.; Barbas III, C. F. *J. Am. Chem. Soc.* **2000**, *122*, 2395. (b) Notz, W.; List, B. *J. Am. Chem. Soc.* **2000**, *122*, 7386. (c) List, B; Pojarliev, P.; Castello, C. *Org. Lett.* **2001**, *3*, 573.

[10] (a) Clemente, F. R.; Houk, K. N. *Angew. Chem. Int. Ed.* **2004**, *43*, 5766. For a review on the theory of asymmetric organocatalysis of aldol reaction, see: (b) Allmann, C.; Goldilld, R.; Clemente, F. R.; Cheong, P. H.; Houk, K. N. *Acc. Chem. Res.* **2004**, *37*, 558.

[11] Akiyama, T.; Itoh, J.; Yokota, K.; Fuchibe, K. *J. Angew. Chem. Int. Ed.* **2004**, *43*, 1566.

[12] Uraguchi, D.; Terada, M. *J. Am. Chem. Soc.* **2004**, *126*, 5356.

[13] Uraguchi, D.; Sorimachi, K.; Terada, M. *J. Am. Chem. Soc.* **2004**, *126*, 11804.

[14] Trost, B. M.; Weiss, A. H. *Adv. Synth. Catal.* **2009**, *351*, 963.

[15] Anand, N. K.; Carreira, E. M. *J. Am. Chem. Soc.* **2001**, *123*, 9687.

[16] Kang, Y.-F.; Liu, L.; Wang, R.; Yan, W.-J.; Zhou, T.-F. *Tetrahedron Asymmetry*. **2004**, *15*, 3155.

[17] (a) Takita, R.; Fukuta, Y.; Tsuji, R.; Ohshima, T.; Shibasaki, M. *Org. Lett.* **2005**, *7*, 1363. (b) Takita, R.; Yakura, K.; Ohshima, T.; Shibasaki, M. *J. Am. Chem. Soc.* **2005**, *127*, 13760.

[18] Ito, J.; Asai, R.; Nishiyama, H. *Org. Lett.* **2010**, *12*, 3860.

[19] Armas, P, D.; Tejedor, F.; Garcia-Tella-do. *Angew. Chem. Int. Ed.* **2010**, *49*, 1013.

[20] Wei, C.; Li, C.-J. *J. Am. Chem. Soc.* **2002**, 124, 5638.

[21] Lu, Y.; Johnstone, T. C.; Arndtsen, B. A. *J. Am. Chem. Soc.* **2009**, *131*, 11284.

[22] Motoki, R.; Kanai, M.; Shibasaki, M. *Org. Lett.* **2007**, *9*, 2997.

[23] (a) Asano, Y.; Hara, K.; Ito, H.; Sawamura, M. *Org. Lett.* **2007**, *9*, 3901. (b) Asano, Y.; Ito, H.; Hara, K.; Sawamura, M. *Organometallics* **2008**, *27*, 5984.

Chapter 1

Cooperative Catalysis of Metal and O–H···O/sp^3-C–H···O Two-point Hydrogen Bonds in Alcoholic Solvents: Copper-catalyzed Enantioselective Direct Alkynylation of Aldehydes with Terminal Alkynes

1. Introduction

Enantioselective cooperative catalysis using transition metal complexes comprising of organocatalytic secondary functional groups is a privileged concept for opening new possibilities in catalytic asymmetric synthesis.[1] This approach has already allowed the development of numbers of innovative molecular transformations that had not been achieved by a naive use of either metal complexes or organocatalysts,[2–5] but the field is still immature. Capter 1 describes the author's efforts toward the development of the Cu(I)-catalyzed enantioselective alkynylation of aldehydes, which has been enabled by the cooperative catalysis of Cu(I) complexes with chiral amino phosphine ligands bearing a hydrogen-bonding site. To the author's knowledge, no non-metal organocatalyst for the enantioselective aldehyde alkynylation has been reported to date. It seems that the poor kinetic and thermodynamic acidities of terminal alkyne pronucleophiles makes the organocatalytic approach for this molecular transformation difficult.

The enantioselective carbonyl addition of terminal alkynes to aldehydes is an important carbon–carbon bond formation reaction to prepare enantioenriched propargylic alcohols.[6–10] Conventionally, this transformation has used stoichiometric amount of an organometallic base for converting the alkynes into the corresponding metal acetylide. Specifically, zinc has been the most successful and popular metal. Given the recent demand for highly efficient and environmentally friendly processes, however, the direct enantioselective alkynylation of aldehydes that avoids the use of a stoichiometric amount of a reagent has become highly desirable. Specifically, Carreira and co-workers reported the enantioselective alkynylation of aldehydes that uses catalytic amounts of $Zn(OTf)_2$ (20 mol%) and N-methylephedrine (22 mol%).[7] Unfortunately however, the usable aldehydes are generally limited to aliphatic aldehydes. Furthermore, the system required the use of a substoichiometric amount of base (Et_3N, 50 mol%). Shibasaki and co-workers reported the enantioselective alkynylation catalyzed by indium(III)/BINOL system (10 mol%), which shows a broad substrate scope including both aromatic and aliphatic aldehydes.[8] Nevertheless, this protocol also employs a tertiary amine base (Cy_2NMe, 50 mol%) in a substoichiometric amount together with a relatively large quantity of preciousness metal indium (10 mol%). More recently, Nishiyama and co-workers introduced a ruthenium-based system (5 mol%) with a bis(oxazolinyl)arene ligand, but high

enentioselectivities were reported only for substrate pairs between aromatic aldehydes and phenylacetylene derivatives.[10] Accordingly, the enantioselective addition reaction of alkynes to carbonyl groups remains much room for improvement from various aspects, and the development of an effective catalytic system for this important molecular transformation is highly desirable.

Sawamura's earlier investigation on the Cu(I)-catalyzed enantioselective addition of terminal alkynes to aldehydes identified the TRAP class of chiral bisphosphines to be specific ligands that render a Cu(I) complex catalytically active so as to promote the alkynylation under mild conditions: the nature of the TRAP ligands exerting large bite angles and hence monomerizing Cu(I) acetylides was indispensable for the Cu catalysis.[9] Nonetheless, the substrate scope was severely limited to aromatic aldehydes and phenylacetylene derivatives, and enantioselectivities were only moderate. Under such a background, the author initiated a program for developing a second-generation copper catalyst system.

This chapter describes the enantioselective direct alkynylation of aldehydes with terminal alkynes catalyzed by copper(I) complexes with prolinol-based hydroxy amino phosphine chiral ligands, and present experimental as well as computational evidence for directional hydrogen-bonding interactions between chiral catalysts and substrates in alcoholic solvents. This cooperative catalysis provides an efficient method for accessing a wide range of enantioenriched secondary propargylic alcohols that are versatile synthetic intermediates for more complex non-racemic compounds.[11,12] A hydroxy group of the ligand plays a critical role in promoting the reaction, and protic solvents promote a favorable reaction rate and enantioselectivity. Guided by quantum mechanical calculations, the author proposes the existence of a non-classical sp^3-C–H···O hydrogen bond as a secondary interaction between the ligand and the substrate, which results in highly directional catalyst–substrate two-point hydrogen-bonding.

2. Results and Discussion

2.1. Catalyst Design

Upon designing the second-generation catalyst system, the author paid his attention to the fact that, in the aldehyde alkynylation with the first-generation catalyst system based on the TRAP ligands, alcoholic solvents played an important role in accelerating the reaction

and in improving the enantioselectivity. This observation suggested a possibility that a Cu-coordinated alcohol may provide a cooperative Brønstead acid site, which assists the carbonyl addition of a copper acetylide by stabilizing a developing propargylic oxyanion (Figure 1a). This assumption prompted us to design a copper-based chiral catalyst system that incorporates an alcoholic Brønstead acid site and a phosphine-based bidentate coordination site within a chiral organic scaffold so as to render the ligand–substrate hydrogen-bonding interaction and the stereodifferentiating transition state well defined. Having an additional oxygen-based coordination site, such a hydroxylated phosphine ligand would function as a tridentate ligand for copper(I) center. The author expected that such a tridentate coordination would realize monomerization of a copper(I) acetylide, for which Sawamura used previously chelation by the large-bite-angle ligands.

Figure 1. Cooperative transition state hypotheses: (a) First-generation, (b) Second-generation.

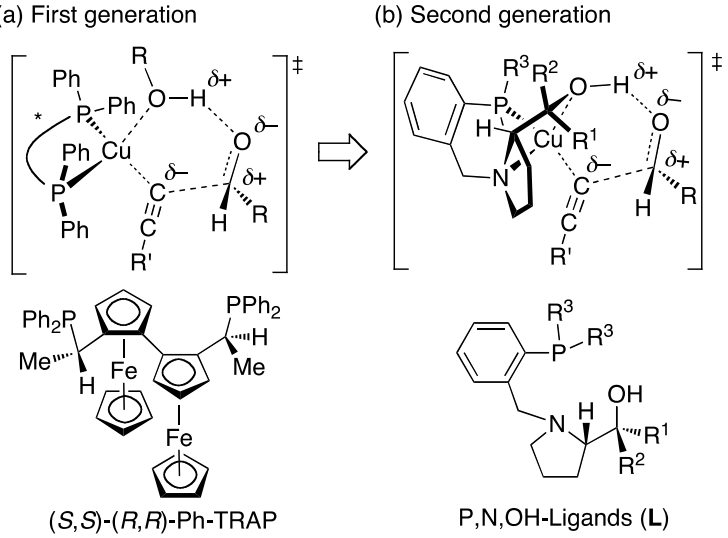

Another important designing strategy was to place a pyramidal sp^3-hybridized atom rather than a planer sp^2-hybridaized atom at the pivotal position that connects the phosphine site and the alcoholic site, so that the chiral tridentate ligand fits to a tetrahedral geometry of copper(I) center. Taking structural simplicity and the ease of synthesis and structural diversification into account as well, the author thought that chiral β-*tert*-amino alcohols would be reasonable candidates for part structures that include the pivotal site and the alcoholic Brønstead acid site. These considerations led to identify a class of natural

proline-derived hydroxy amino phosphines **L** as the first synthetic target (Figure 1b). As a result, the ligands could be efficiently synthesized and some of them showed satisfactory to excellent ligand performances, which are in accordance with the author's designing concept and mechanistic hypothesis based on the cooperative catalysis involving hydrogen-bonding interaction between the alcoholic Brønstead acid site and the oxygen atom of aldehyde substrates.

2.2. Ligand Synthesis.

The synthetic routes to the P,N,OH-ligands used in this study were outlined in Scheme 1. The prototype P,N,OH-ligand **L1** was synthesized through acylation of L-proline methyl ester with *o*-(diphenylphosphino)benzoic acid followed by $LiAlH_4$ reduction. For the synthesis of the tertiary alcohol type ligands **L2** (R = Me) and **L3** (R = Ph), the amide intermediate was reacted with Grignard reagents to introduce a branch before the reduction of the amide moiety. The secondary alcohol type ligands, having an additional stereogenic center, were synthesized in two ways. The Me-branched (**L4a**,**b**) and Ph-branched (**L5a**,**b**) ligands were first prepared as diastereomeric mixtures through stereodivergent Grignard addition to *N*-Cbz-prolinal, and then the isomers were separated by chromatography. The other secondary alcohol ligands **L6–8** were prepared through the stereocontrolled Grignard addition to *N*-trityl-prolinal, developed by Chemla and co-workers[13] For the synthesis of the P,N,OH-ligand derivatives (**L10**,**11**) with P-substituents other than Ph were prepared by using the corresponding phosphinated benzaldehydes.

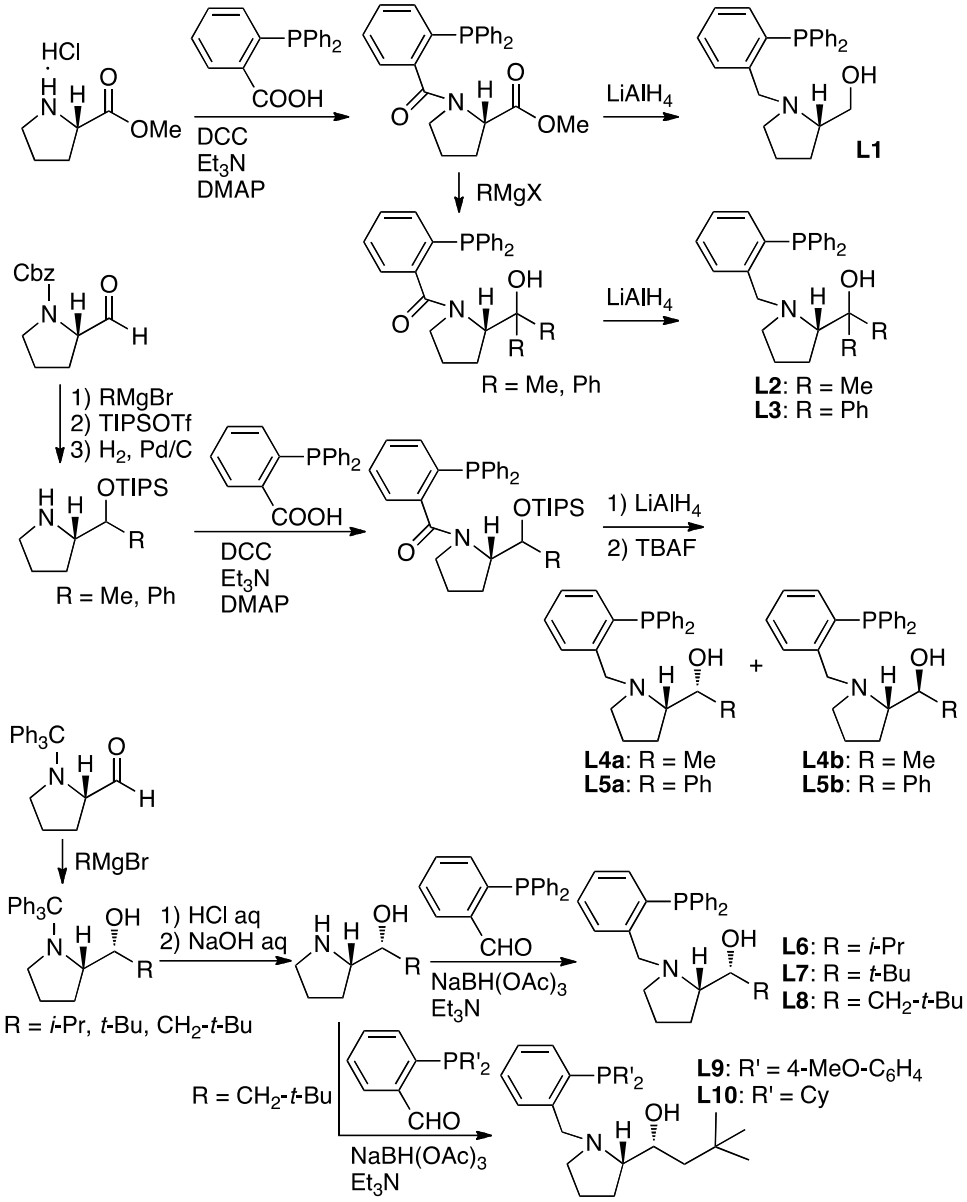

Scheme 1. Synthetic routes to P,N,OH-ligands **L1–10**

2.3. Optimization of Reaction Conditions with Prototype Chiral Ligand L1 (Solvent Effect)

As described above, the first-generation catalyst systems based on the TRAP ligands and Cu(O-*t*-Bu) had a serious limitation of substrate scope toward aliphatic aldehydes, which showed no reactivity under the reaction conditions examined.[9] Furthermore, the Ph-TRAP–Cu catalyst showed significant decrease in catalytic activity in the reactions

with alkylacetylenes and silylacetylenes. Aiming to solve these problems, the prototype P,N,OH-ligand **L1** was used for the copper-catalyzed alkynylation of an branched aliphatic aldehyde with a silylacetylene. Specifically, the **L1**/Cu(O-*t*-Bu) catalyst system (10 mol%) was examined for catalytic activity and enantioselectivity for the reaction between cyclohexanecarboxaldehyde (**1a**) and triisopropylsilylacetylene (**2a**) in various medias including aprotic, nonpolar and polar solvents and protic solvents with a constant reaction time of 48 h. Results are summarized in Table 1. To the author's delight, the reaction of this challenging substrate pair did proceed at 40 °C in aprotic solvents such as hexane, toluene, THF, DMF, and CH_3CN although the yields and the enantioselectivities were low or moderate (entries 1–5). Among these solvents, nonpolar toluene caused the highest yield (43%) with moderate enantioselectivity (32%) (entry 2), while polar solvents such as DMF and CH_3CN gave slightly higher enantioselectivities (36% ee and 43% ee, respectively) albeit with significantly reduced yields (15% and 18%) (entries 4 and 5). These results suggest that the alcoholic site in **L1** functioned as a proton source as the alcoholic solvents did in the catalysis of Cu-TRAP systems (Figure 1) [*vide infra* (section 2.8) for the effect of the protection of the ligand OH group and for related studies].

The promising results with the aprotic polar solvents prompted us to dare to use protic solvents even though its negative effect was strongly concerned because the protic solvents might break the designed hydrogen bond between the ligand hydroxy group and the aldehyde substrate. To the author's delight, however, the alcoholic solvents such as EtOH, *i*-PrOH, and *t*-BuOH caused much higher conversion and yield, and, very interestingly, these increases in the yield were accompanied by significant improvement of the enantioselectivity (up to 65% ee with EtOH and *i*-PrOH). The reaction at 25 °C resulted in a slightly higher enantiomeric excess (70% ee) at the expense of conversion rate (96 h, 91% conv.). Interestingly, the enantiomeric excess could be increased furthermore up to 71% upon addition of a small amount of water (5 equiv to **1a**).

Although the enantioselectivities thus obtained with the **L1** ligand are still only moderate, the simplicity of the ligand chiral scaffold would be surprising, having only a single stereogenic carbon center substituted with a primary alcohol moiety. Furthermore, the effects of the protic reaction medias were quite intriguing. These observations prompted us to carry out the ligand screening based on the P,N,OH motif in alcoholic solvents.

Table 1. Alkynylation of **1a** with **2a** in the presence of Cu(O-*t*-Bu)/**L1** catalyst in various solvents.

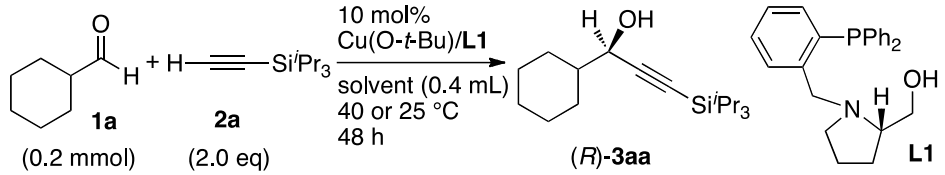

entry	solvent	additive	temp,°C	conv of **1a**, %[a]	yield, %[b]	ee, %[c]
1	hexane	–	40	42	37	34 (*R*)
2	toluene	–	40	48	43	32 (*R*)
3	THF	–	40	32	32	26 (*R*)
4	DMF	–	40	15	15	36 (*R*)
5	CH_3CN	–	40	19	18	43 (*R*)
6	EtOH	–	40	71	70	65 (*R*)
7	*i*-PrOH	–	40	92	92	65 (*R*)
8[d]	*i*-PrOH	–	25	91	89	70 (*R*)
9[d]	*i*-PrOH	H_2O[e]	25	80	80	71 (*R*)

[a] Determined by ^1H NMR analysis of crude mixture with 1,1,2,2-tetrachloroetane as an internal standard unless otherwise noted. [b] Yield of the isolated product (silica gel chromatography). [c] Determined by HPLC analysis. [d] Reaction time was 96 h. [e] H_2O (5 equiv of to **1a**) was added.

2.4. Ligand Optimization

Considering that the alcoholic site of the chiral P,N,OH-ligand plays a key role in the catalytic activity and the stereocontrol, the author investigated effects of the ligand modification at this site. In fact, the use of the tertiary alcohol type ligands **L2** and **L3** in *i*-PrOH at 40 °C caused slight improvement of the stereocontrol (71 and 67% ee v.s. 65% ee with **L1**), but, unfortunately, the slowing down of reaction was serious (Table 2, entries 1 and 2 v.s. Table 1, entry 7). On the other hand, when the secondary alcohol type ligands such as **L4a**,**b** and **L5a**,**b** were employed, the reaction rate was maintained as compared to that with **L1** with apparent improvements of the stereocontrol exept for the case with **L5b** (up to 73% ee with **L4a**) (Table 2, entries 3–6). Although the configuration at the

stereogenic center to the hydroxy group had only small impacts on both the reaction rate and the stereocontrol, **L4a** and **L5a** (R^2 = H) gave the apparently higher ee values than **L4b** and **L5b** (R^1 = H), respectively. According to these results, the author decided to focus on the diastereomerically pure secondary alcohol type ligands having a substituent as R^1 (R^2 = H) in the following experiments.

Table 2. Screening of chiral ligands for the reaction between **1a** and **2a**

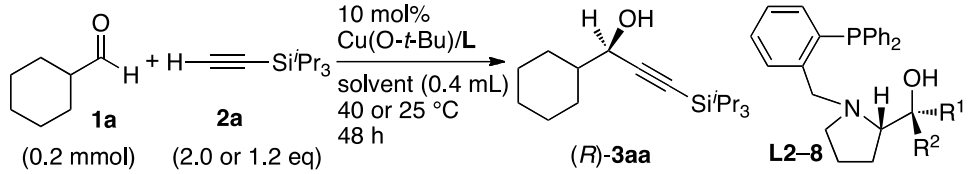

	chiral ligand					
entry	**L**	R^1	R^2	solvent	yield, %[a]	ee, %[b]
1[c]	**L2**	Me	Me	*i*-PrOH	20	71 (*R*)
2[c]	**L3**	Ph	Ph	*i*-PrOH	18	67 (*R*)
3[c]	**L4a**	Me	H	*i*-PrOH	98	73 (*R*)
4[c]	**L4b**	H	Me	*i*-PrOH	87	68 (*R*)
5[c]	**L5a**	Ph	H	*i*-PrOH	66	69 (*R*)
6[c]	**L5b**	H	Ph	*i*-PrOH	66	62 (*R*)
7[c]	**L6**	*i*-Pr	H	*i*-PrOH	94	81 (*R*)
8[c]	**L7**	*t*-Bu	H	*i*-PrOH	96	85 (*R*)
9[c]	**L8**	CH_2-*t*-Bu	H	*i*-PrOH	95	88 (*R*)
10[d]	**L8**	CH_2-*t*-Bu	H	*i*-PrOH	99	91 (*R*)
11[d]	**L8**	CH_2-*t*-Bu	H	*t*-BuOH	98	92 (*R*)
12[d, e]	**L8**	CH_2-*t*-Bu	H	*t*-BuOH	98	94 (*R*)
13[d, e, f]	**L8**	CH_2-*t*-Bu	H	*t*-BuOH	98	94 (*R*)

[a] Yield of the isolated product (silica gel chromatography). [b] Determined by HPLC analysis. [c] Reaction at 40 °C. [d] Reaction at 25 °C. [e] H_2O (5 equiv of to **1a**) was added. [f] 1.2 equiv of **2a** was used.

The ligand modification by increasing the steric demand of the α-substituent R^1 of the secondary alcohol type ligands was quite fruitful. By replacing the Me group of **L4a** with *i*-Pr and *t*-Bu groups, the ee values of (*R*)-**3aa** was increased from 74% to 81 and 85%, respectively, with retention of the complete substrate conversion (Table 2, entries 3, 7, 8). Although the straightforward increase of the steric demand of the R^1 group failed to improve the enantiocontrol furthermore, extensive ligand screening led to find the ligand **L8**, having a neopentyl group, to be more efficient chiral ligand, which afforded (*R*)-**3aa** with 88% ee (entry 9). The ee value with **L8** became as high as 91% by lowering the reaction temperature to 25 °C, and was further increased to 92% by changing the solvent to *t*-BuOH (entries 10 and 11). As observed in the case with the prototype **L1** ligand (Table 1, entry 9), the addition of a small amount of H_2O (5 equiv to **1a**) was effective for increasing the enantioselectivity, giving (*R*)-**3aa** with 94% ee. It should be noted that the alkynylation with the optimal secondary alcohol type ligand **L8** is markedly faster than that with the primary alcohol type ligand **L1**, and the quantitative substrate conversion was observed in the reaction at 25 °C (Table 1, entries 8 and 9 v.s. Table 2, entries 10–12). The amount of alkyne substrate (**2a**) could be reduced to 1.2 equiv with the quantitative yield and the high ee values unchanged (Table 2, entry 13).

2.5. Scope of Aldehydes

The influence of aldehydes on the reactivity and enantioselectivity were examined using the reaction with triisopropylsilylacetylene (**2a**). The reaction was carried out with 1.2 equiv of **2a** in the presence of 10 mol% of the Cu(O-*t*-Bu)/P,N,OH-ligand systems in *t*-BuOH at 25 °C (Table 3). The chiral ligands **L8**–**10** having a neopentyl substituent in the alcoholic site were used. A small amount of H_2O (5 equiv to **1**) was occasionally added in order to improve the enantioselectivity. Results are summarized in Table 3. Unbranched hexanal (**1b**) reacted with high enantioselectivities with Cu(O-*t*-Bu)/**L8** system, while the yield was low due to the self-condensation of the aldehyde (entry 1). Branching at the β-position of aldehydes suppressed the self-condensation significantly, the high level of enantioselectivity being unchanged (entries 2 and 3). α-Branched aldehydes are generally suitable substrates in terms of both the yield and enantioselectivity with the **L8** ligand (entries 4–6 and see also Table 2, entry 13). Neverthless, sterically more demanding

pivalaldehyde (**1i**) reacted with a moderate enantioselectivity with **L8** (entry 7). Further ligand examination with **L8** and **L9** revealed that **L9** gave a slightly improved enantiomeric excess (76% ee) (entries 8 and 9).

The reaction of benzaldehyde (**1i**) showed ligand suitability different with that of aliphatic aldehydes. The Cy_2P-type ligand **L10** gave apparently higher ee value (90% ee) than the Ar_2P-type ligands **L8** and **L9** (entries 10–12). The superiority of **L10** was general for the reaction of a range of aromatic aldehydes (entries 13–19). The aromatic aldehydes having electron-withdrawing groups such as ester, fluoro and chloro moieties were suitable substrates for the both yield and enantioselectivity (entries 13–15). The electron-donating group (OMe) on the *meta*-position of the aromatic ring was compatible (entry 16), albeit that the *p*-OMe group inhibited the reaction completely (data not shown). Heteroaromatic aldehydes such as 3-thiophenealdehyde (**1n**) and 3-furylaldehyde (**1o**) were suitable substrates (entries 17 and 18). The ortho-substituted aromatic aldehyde **1p** reacted with a poor enantioselectivity (entry 19).

The applicability of the Cu-catalyzed protocol toward both aliphatic and aromatic aldehydes is significant: the reported Zn-based catalytic systems encountered a problem of competitive Cannizzaro reaction of aromatic aldehydes, first-generation copper catalyst system did not promote the reaction of aliphatic aldehydes, and the Ru-based catalyst system was not effective for the reaction of aliphatic aldehydes. The In-based system is only the precedent effective for the both types of aldehydes.

Table 3. Scope of aldehydes. [a]

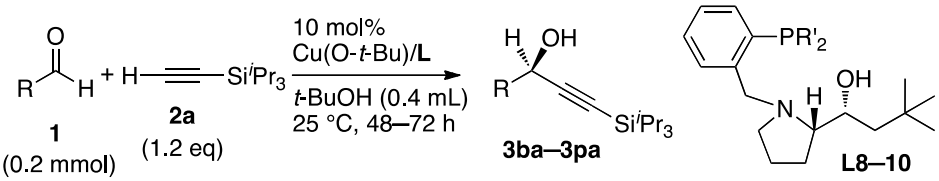

entry	aldehyde	gand	product	yield, %	ee, %
1	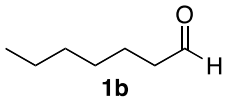 **1b**	**L8**	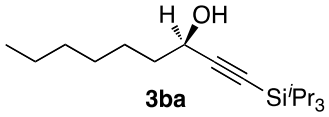 **3ba**	45	87
2	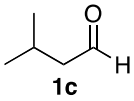 **1c**	**L8**	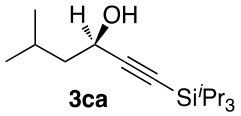 **3ca**	73	85
3	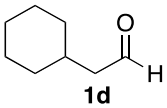 **1d**	**L8**	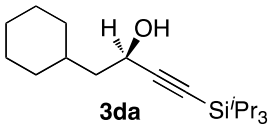 **3da**	75	90
4	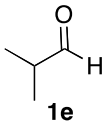 **1e**	**L8**	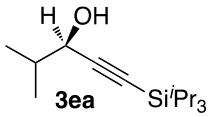 **3ea**	87	87
5	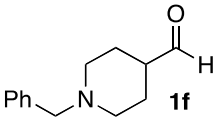 **1f**	**L8**	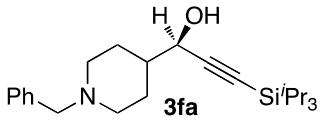 **3fa**	99	94
6	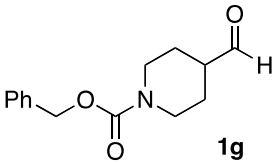 **1g**	**L8**	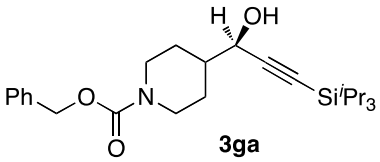 **3ga**	98	94
7		**L8**		42	64
8	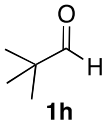 **1h**	**L9**	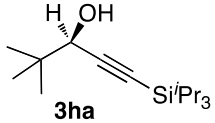 **3ha**	85	76
9		**L10**		0	–

10	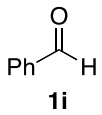 **1i**	**L8**	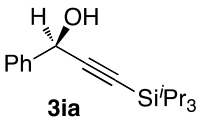 **3ia**	71	78
11		**L9**		70	76
12		**L10**		80	90
13	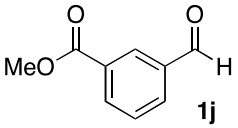 **1j**	**L10**	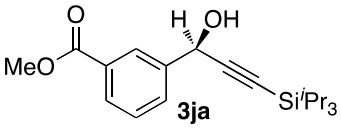 **3ja**	93	86
14	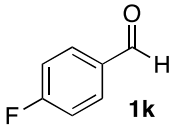 **1k**	**L10**	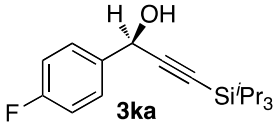 **3ka**	91	88
15	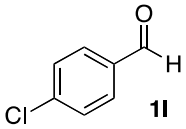 **1l**	**L10**	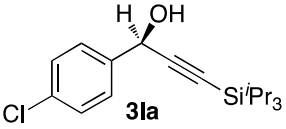 **3la**	95	90
16	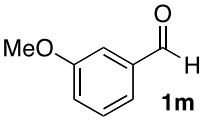 **1m**	**L10**	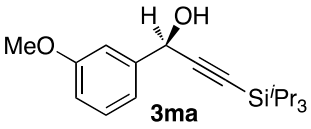 **3ma**	95	91
17	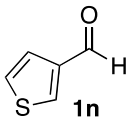 **1n**	**L10**	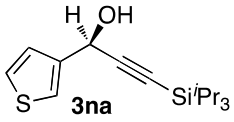 **3na**	73	90
18	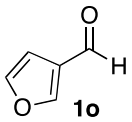 **1o**	**L10**	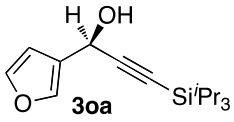 **3oa**	52	91
19	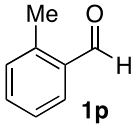 **1p**	**L10**	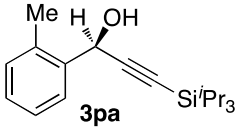 **3pa**	45	36

[a] Conditions: **1** (0.2 mmol), **2** (0.24 mmol), Cu(O-*t*-Bu)/**L8–10** (10 mol %), *t*-BuOH (0.4 mL), 25 °C, 48 h (entries 1, 5–8, 10, 11, 13), 60 h (entry 16), 72 h (entries 2, 3, 5, 12, 14–16, 18, 19). H_2O (5 equiv to **1**) was added in entries 1–8.

2.6. Scope of Alkynes

Various alkynes were examined using the reaction with cyclohexanecarboxaldehyde (**1a**) (Table 4, entries 1–11). The reaction was carried out with 1.2 equiv of **2** in the presence of 10 mol% of a Cu(O-*t*-Bu)/**L8** system in *t*-BuOH at 25 °C. Various aliphatic alkynes (**2b**-**e**) with different degrees and patterns of branching reacted with high enantioselectivities, although liner aliphatic alkyne **2b** specifically showed lower reactivity (entries 1–4). *N*,*N*-dibenzylpropargyl amine (**2f**) or *o*-protected propargylic alcohol (**2g**) also reacted with high product yields and enantioselectivities (entries 5 and 6). The reaction of aromatic alkynes proceeded with somewhat lower enantioselectivities (72–83% ees) than those of aliphatic alkynes, while the yields were generally high (entries 7–9). Electron-donating substituent effect on the aromatic ring seems to be beneficial for the enantioselectivity at the small expense of the product yield. The silylacetylenes (**2a**, **l**, **m**) are generally reactive alkylating reagents, while the enantioselectivity was significantly dependent on the steric demand of the triorganosilyl moiety: sterically more demanding groups affording higher enantioselectivities ($SiEt_3$, 78%; Si-*t*-$BuMe_2$, 80%; Si-*i*-Pr_3, 94%) (entries 10, 11 and Table 2, entry 13).

Table 4. Scope of alkynes for the reaction of **1a**.[a]

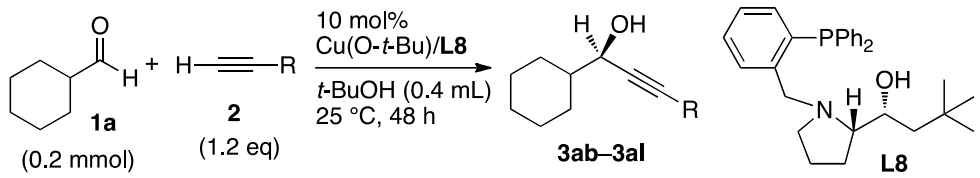

entry	alkyne	product	yield, %	ee, %
1	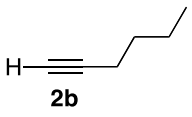 **2b**	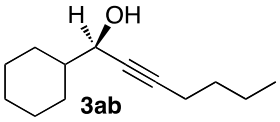 **3ab**	62	84
2	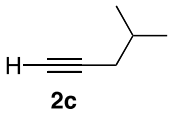 **2c**	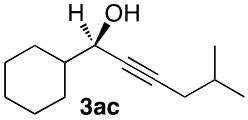 **3ac**	92	86
3	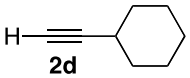 **2d**	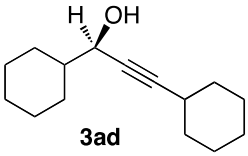 **3ad**	95	85
4	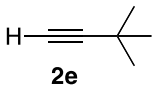 **2e**	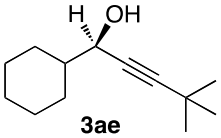 **3ae**	97	87
5	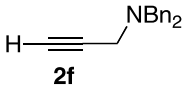 **2f**	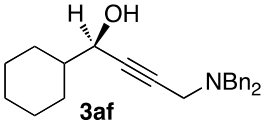 **3af**	91	83
6	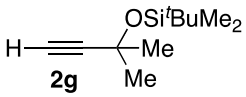 **2g**	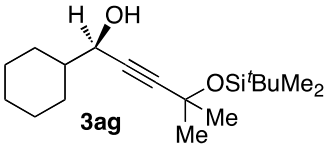 **3ag**	96	88
7	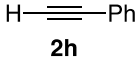 **2h**	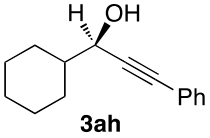 **3ah**	94	78

8	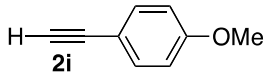 **2i**	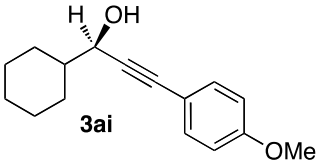 **3ai**	81	83
9	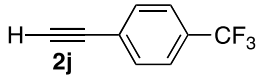 **2j**	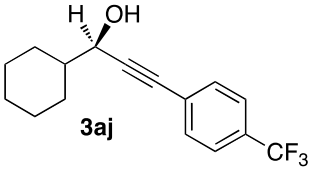 **3aj**	98	72
10	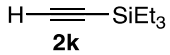 **2k**	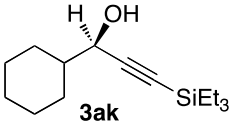 **3ak**	96	78
11	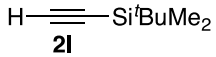 **2l**	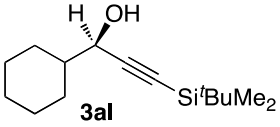 **3al**	97	80

[a] Conditions: **1a** (0.2 mmol), **2** (0.24 mmol) Cu(O-*t*-Bu)/**L8** (10 mol %), *t*-BuOH (0.4 mL), 25 ˚C, 48 h.

2.7. Modified Reaction Conditions: CuCl/L/K_2CO_3 System and Scalability

The reaction conditions, which were used for the initial research, employ air-sensitive copper source Cu(O-*t*-Bu), and it necessitates a glovebox operation. Accordingly, the author explored alternative reaction conditions that use more easy-to-handle copper source. As a result, the author found that the reaction can be performed almost equally with a catalyst system consisting of CuCl, the P,N,OH-ligands and K_2CO_3 (Table 5). For instance, the reactions of α-branched aliphatic aldehydes such as **1a** and **1g** or a β-branched aliphatic aldehyde **1c** with triisopropylsilylacetylene (**2a**) in the presence of CuCl/**L8** (10 mol %) and K_2CO_3 (30 mol %) proceeded with enantioselectivities as high as those with the Cu(O-*t*-Bu)/**L8** system (entries 1–3). The reaction of aromatic aldehydes such as **1i**, **1j**, **1l** and **1n** could also be conducted under the modified reaction conditions employing the CuCl/**L10**/K_2CO_3 system (entries 4–7).

Table 5. Enantioselective alkynylation of various aldehydes with **2a** using CuCl/P,N,OH-ligand/K_2CO_3 system.

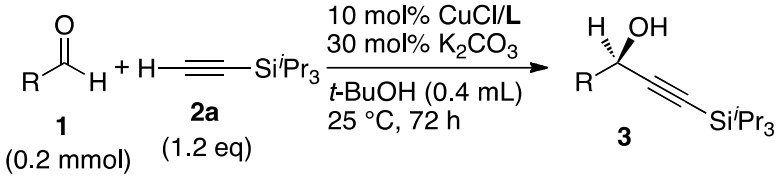

entry	aldehyde	ligand	product	yield, %	ee, %
1	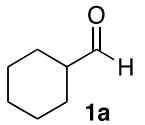 **1a**	**L8**	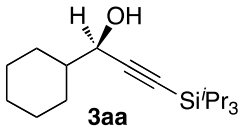 **3aa**	98	94
2	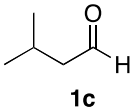 **1c**	**L8**	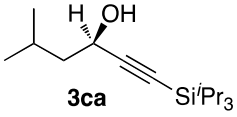 **3ca**	84	86
3	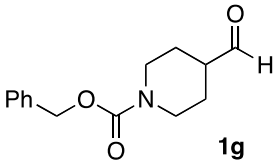 **1g**	**L8**	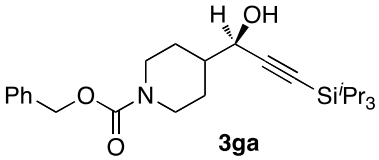 **3ga**	94	94
4	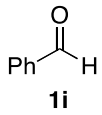 **1i**	**L10**	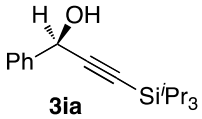 **3ia**	65	88
5	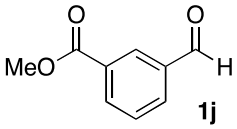 **1j**	**L10**	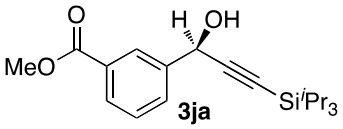 **3ja**	99	91
6	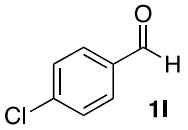 **1l**	**L10**	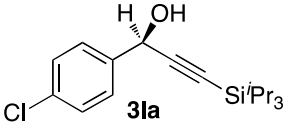 **3la**	97	89
7	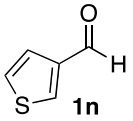 **1n**	**L10**	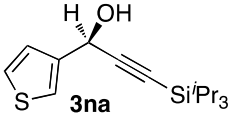 **3na**	56	89

[a] Conditions: **1** (0.2 mmol), **2a** (0.24 mmol), CuCl/**L** (10 mol %), K_2CO_3 (30 mol %), *t*-BuOH (0.4 mL), 25 ˚C, 48 h.

The glovebox-free protocol could be scaled up without a loss of the product yield and the enantioselectivity as exemplified in the 10 mmol scale reaction between **1a** and **2a** (Scheme 2). The author notes that the catalyst loading was successfully reduced to 5 mol % (Cu) upon the scale-up.

Scheme 2. A gram-scale reaction of **1a** and **2a** under the glovebox-free conditions.

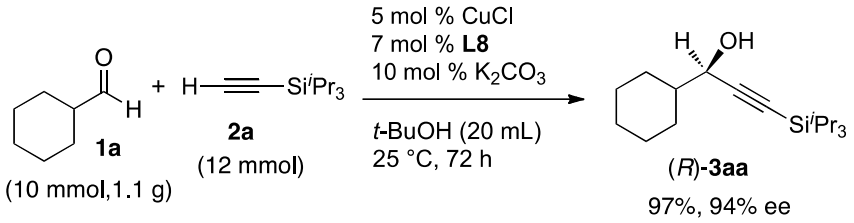

2.8. Other Chiral Ligands: Importance of the Ligand OH Group

Figure 2 summarizes the effect of various chiral ligands other than **L1–10** on the copper-catalyzed alkynylation of cyclohexanecarboxyaldehyde (**1a**). Protection of the hydroxy groups of the P,N,OH ligands **L1** and **L8** as a methyl ether caused complete inhibition of the alkynylation reaction (with **L11**, **12**). The results indicate that the alcohol sites in the P,N,OH ligands such as **L1–10** play a critical role in promoting the alkynylation reaction. The P,N,OH ligands **L13** and **L14** were also totally ineffective. These ligands have a hydroxy group at the position β to the nitrogen atom as the effective P,N,OH ligands **L1–10** have, but the alcoholic sites of **L13** and **L14** are endocyclic, while those of **L1–10** ligands are exocyclic. In addition, the P,N,OH ligand **L15**, which has an exocyclic γ-hydroxy group, was also ineffective. These results with P,N,OH ligands **L13–15** indicate that the effect of the hydroxy group on the catalysis is very sensitive to its location relative to the P,N moiety. Furthermore, the P,N,OH-ligand **L16**, which has an sp^2-hybridized nitrogen and a β-hydroxy group, gave a low yield and poor enantioselectivity. Thus, the low efficiency of **L16** relative to the **L1–10** ligands may be due to the electronic effect of the nitrogen atom or to the directionality of the alcoholic pendant.

Among various chiral bidentate ligands including bisphosphines with different backbone structures and natures of *p*-substitutuents as well as nitrogen-based ligands [(*R*,*R*)-*i*-Pr-DUPHOS, (*R*)-BINAP, (*R*)-Segphos, (*R*,*R*)-QuninoxP* and (*R*)-Ph-Box], only

(*R*,*R*)-*i*-Pr-DUPHOS afforded the alkynylation product (**3ah**, 65 °C, 88%) but no enantioselectivity was observed.

Figure 2. Other chiral ligands.

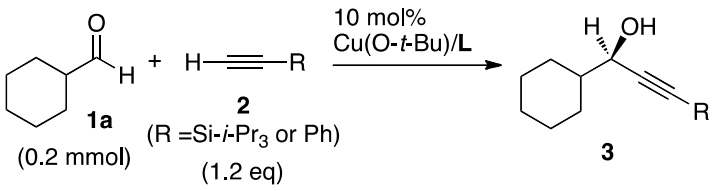

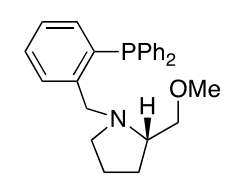

L11
N.R.
2a, *t*-BuOH, 65 ˚C

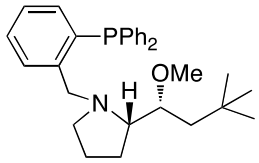

L12
N.R.
2a, *t*-BuOH, 25 ˚C

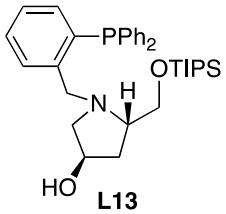

L13
N.R.
2a, *t*-BuOH, 25 ˚C

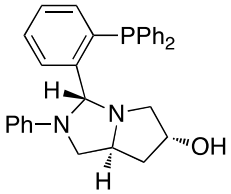

L14
N.R.
2h, *i*-PrOH, 65 ˚C

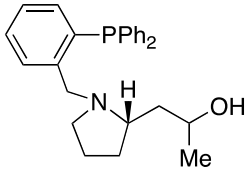

L15
N.R.
2h, *i*-PrOH, 40 ˚C

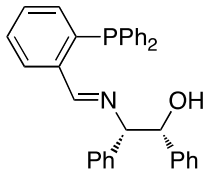

L16
17%, 9% ee
2a, *i*-PrOH, 65 ˚C

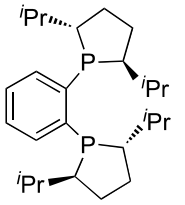

(*R*,*R*)-*i*Pr-DUPHOS
88%, 0%ee
2h, *i*-PrOH, 65 ˚C

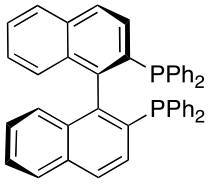

(*R*)-BINAP
N.R.
2h, *i*-PrOH, 65 ˚C

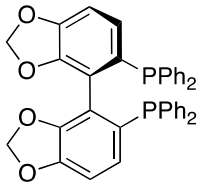

(*R*)-Segphos
N.R.
2h, *i*-PrOH, 65 ˚C

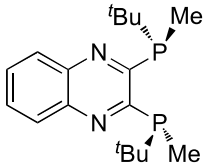

(*R*,*R*)-QuinoxP*
N.R.
2h, *i*-PrOH, 65 ˚C

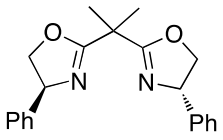

(*R*)-Ph-Box
N.R.
2h, *i*-PrOH, 65 ˚C

2.9. Effects of Enantiomeric Purity of L8 on the ee of the Product 3aa

To shed light on the structure of catalytically active species, the relationship between the enantiomeric purity (% ee) of chiral ligand **L8** and the enantioselectivity (% ee) for the reaction between **1a** and **2a** was investigated. As shown in Figure 3, a non-linear effect was not observed both with *t*-BuOH and toluene as a solvent, supporting a monomeric nature of catalytic species. The enantiomeric purity of **L8** did not affect the yield of **3aa** with the both solvents. This is in accord with the author's catalyst design for rendering a copper(I) acetylide species monomeric by tridentate coordination with P,N,OH ligands.

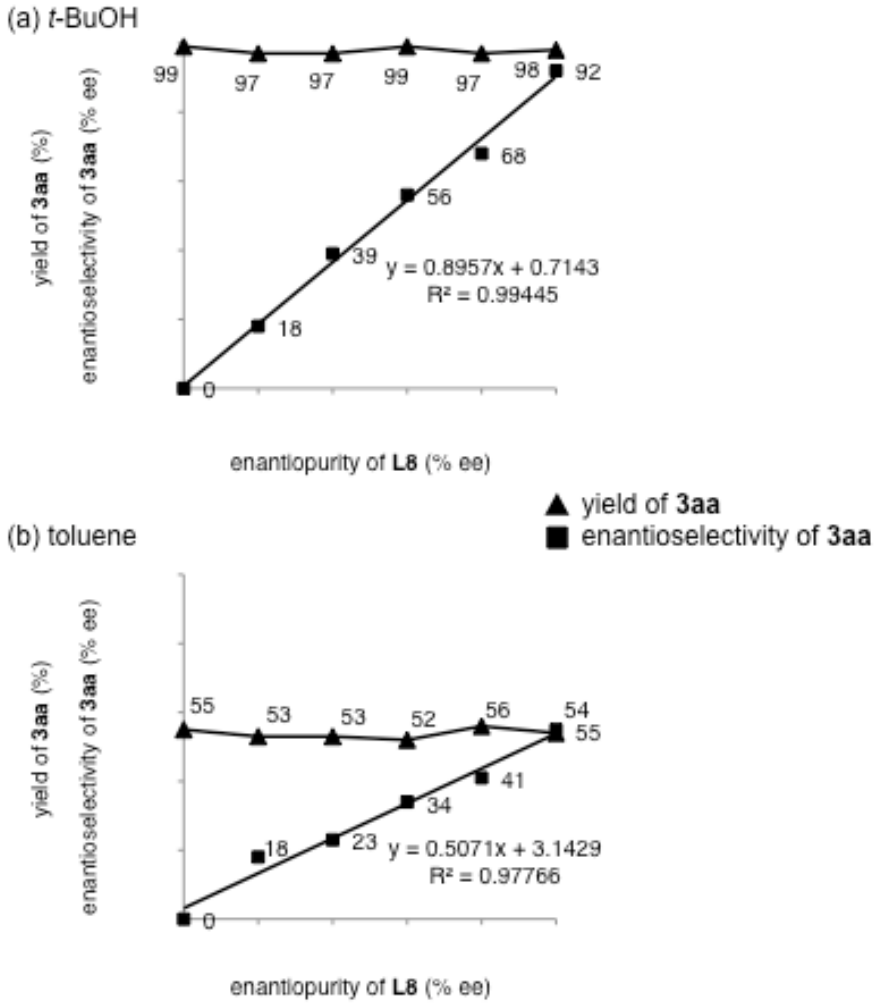

Figure 3. Linear correlation between enantiomeric purity of **L8** and enantioselectivity of the reaction between **1a** and **2a** catalyzed by Cu(O-*t*-Bu)/**L8** system (10 mol %) at 25˚C for 48 h (a) with *t*-BuOH or (b) with toluene as a solvent.

2.10. Proposed Reaction Pathway

A proposed reaction pathway, which accounts for most of the mechanistically important experimental results, is illustrated in Figure 4. This cycle is based on the hydrogen-bond-based, cooperative, six-centered transition state model shown in Figure 1b. It is to be noted that a non-linear effect in enantiomeric excess was not observed between **L8** and the product **3aa**, supporting the monomeric nature of the catalytic species (see Experimental Section; Figure 6). Since the reaction was conducted in an alcoholic solvent, participation of alcohol through hydrogen-bonding was considered throughout the catalytic cycle.

First, a Cu(I) alkoxide complex (**A)** with an h^2-coordinated alkyne ligand is produced through the reaction between a P,N,OH ligand (**L**) and Cu(O-*t*-Bu) or $CuCl/K_2CO_3$ in the presence of an alkyne (**2**). The alkoxide oxygen atom and the terminal hydrogen atom of the alkyne likely form a hydrogen bond bridge with an alcohol molecule, which is either from the alkoxide complex or a solvent. The *p*-complex **A** should be in equilibrium with h^1-acetylide complex **B** through intramolecular proton transfer. In the acetylide complex **B**, the OH group of **L** stays bound to the Cu atom at the oxygen atom and provides an acidic hydrogen bond donor site while the acetylide carbon offers a basic (nucleophilic) site. Replacement of the alcohol molecule of **B** with an aldehyde (**1**) forms a hydrogen-bonded complex **C**, which is a precursor for a nucleophilic addition step. The aldehyde in **C** should have an interaction with an alcoholic solvent. The proton-assisted, carbon–carbon bond forming, nucleophilic addition proceeds through a six-centered transition state [**D(TS)**], to yield an alkoxocopper(I)–propargylic alcohol complex (**E**). Finally, the alkyne exchange equlibrium between **E** and the substrate **2** releases the propargylic alcohol **3** to complete a catalytic cycle. The proton-assisted nucleophilic addition should be an enantiodiscriminating step.

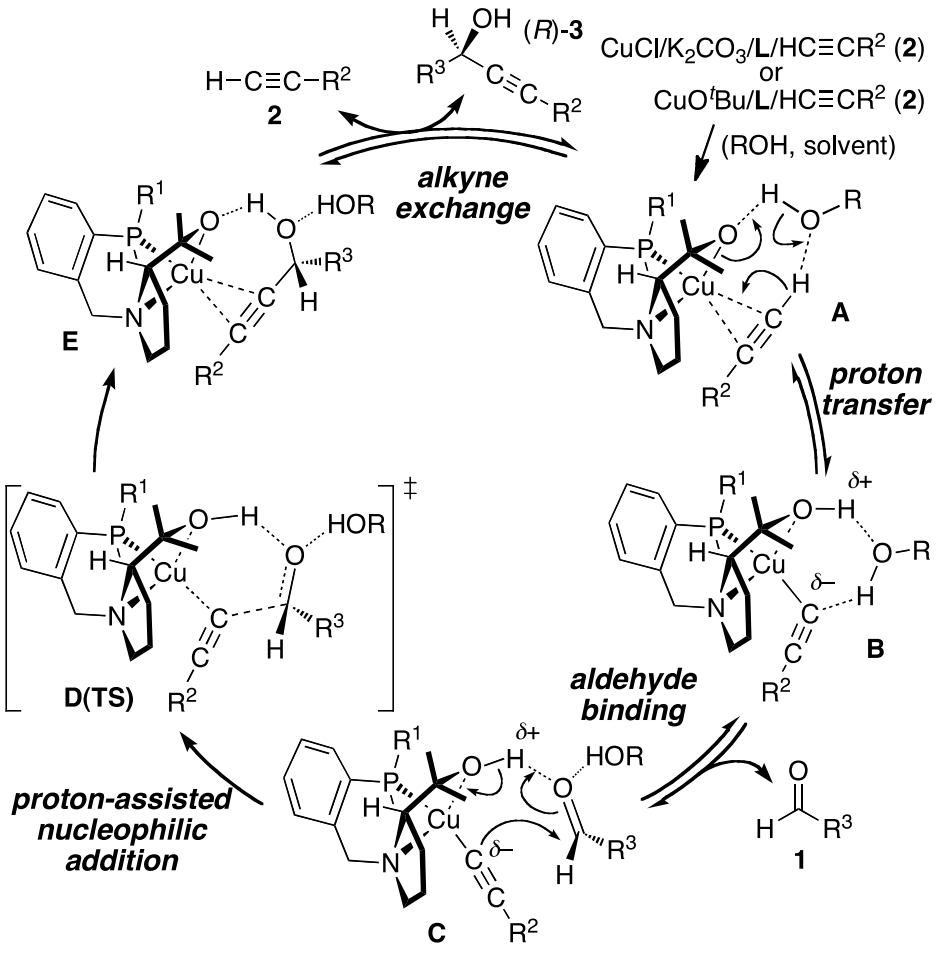

Figure 4. A proposed reaction pathway.

2.11. Quantum Mechanical Studies

To understand how the chiral catalysts impart high enantioselectivity, DFT calculations was carried out for the transition states (TSs) of the enantiodiscriminating C–C bond formation step [cf. **D(TS)** in Figure 4], not only for modeled reactions between MeCHO and HC≡CSiMe$_3$ (Model-1a with **L1**; Model-2a with **L8**), but also for the reactions between *c*-HexCHO (**1a**) and HC≡CSi-*i*-Pr$_3$ (**2a)** (Model-1b with **L1**, Table 1, entry 6–8; Model-2b with **L8**, Table 2, entries 9–13 and Scheme 2). Geometry optimizations were performed at the B3LYP[14,15] level with the TZVP basis set[16] for Cu and with the 6-31G(d) basis set[17] for the other atoms (termed BI basis sets). Single-point energies of the optimized geometries were calculated at the B3LYP-D(PCM) level[18–20] with the TZVP basis set for Cu and with the 6-311+G(d,p) basis set[19] for the other atoms (termed BII basis sets); energy was adjusted to introduce

the effects of the solvent polarity of *t*-BuOH (*e* = 12.0) and empirical dispersion corrections.

First, TS geometries were optimized for a simplified model (Model-1a) with **L1**, MeCHO, and a C≡CSiMe$_3$ group to investigate the range of conformers (40 for each of the major and minor enantiomers, 80 in total) of the pyrrolidine[21] and P, N-chelate rings with the copper atom at the B3LYP level with a smaller basis set (termed B0 basis sets; see Experimental Section for details). This resulted in convergence to eight TS structures for each isomer (Table 7). The two most meaningful conformers out of the eight were further optimized at the B3LYP level with a larger basis set BI (Figure 10). Figure 5 shows the most stable structures of TSs leading to the major (denoted as **M**) and minor (denoted as **m**) enantiomeric products, in which the pyrrolidine ring adopts an envelope-type conformation with an out-of-plane N atom and an equatorial hydroxymethylene side chain. A reasonable value of 72.9 kJ/mol was obtained for the Gibbs activation energy of alkynylation through the most stable TS(**M**) (Figure 12). In contrast, four-centered TSs, in which the carbonyl oxygen is directly coordinated to the Cu atom with the OH group ligand free from coordination, were greater than 70 kJ/mol higher in total electronic energy compared with the six-centered TSs (Table 10, Figures 13 and 14). Accordingly, for further studies, only six-centered TSs that adopted the pyrrolidine and P, N-chelate ring conformations as in the most stable Model-1a TSs were considered (Figure 5).

A surprising feature of the Model-1a TSs (Figure 5) is that, in addition to the hydrogen bond between the OH group and aldehyde oxygen atom with H···O atomic distances of 1.52 and 1.51 Å, the pyrrolidine ring has a direct interaction with the carbonyl oxygen through a non-classical C^2–H···O hydrogen bond with an H···O atomic distance of 2.24 Å for both **TS M** and **TS m**. Although the C–H bond lengths are normal, the H···O atomic distances are considerably shorter than the sum of van der Waals radii of H and O atoms (ca. 2.6 Å). Similar sp^3-C–H···O interactions are found in organic crystal structures[22] and biomolecules,[23] though they have not been concerned in common in the studies on artificial catalyst systems.[24–28] Other optimized conformers without a C^2–H···O hydrogen bond are no less than 16.0 kJ/mol higher in Gibbs free energy [B3LYP-D(PCM)/BI//B3LYP/B0, Table 8]. Consequently, the directional two-point hydrogen-bonding orients the carbonyl group. Nevertheless, the **M** and **m** structures are almost equal in stability, and calculations of the Boltzmann

distribution at 25 °C from the Gibbs free energies of all the optimized structures for this modeled system give an **M**/**m** abundance ratio (er) as low as 57.4:42.6 (Table 9).

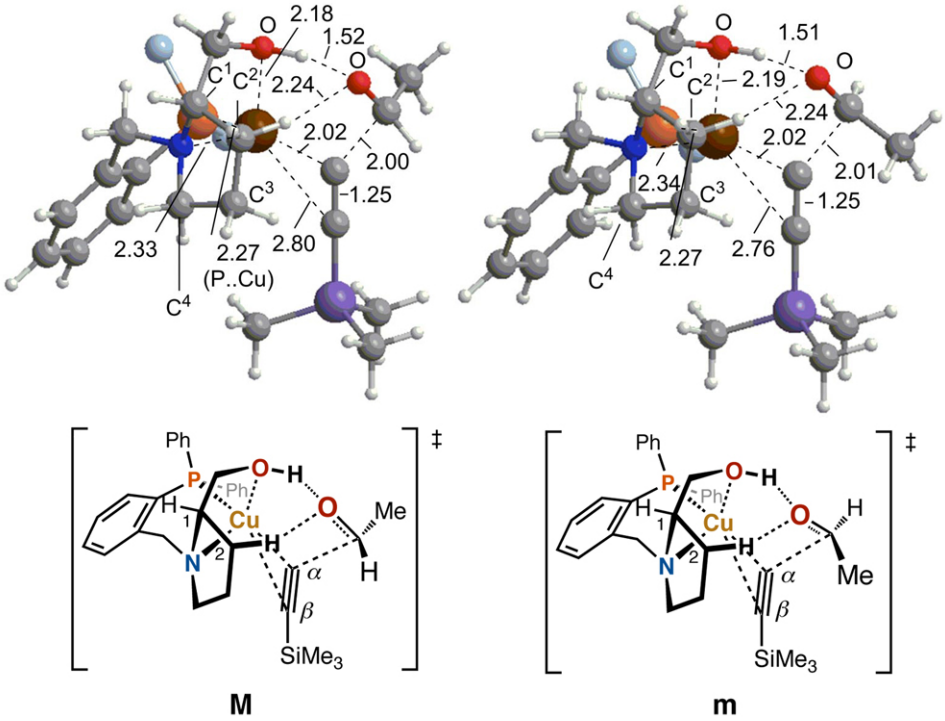

Figure 5. The most stable structures of **M** (major) and **m** (minor) transition states for Model-1a (**L1**, MeCHO, -C≡CSiMe$_3$). Phenyl groups are shown as light-blue balls for clarity.

The calculations were performed for a more advanced model system (Model-1b) with **L1**, *c*-HexCHO (**1a**), and a C≡CSi-*i*-Pr$_3$ group (**2a**–H), which corresponds to the experiment that showed the moderate enantiomeric ratio of 85:15 (Table 1, entry 8). For reducing the cost of calculations, only a single conformation of the *c*-HexCHO molecule and the most stable three conformations of the Si-*i*-Pr$_3$ moiety were considered; the latter were obtained by conformational analysis of **2a** at the HF/6-31G* level with the Spartan '08 program.[29] The calculations, albeit having considerable ambiguity due to the conformational constraints in the *c*-HexCHO molecule, gave a reasonable **M**/**m** abundance ratio (er) of 74.9:25.1 (Figure 15 and Table 11).

After preliminary examination of the other simplified model system (Model-2a) with a neopentyl-substituted ligand **L8** (Figure 16, Table 12), which gave a **M**/**m** ratio of 64.0:36.0, the calculations was performed for a system (Model-2b) with **L8**, *c*-HexCHO (**1a**), and a C≡CSi-*i*-Pr$_3$ group (**2a**–H). This corresponds to the optimal reaction

conditions in the experiments (Table 2, entries 9–13). Geometry optimizations were conducted for 27 conformers for each of TS(**M**) and TS(**m**) with different conformations of the neopentyl group (x 3), the *c*-HexCHO molecule (x3), and the Si-*i*-Pr_3 group (x 3) (Table 13, Figure 17). The most stable structures of **M** and **m** are shown in Figure 6a. The **M**/**m** abundance ratio (er) based on the Boltzmann distribution at 25 °C from the Gibbs free energies of all the optimized structures was 96.9:3.1 (Table 13) in accord with the efficient enantiocontrol (er up to 97:3 in *t*-BuOH at 25 °C) with the Cu-**L8** system in the experiments.

The neopentyl group of **L8** is relatively distant from both the alkyne and aldehyde substrates, overhanging the Cu-bound hydroxy group with its *t*-Bu hammerhead: the hydrogen atom on the carbon α to the OH group and the OH oxygen atom have van der Waals contacts with the nearest *t*-Bu-H atoms (Figure 6a). The *P*-phenyl groups (omitted in Figure 6a) are also located in regions where no direct interaction with the substrates occurs. Despite a lack of chiral ligand–substrate steric interactions (which is unusual in enantioselective catalysis), the directional two-point hydrogen bond arranges the aldehyde carbonyl group asymmetrically in a well-defined manner. As a result, the difference in steric environment around the aldehyde between TS(**M**) and TS(**m**) is evident as shown in the views from the plane of the aldehyde along the developing C–C bond (Figure 6b). The *c*-Hex substituent in TS(**M**) is arranged perpendicularly to the axis of the acetylide while that in TS(**m**) is eclipsed. Consequently, TS(**m**) encounters larger steric repulsion between the *c*-Hex substituent of the aldehyde and the Si-*i*-Pr_3 substituent of the alkyne. The neopentyl group in **L8**, being distal to the substrates, might play the role of an anchor to enhance the directionality of the hydrogen bonds, producing a well-defined chiral reaction environment.

To confirm that the sp^3-C–H···O hydrogen bond exists even in an alcoholic solvent, the a single MeOH molecule was attached to the aldehyde C=O oxygen of the most stable conformer of TS(**M**) of Model-2b through a hydrogen bond [cf. **D(TS)** in Figure 4]. This caused only a small structural change in the TS involving the two-point hydrogen bonds, except for the elongation of the C^2–H···O and O–H···O hydrogen-bonding distances by ca. 5% (Figure 18). Although the possibility of a certain degree of overestimation of the sp^3-C–H···O hydrogen bond is not ruled out, it is difficult to explain the efficient enantiocontrol without considering this secondary

interaction (see Figure 9 for various higher-energy conformers without a C–H···O hydrogen bond in Model-1a).

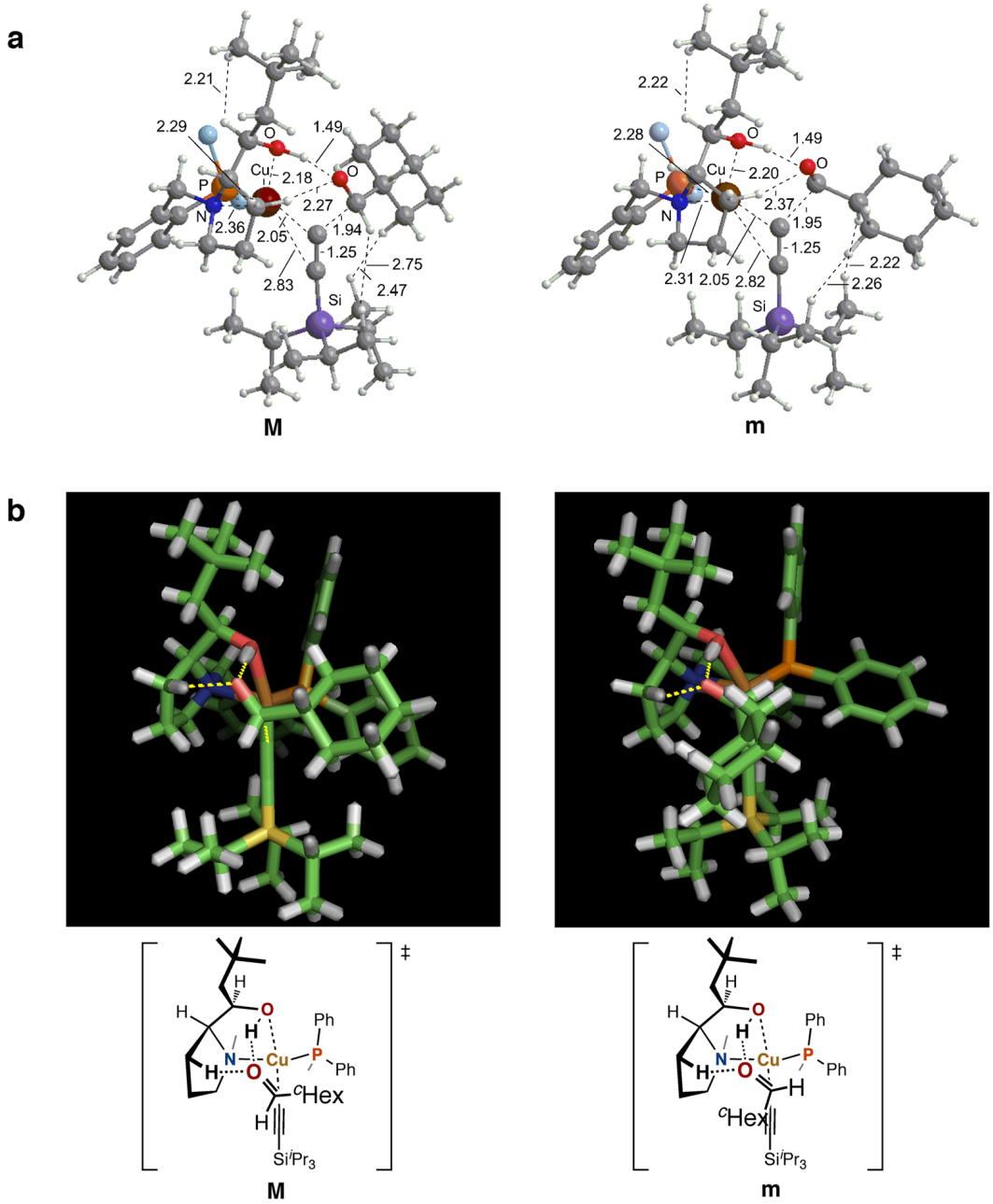

Figure 6. The most stable structures of **M** (major) and **m** (minor) transition states for Model-2b [**L8**, *c*-HexCHO (**1a**), -C≡CSi-*i*-Pr$_3$ (**2a**–H)]. a) Side views. Phenyl groups are shown as light-blue balls for clarity. b) Views (from the front) from the plane of the aldehyde along the developing C–C bond.

3. Summary

A copper-catalyzed enantioselective alkynylation of aldehydes with terminal alkynes with prolinol-based hydoroxy amino phosphine chiral ligands was developed. This reaction presents a case in which ligand–substrate hydrogen bonding interactions cooperate with a metal center in protic solvents. Quantum mechanical calculations show the occurrence of a non-classical sp^3-C–H···O hydrogen bond as a secondary interaction between the ligand and the carbonyl substrate, which results in highly directional catalyst–substrate two-point hydrogen-bonding. The enantioselective catalysis is applicable for both aliphatic and aromatic aldehydes in combination with various alkynes with different terminal substituents, thus providing a useful method for preparing enantioenriched propargylic alcohols, which eliminates problems of existing systems such as a limited substrate range or use of precious metals and organic bases in large quantities. Catalyst–substrate hydrogen-bonding interactions in protic solvents and sp^3-C–H···O hydrogen-bonds would be useful new concepts for understanding the mechanisms of cooperative asymmetric catalysis and for future catalyst design. On the other hand, questions of why aliphatic aldehydes and aromatic aldehydes favor different P-substituents (PPh_2 vs. PCy_2) and of how the alcoholic solvents participate in the catalysis remain to be elucidated.

4. Details for Computational Studies

All calculations in the present study were performed with the Gaussian 09 program[30] and by using the restricted Becke-three-parameter plus Lee-Yang-Parr (B3LYP) DFT method. The B3LYP functional is able to provide a satisfactory description for structures and energetics of the copper-containing system. [31] The B3LYP functional was employed for geometry optimizations and normal coordinate analyses. The B3LYP-D functional was used with empirical dispersion corrections for the single point calculations. The TZVP basis set with a basis set for Cu, the 6-31G(d) basis set for blue atoms in Figure 7, and the 3-21G basis set for the others (black atoms in Figure 7) was used. This basis set combination is termed B0 in this paper. For the single-point calculations for TSs and geometry optimization of representative TSs, the TZVP basis set for Cu, and the 6-31G(d) basis set for the others was used. This combination is denoted as BI. For single-point calculations, the TZVP basis set for Cu, and the 6-311+G(d,p) basis set for the others was used. This combination is denoted as BII. Solvent polarity of *t*-BuOH has also been considered as the polarizable continuum model (PCM). Natural charges were computed with NBO 5.9. [32] Zero-point energies (ZPE) and standard Gibbs energies at 298.15 K and 1 atm were calculated based on normal coordinate analyses. For the most stable **TS M** of Model-2b (B-E6 2b-2-1-3 M), geometry optimization (10 optcycles) and normal coordinate analysis at the B3LYP/BI level (907 basis functions) required 1630 min and 2843 min, respectively, on eight processors of a server Fujitsu PRIMERGY RX300 in the research center for computational sciences, Okazaki research facilities.

Setup of Models for Computational Studies.

The schematic representations of the six-centered TSs are shown in Figure 7. The TSs leading to the major and minor enantiomers are coded as M and m, respectively. The two conformers for the 6-membered P,N-chelate ring including Cu, C^a, N, and P atoms are named as conformers A and B. Several conformers for the pyrrolidine ring were considered (vide infra).

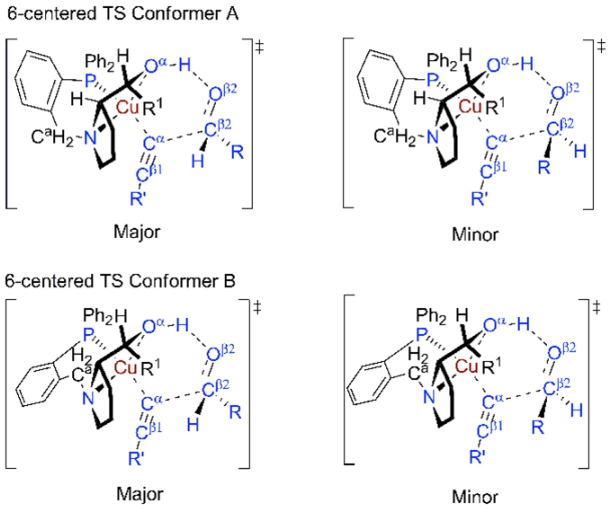

Figure. 7. Schematic representation of six-centered TS. The 6-31G(d) basis set was used for atoms and groups in blue, TZVP basis set used for Cu atom, and the 3-21G basis set used for the other atoms.

The two types of models, Models 1 and Models 2, were examined, which differ in the chiral ligands (Table 6). Model-1a and Model-1b have the **L1** ligand, while Model-2a and Model-2b have the neopentyl-substituted **L8** ligand. Model-1a and Model-2a are simpler models having MeCHO molecule and C≡CSiMe$_3$ moiety. Model-1b and Model-2b, having *c*-HexCHO (**1a**) molecule and C≡CSi-*i*-Pr$_3$ moiety, correspond to Table 1, entries 6–9 and Table 1, entries 9–13, respectively.

Table 6. Computational Models

	R^1	R	R'	Enantiomer ratio (er)	
	in **L**	in aldehyde **1**	in alkyne **2**	BI//B0	BII//BI
Model-1a	H (**L1**)	Me	SiMe$_3$	48.7:51.3	57.4:42.6
Model-1b	H (**L1**)	*c*-Hex (**1a**)	Si-*i*-Pr$_3$ (**2a**)		74.9:25.1
Model-2a	CH$_2$-*t*-Bu (**L8**)	Me	SiMe$_3$		64.0:36.0
Model-2b	CH$_2$-*t*-Bu (**L8**)	*c*-Hex (**1a**)	Si-*i*-Pr$_3$ (**2a**)		96.9:3.1

Model-1a (Six-centered TSs).

The previous theoretical and electron diffraction studies on the pyrrolidine show that an envelop conformation, in which the N atom is out of the plane, is the most stable.[33-36] The coding of each conformation in ref. 35 is used. Hence, ten twist-conformations and ten envelop-conformations of the pyrrolidine ring were examined in Model-1. Among 40 conformers of the TSs (M and m), 16 conformers were successfully optimized, and the optimization of the other 24 conformers merged to the 16 conformers. The name of the conformers is shown in Figure 9. For example, E1 and E6 have a planar C^1-C^2-C^3-C^4 moiety, and N is out of the C^1-C^2-C^3-C^4 plane. In E*n* and E*n*+5, C^{n-1} (*n* = 2,3,4,5) is out of the plane (Figure 8). In twist conformation T1, C^4-C^3-C^2 lies in a horizontal plane and the other N and C^1 atoms are located above and below the horizontal plane, respectively. The T1 conformer is located between E1 and E2 conformers.

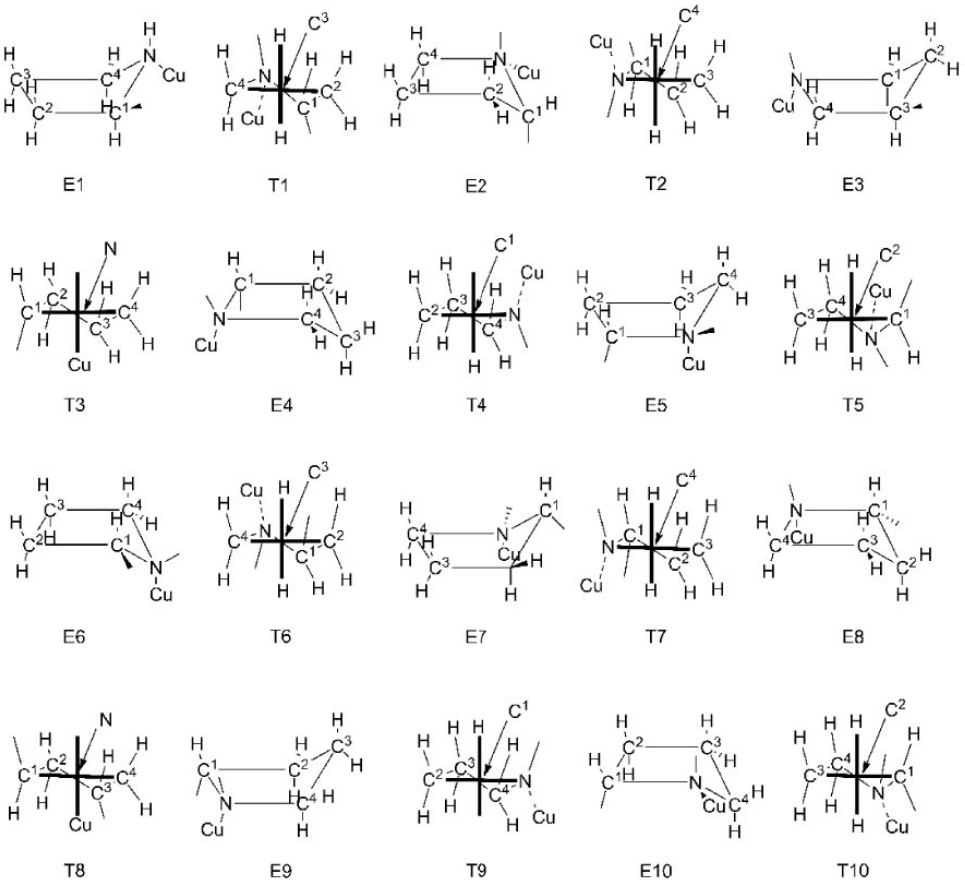

Figure. 8. Conformations of the pyrrolidine ring.

Structures of Model-1a TSs optimized at the B3LYP/B0 level are shown in Figure 9. Total electronic energies and relative Gibbs energies of the optimized TSs are shown in Table 7 and Table 8, respectively.

B-E6 is the most stable TSs (**M** 48.4%; **m** 51.0%) and A-T10 (**M** 0.3%; **m** 0.2%) is the second. The pyrrolidine conformation in the most stable TS is close to those in the previous theoretical studies on pyrrolidine derivatives.[34-36] Only A-T10 and B-E6 have a non-classical C^2-H···O interaction, suggesting the importance of this interaction. According to Table 8, low enantiomeric ratio of 48.7:51.3 can be predicted in Model-1a.

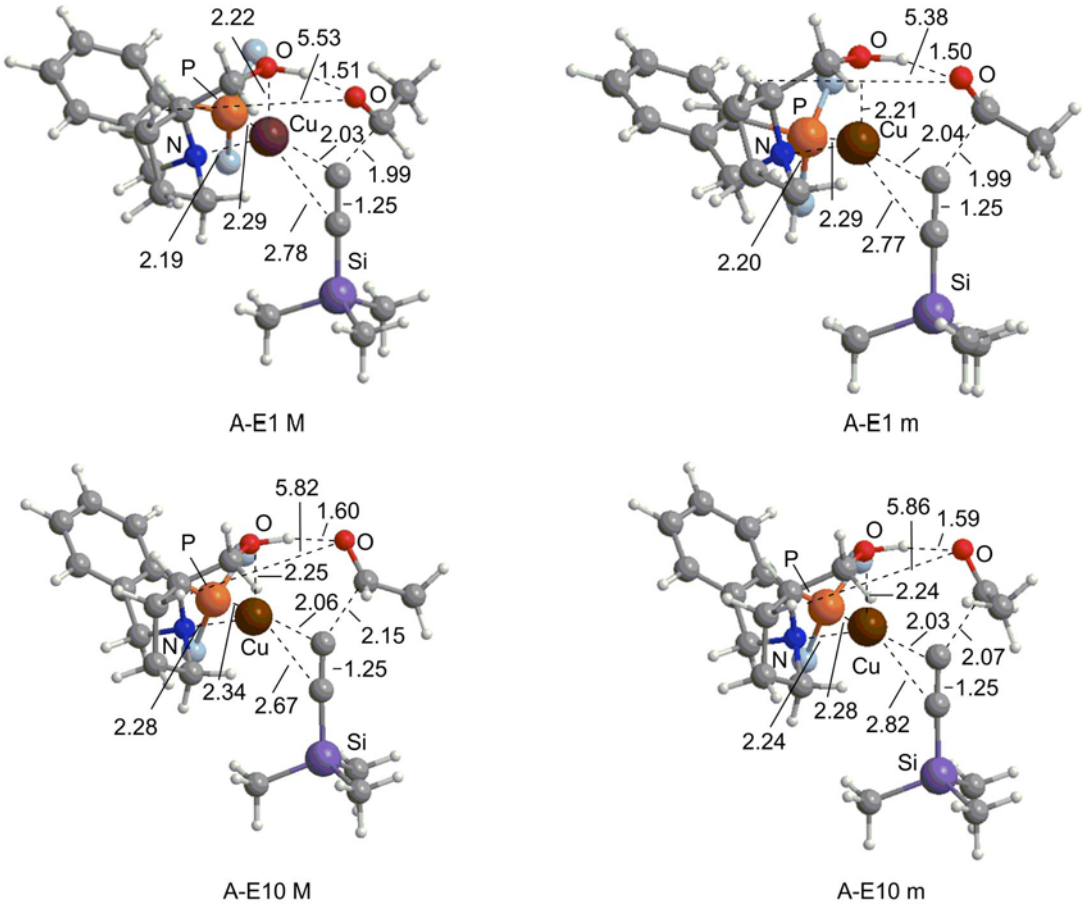

Figure. 9 continued.

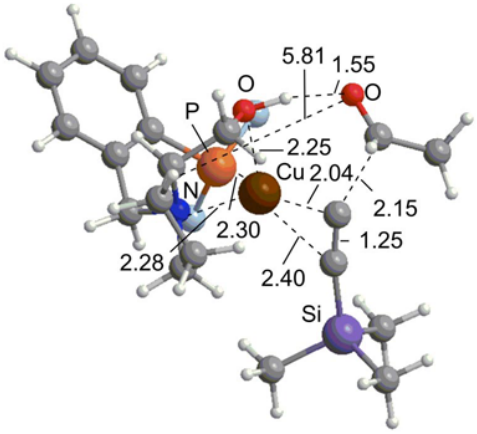

A-T2 M

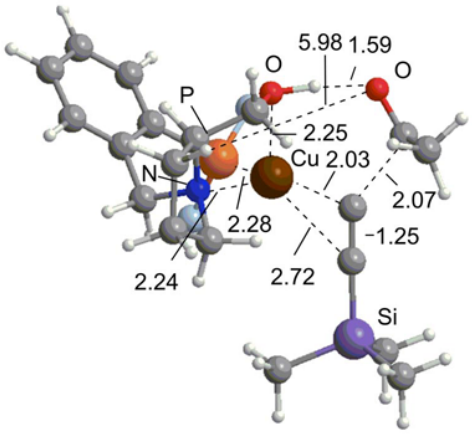

A-T2 m

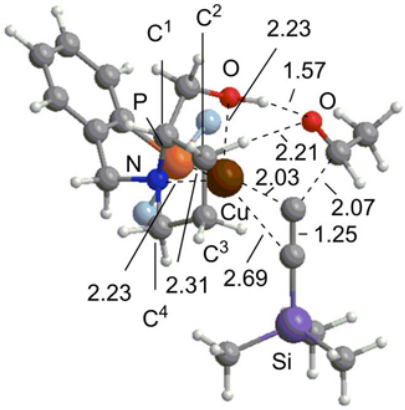

A-T10 M

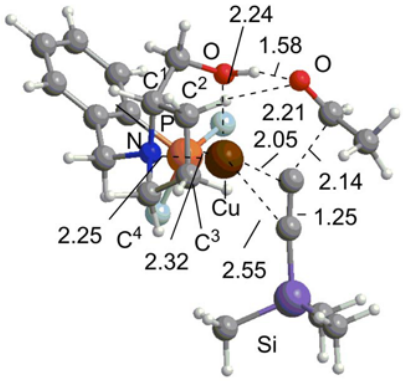

A-T10 m

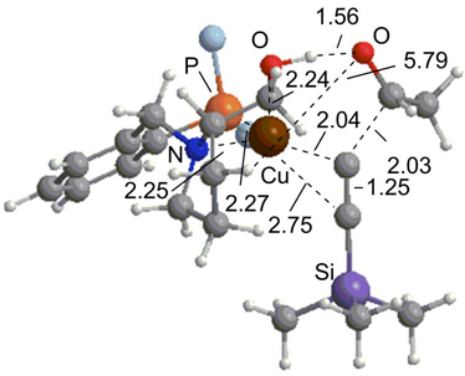

B-E4 M

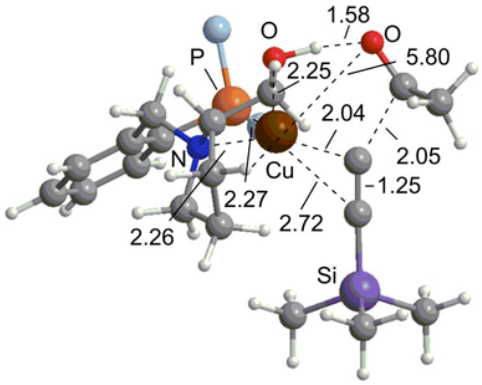

B-E4 m

Figure. 9. continued.

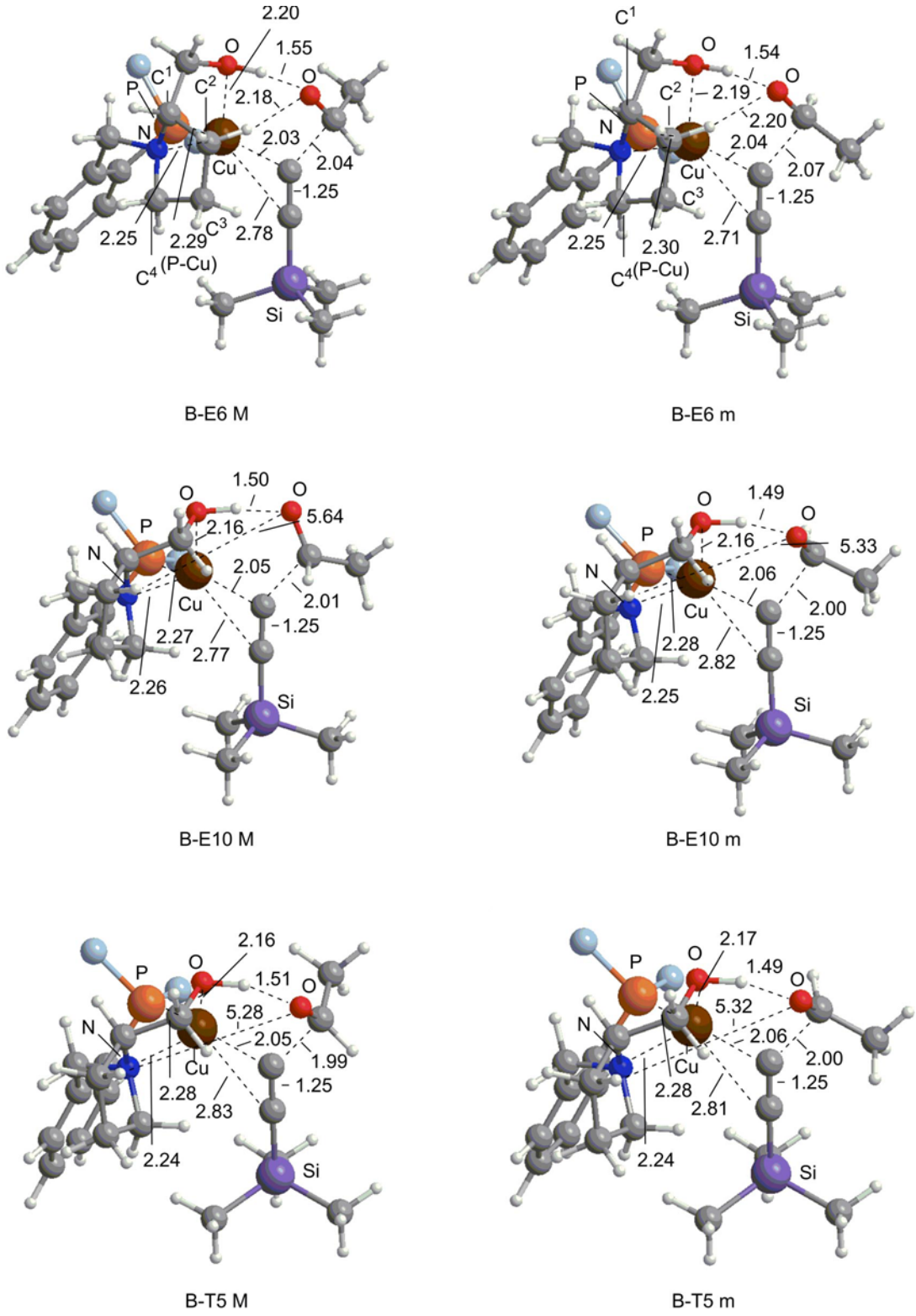

Figure 9. D structures of six-centered TSs for Model-1a optimized at the B3LYP/B0 level. Phenyl groups are shown as light-blue balls for clarity. Atomic distances are shown in Å.

Table 7. Total electric energies (*E*) and Gibbs free energies (*G*) for Model-1a (B3LYP/B0//B3LYP/B0) [A.U.]

	E (M)	*E* (m)	*G* (M)	*G* (m)
A-E1	-2231.255873	-2231.255195	-2230.701171	-2230.700507
A-E2	To A-E10 M	To A-E10 m		
A-E3	To A-T2 M	To A-T2 m		
A-E4	To A-E8 M	To A-E10 m		
A-E5	To A-T2 M	To A-T2 m		
A-E6	To A-T10 M	To A-T10 m		
A-E7	To A-T2 M	To A-T2 m		
A-E8	To A-E10 M	To A-E6 m		
A-E9	To A-E10 M	To A-E10 m		
A-E10	-2231.254144	-2231.253960	-2230.700435	-2230.699170
A-T1	To A-E6 M	To A-E6 m		
A-T2	-2231.252655	-2231.252337	-2230.697298	-2230.698186
A-T3	To A-E6 M	To A-E6 m		
A-T4	To A-E6 M	To A-E6 m		
A-T5	To A-E6 M	To A-E6 m		
A-T6	To A-E6 M	To A-E6 m		
A-T7	To A-E10 M	To A-E6 m		
A-T8	To A-E6 M	To A-E6 m		
A-T9	To A-E6 M	To A-E6 m		
A-T10	**-2231.258452**	**-2231.258560**	**-2230.702257**	**-2230.702792**
B-E1	To B-T5 M	To B-T5 m		
B-E2	To B-T5 M	To B-T5 m		
B-E3	To B-T5 M	To B-E10 m		
B-E4	-2231.254157	-2231.253337	-2230.699659	-2230.698375
B-E5	To B-T5 M	To B-E10 m		
B-E6	**-2231.263286**	**-2231.262926**	**-2230.706219**	**-2230.706702**
B-E7	To B-T5 M	To B-T5 m		
B-E8	To B-T5 M	To B-E10 m		
B-E9	To B-T5 M	To B-E10 m		
B-E10	-2231.255184	-2231.256373	-2230.701190	-2230.702070
B-T1	To B-T5 M	To B-T5 m		
B-T2	To B-T5 M	To B-T5 m		
B-T3	To B-T5 M	To B-E6 m		
B-T4	To B-T5 M	To B-E4 m		
B-T5	-2231.256954	-2231.256407	-2230.701519	-2230.701285
B-T6	To B-T5 M	To B-T5 m		
B-T7	To B-E6 M	To B-E6 m		

B-T8	To B-E10 M	To B-T5 m
B-T9	To B-E10 M	To B-E10 m
B-T10	To B-T5 M	To B-T5 m

Table 8. Standard Gibbs energies *DG* relative to that of the most stable TS B-E6 m and abundance ratios for Model-1a at the B3LYP-D(PCM, *t*-BuOH)/BI//B3LYP/B0 level in kJ/mol.

	DG (M)	*DG* (m)	Abundance ratio[%]	
			M	m
A-E1	22.1	27.5	0.0	0.0
A-E10	27.9	27.8	0.0	0.0
A-T2	31.4	31.3	0.0	0.0
A-T10	**13.0**	**13.9**	**0.3**	**0.2**
B-E4	27.9	29.8	0.0	0.0
B-E6	**0.1**	**0.0**	**48.4**	**51.0**
B-E10	21.4	19.6	0.0	0.0
B-T5	16.0	20.2	0.1	0.0
Total			**48.7**	**51.3**

As mentioned in the main text, further geometry optimizations were performed at the B3LYP level with larger B1 basis set. At the higher B3LYP-D(PCM, *t*-BuOH)/BII//B3LYP/BI level, the A-T10 and B-E6 conformers were selected and examined. The geometries optimized at the B3LYP/BI level are similar to the B3LYP/B0-optimized structures (Figure 10). An enantiomeric ratio predicted at this level is 57.4:42.6 (Table 9).

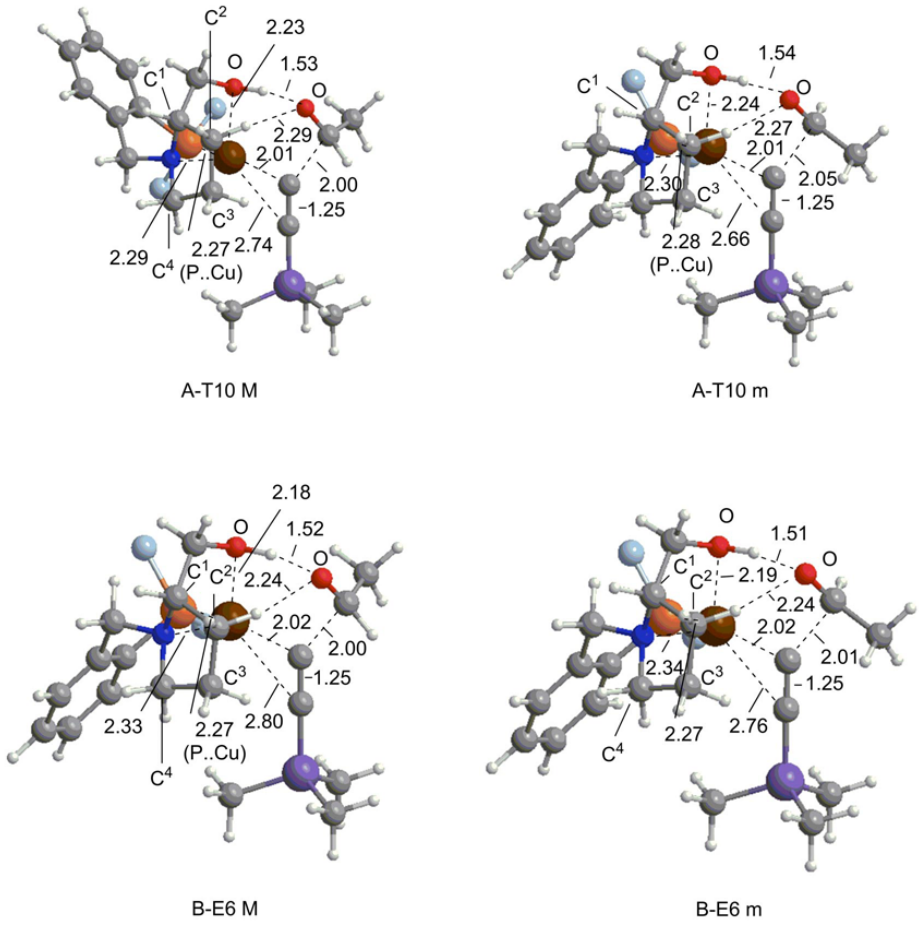

Figure 10. Structures of four most stable six-centered TSs (Model-1a) with A-T10 and B-E6 conformation (B3LYP/BI). Phenyl groups are shown as right-blue balls for clarity. Cu, P, N, Si atoms are shown in brown, orange, blue, and purple, respectively. Atomic distances are shown in Å. The sign "1" after the sign for conformation (e.g. B-E6) means Model-1.

Table 9. Standard Gibbs energies *DG* relative to that of the most stable TS B-E6 m and abundance ratios for Model-1a at the B3LYP-D(PCM, *t*BuOH)/BII//B3LYP/BI level in kJ/mol.

	DG (M)	*DG* (m)	Abundance ratio[%]	
			M	m
A-T10	6.1	7.9	4.6	2.2
B-E6	**0.0**	**0.7**	**52.8**	**40.4**
Total			**57.4**	**42.6**

Localized Molecular Orbital Analyses for Model-1a

In TS B-E6 M (Figure 10), the Cu-C^{a} distance of 2.02 Å is shorter than the Cu-C^{b1} distance of 2.80 Å. To examine the nature of bonding, localized molecular orbital analyses[37] were carried out. As shown in Figure 11, not only donation from the C^{a}-C^{b1} p-orbital to a copper vacant orbital (Figure 11a), but also back-donation from a Cu d orbital to the C^{a}-C^{b1} p*-orbital (Figure 11b) were observed. In this back-donation interaction, the Cu d orbital interacts mostly with the C^{a} orbital rather than with the C^{b1} orbital.

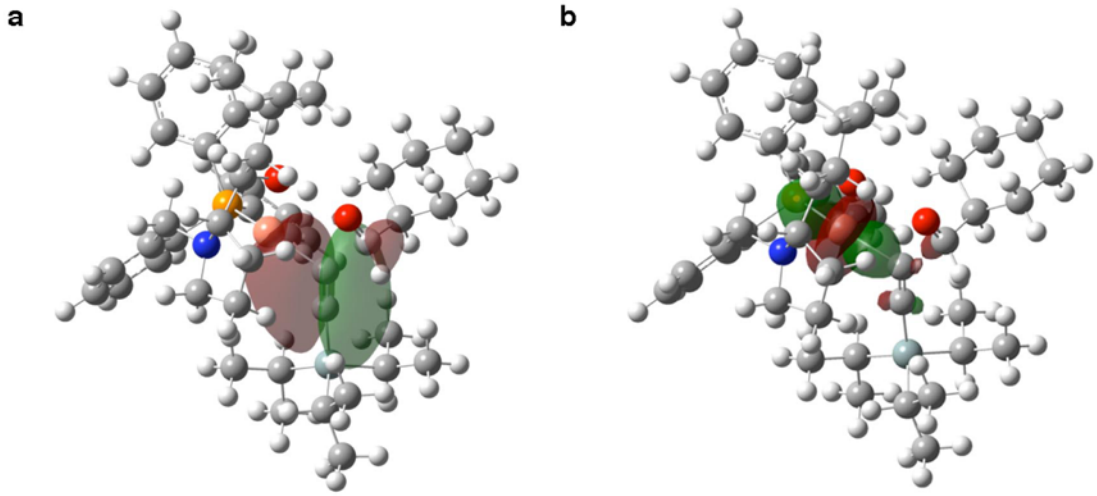

Figure 11. Two representative localized MOs of the six-centered TS B-E6 M for Model-1a (B3LYP/BI).

Reaction Pathways through TS B-E6 for Model-1a

The intrinsic reaction coordinate (IRC) analyses[38-43] were performed from the most stable structures TSs B-E6 M and B-E6 m toward precursor complexes (PCCs) and alkynylated alcohol intermediates (PDCs). The obtained structures were subjected to further geometry optimization at the B3LYP/BI level. In the precursor complexes PCC B-E6 M and PCC B-E6 m, the Cu-C^{a}-C^{b1} angles of 177° and 176°, respectively, indicates an alkynylcopper character in the precursor complexes (Figure 12). The activation Gibbs energy for M of 72.9 kJ/mol at the B3LYP/BII//B3LYP/BI level is reasonable for the reaction to proceed at room temperature.

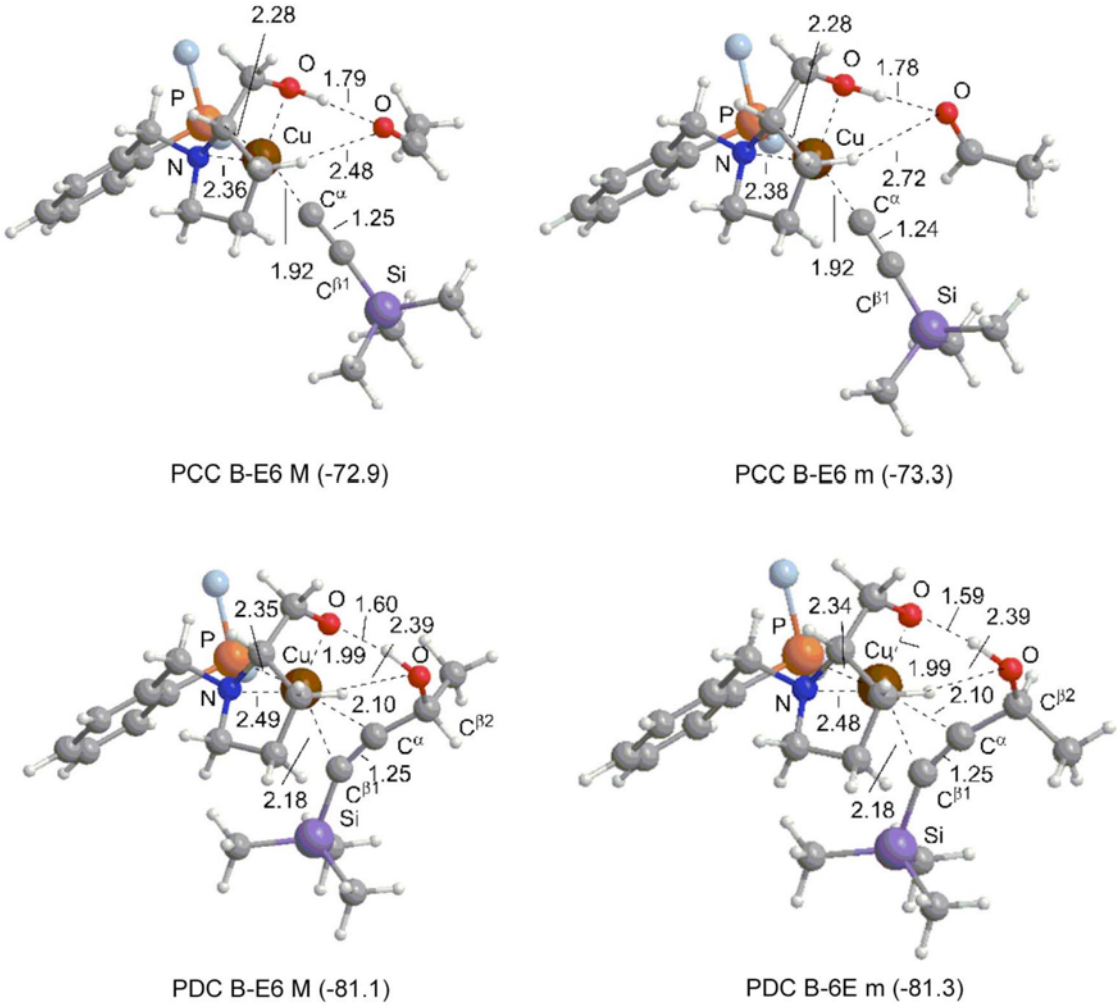

Figure 12. Structures of B-E6 conformers of precursor and product complexes for Model-1a (B3LYP/BI). The Gibbs energies in kJ/mol are relative to TS B-E6 M. Phenyl groups are shown as right-blue balls for clarity. Atomic distances are shown in Å.

Model-1f TSs (Four-centered TSs).

Four-centered transition states for Model-1a, which involve coordination of the carbonyl oxygen to the copper atom instead of the OH proton of the ligand in the six-centered TS were also examined. These TSs are denoted as "Model-1f", in which "f" means four-centered TSs. B-E6-type conformations for the copper N,P-chelate ring and the pyrrolidine ring were adopted. Three types of the 4-centered TS models (Figure 13), which differ in the orientation of alcohol moiety of the ligand (-CH(OH)-R^1), were subjected to geometry optimization at the B3LYP/B0 level to afford four TS structures (Figure 14). The other two TSs (B-E6 1f-3 M and B-E6 1f-3 m) led to the six-centered TSs B-E6 (M and m). The energies of the optimized structures are 60.8 kJ/mol higher than that of the six-centered TS B-E6 M, suggesting that the reaction prefers to proceed through six-centered TSs (Table 10).

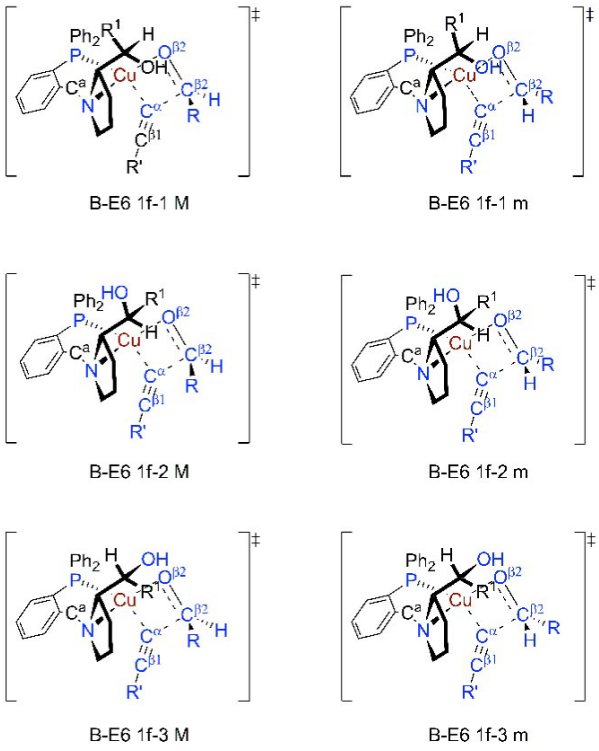

Figure 13. Four-centered TSs (Model-1f). The 6-31G* basis set is used for atoms and groups in blue, TZVP basis set used for Cu atom, and the 3-21G basis set used for the other atoms.

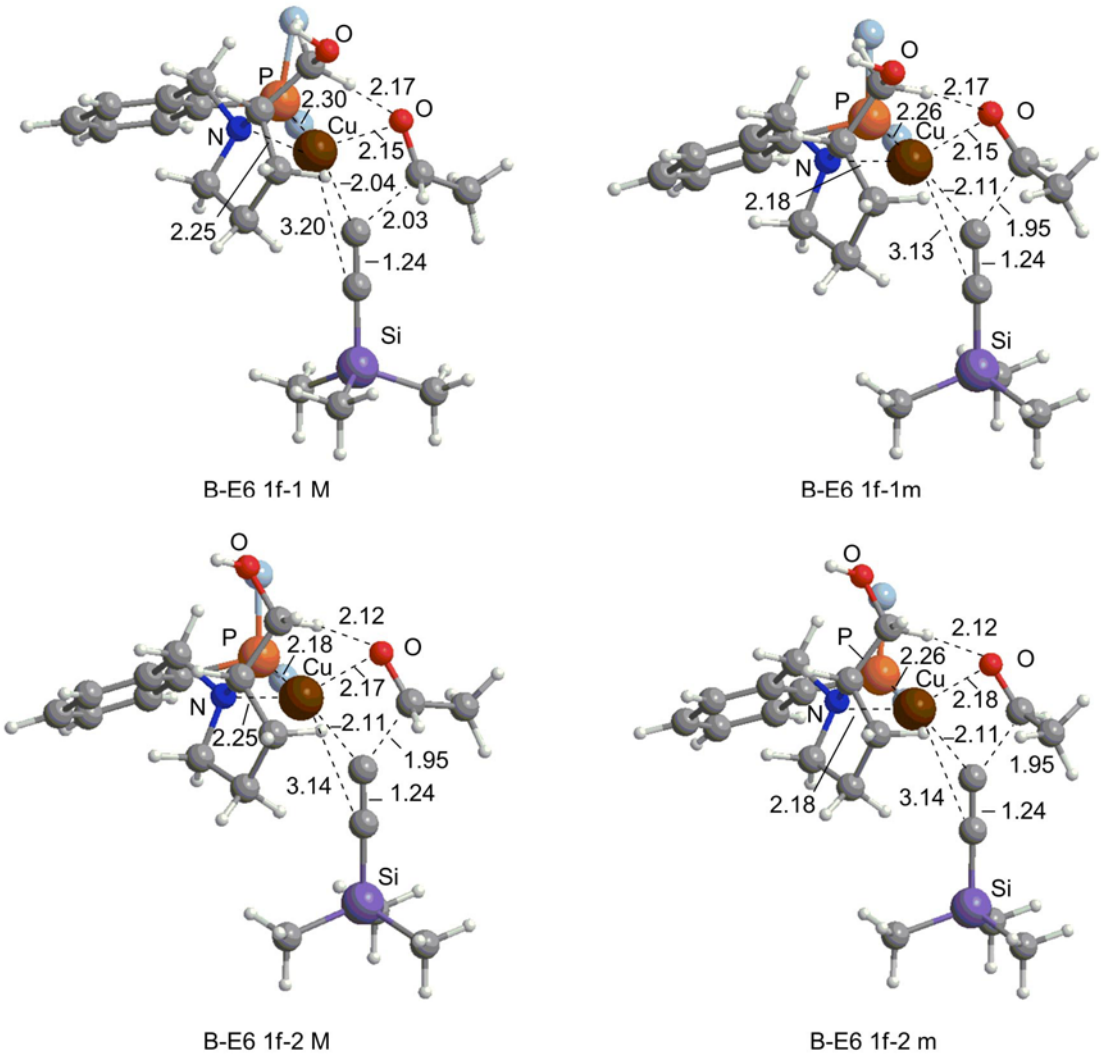

Figure 14. Structures of four-centered TSs of B-E6 conformer for Model-1f (B3LYP/B0). Phenyl groups are shown as right-blue balls for clarity. Atomic distances are shown in Å.

Table 10 Relative Gibbs energies *DG* to TS B-E6 M for Model-1f (B3LYP/B0) [kJ/mol]

	DG (M)	*DG* (m)
B-E6 1f-1	65.8	66.9
B-E6 1f-2	60.8	61.9
B-E6 1f-3	To B-E6 1 M	To B-E6 1 m

Model-1b (L1, *c*-HexCHO, HC≡CSi-*i*-Pr$_3$).

Model-1b, which consists of **L1**, *c*-HexCHO (**1a**), and a *i*-Pr$_3$Si(TIPS)-substituted acetylide moiety (**2a**–H) was examined. For the conformation of *c*-HexCHO (**1a**), only one rotamer with respect to the C(C=O)–C(a) with a chair cyclohexane conformation was considered. For the Si-*i*-Pr$_3$ moiety, the most stable three conformations obtained by conformational analysis of HC≡CSi-*i*-Pr$_3$ at the Hartree-Fock (HF/6-31G*) level with Spartan '08 program[44] were adopted. 3D structures for Model-1a are shown in Figure 15 and relative Gibbs energies and abundance ratio are shown in Table 11. The enantiomeric ratio based on the Boltzmann distribution was calculated to be 74.9:25.1.

Table 11. Relative Gibbs energies *DG* and abundance ratios in canonical (Boltzmann) distribution from relative Gibbs energies of each TS for Model-1b (B3LYP-D(PCM)/BII//B3LYP/BI) [kJ/mol]

	DG		Abundance ratio[%]	
	M	m	M	m
B-E6 1b-1	0.4	3.1	27.9	9.5
B-E6 1b-2	0.0	5.8	**33.0**	3.1
B-E6 1b-3	2.1	2.4	14.0	**12.5**
Total			**74.9**	**25.1**

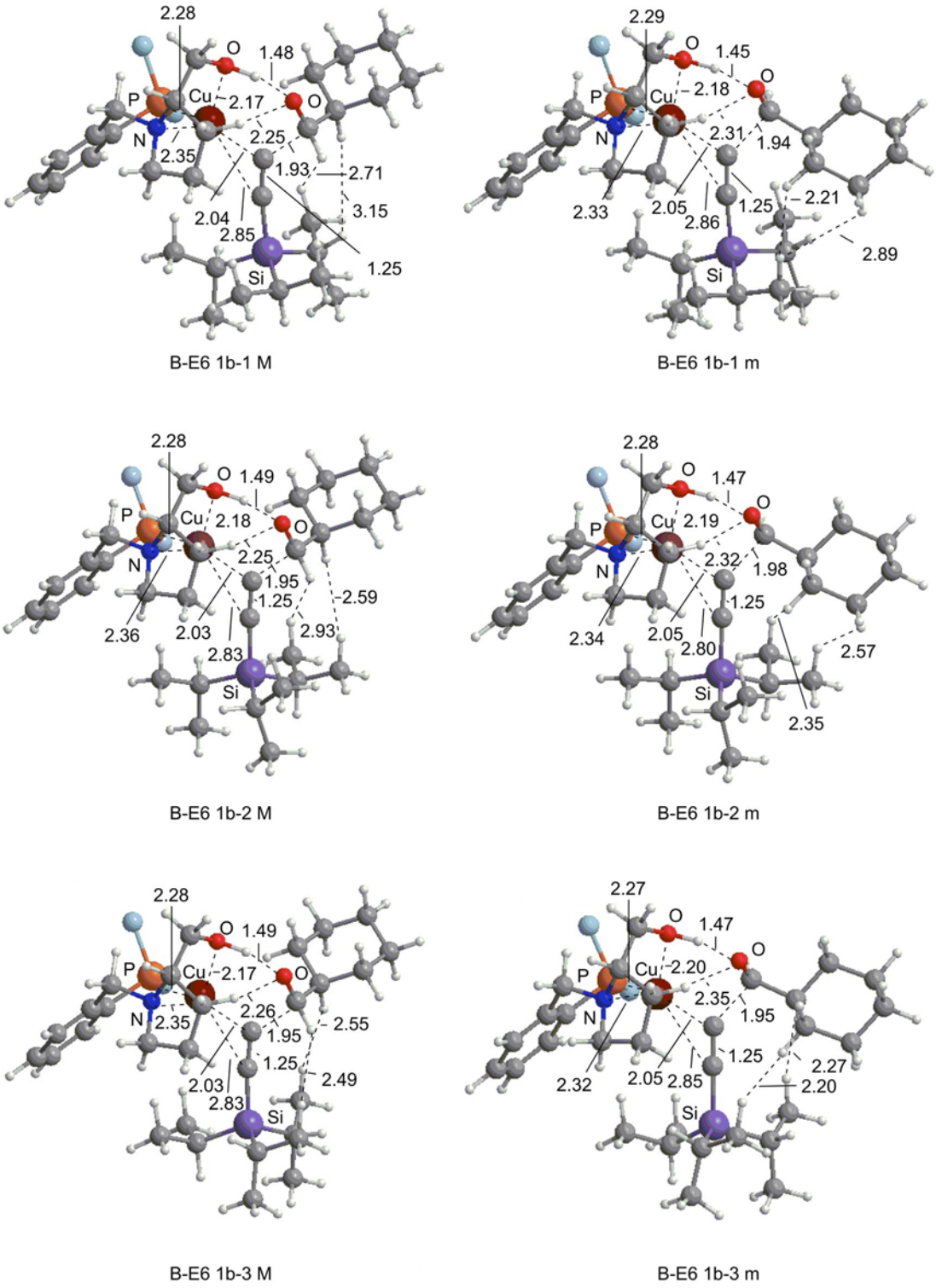

Figure 15. Structures of six-centered TSs for Model-1b with B-E6 conformation (B3LYP/B0). Phenyl groups are shown as right-blue balls for clarity. Cu, P, N, Si atoms are shown in brown, orange, blue, and purple, respectively. Atomic distances are shown in Å.

Model-2a (L8, MeCHO, HC≡CSiMe$_3$).

Model 2 consists of the chiral P, N, OH ligand with a neopentyl group (**L8** in the text), MeCHO, and a Me_3Si-substituted acetylide moiety. Three conformations of the **L8** side arm with different location of the *t*-Bu group were considered for TSs with the B-E6 conformation at the B3LYP/BI level. Optimized structures are shown in Figure 16. Gibbs free energies with abundance ratios based on canonical (Boltzmann) distribution are summarized in Table 12. Among the TSs, B-E6 2-2, which locates the *t*-Bu group to overhang the Cu-bound hydroxy group with van der Waals contacts with the nearest *t*-Bu–H atoms, is the most stable (60.9%) and B-E6 2-3 the second (3.0%). The predicted enantiomer ratio of the product is calculated to be 64.0:36.0.

Table 12. Relative Gibbs energies *DG* and abundance ratios in canonical (Boltzmann) distribution from relative Gibbs energies of each TS for Model-2a (B3LYP-D(PCM)/BII//B3LYP/BI) [kJ/mol]

	DG		Abundance ratio[%]	
	M	m	M	m
B-E6 2a-1	35.1	35.7	0.0	0.0
B-E6 2a-2	**0.0**	**1.2**	**60.9**	**34.7**
B-E6 2a-3	7.4	9.5	3.0	1.3
Total			**64.0**	**36.0**

(**Figure 16** in the next page)

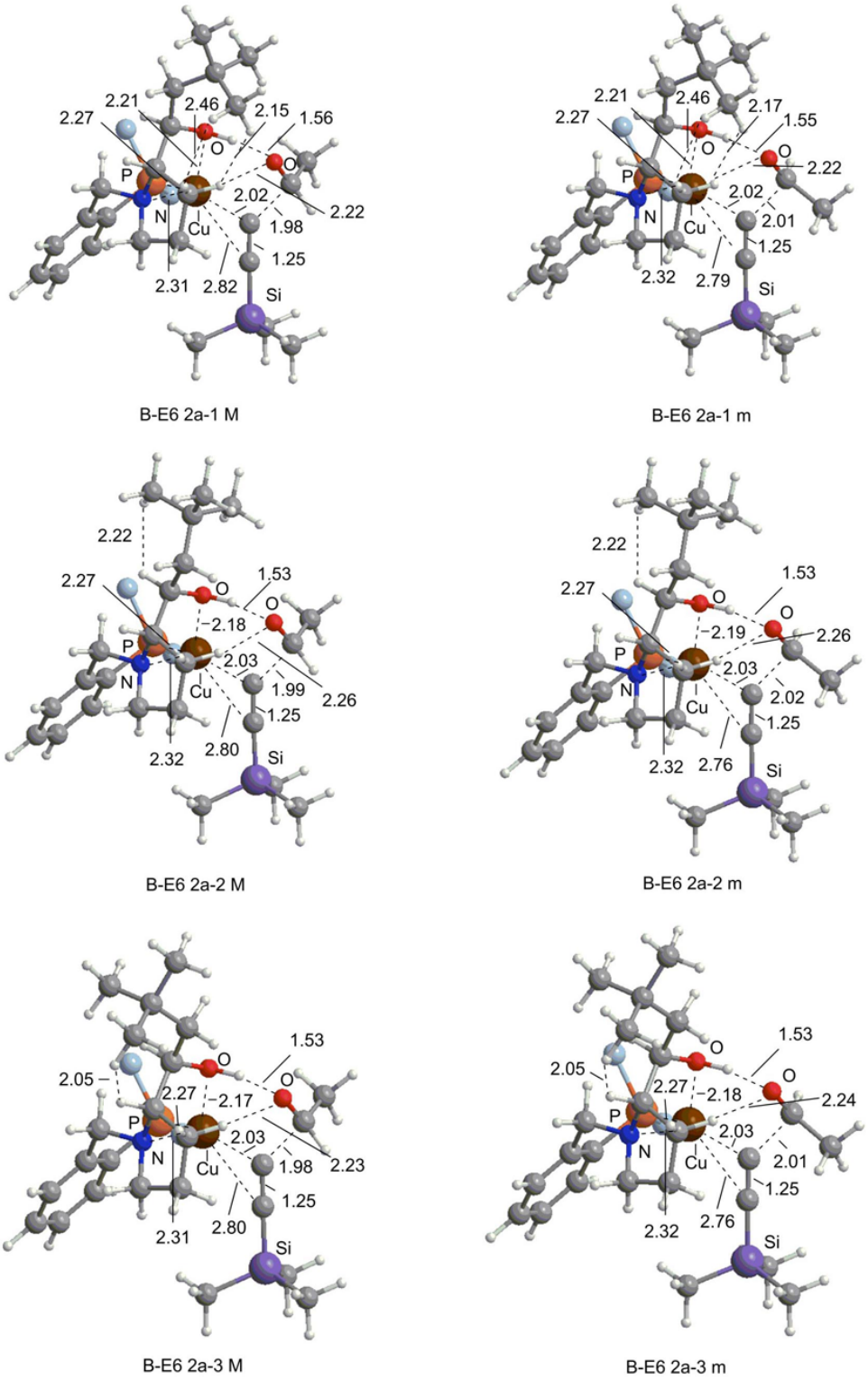

Figure 16. Structures of six-centered TSs of B-E6 conformer for Model-2a (B3LYP/BI). Phenyl groups are shown as right-blue balls for clarity. Atomic distances are shown in Å.

Model-2b (L8, *c*-HexCHO, HC≡CSi-*i*-Pr$_3$).

Model-2b is composed of **L8**, *c*-HexCHO (**1a**), and *i*-Pr$_3$Si(TIPS)-substituted acetylene (**2a**). Based on the examination with Model-1a, TSs with a B-E6-type conformations were examined for Model-2b at the B3LYP/BI level. For each of the alcoholic side arm of **L8**, the C≡CSi-*i*-Pr$_3$ group, and the *c*-HexCHO molecule, three conformations were considered, giving 27 conformers for each of M and m transition states (total of 54). The conformers are named as B-E6 2b-x-y-z M(m), where x, y, and z denote the conformers regarding the **L8** side arm, the C≡CSi-*i*-Pr$_3$ group, and the *c*-HexCHO molecule, respectively (x = 1–3, y = 1–3, z = 1–3). Optimized structures are shown in Figure 17 (Part 1–3). Gibbs free energies with abundance ratios based on canonical (Boltzmann) distribution are summarized in Table 13. Among the TSs, B-E6 2b-2-2-3 M is the most stable (21.8%) and B-E6 2b-2-1-3 M the second (20.5%), and these two are different in the conformation of the C≡CSi-*i*-Pr$_3$ group [Figure 17 (part 3)]. Among the TSs for the minor enantiomer, B-E6 2b-2-3-1 m is the most stable one (0.9%) [Figure 17 (part 1)]. The predicted enantiomer ratio of the product based on the Boltzmann distribution of the optimized transition states is calculated to be 96.9:3.1 (B3LYP-D(PCM)/BII).

Table 13. Relative Gibbs energies *DG* and abundance ratios in canonical (Boltzmann) distribution from relative Gibbs energies of each TS for Model-2b (B3LYP-D/BII//B3LYP/BI and B3LYP-D(PCM)/BII//B3LYP/BI levels) [kJ/mol]

	B3LYP-D/BII				B3LYP-D(PCM)/BII			
	DG [kJ/mol]		Abundance ratio [%]		*DG* [kJ/mol]		Abundance ratio [%]	
	M	m	M	m	M	m	M	m
B-E6 2b-1-1-1	to 2-2-1-1	40.2		0.0		41.0		0.0
B-E6 2b-1-2-1	to 2-2-2-1	46.9		0.0		46.3		0.0
B-E6 2b-1-3-1	to 2-2-3-1	43.5		0.0		43.2		0.0
B-E6 2b-2-1-1	4.8	7.7	3.5	1.1	3.1	9.0	6.2	0.6
B-E6 2b-2-2-1	3.3	8.2	6.3	0.9	1.8	9.3	10.6	0.5
B-E6 2b-2-3-1	5.4	8.7	2.7	0.7	3.4	**8.0**	5.6	**0.9**
B-E6 2b-3-1-1	16.3	17.9	0.0	0.0	12.5	16.0	0.1	0.0
B-E6 2b-3-2-1	16.7	20.9	0.0	0.0	12.9	18.9	0.1	0.0
B-E6 2b-3-3-1	16.7	20.4	0.0	0.0	12.5	16.7	0.1	0.0
B-E6 2b-1-1-2	37.5	43.5	0.0	0.0	38.2	43.3	0.0	0.0
B-E6 2b-1-2-2	36.0	47.1	0.0	0.0	37.1	45.9	0.0	0.0
B-E6 2b-1-3-2	37.8	47.8	0.0	0.0	38.6	48.2	0.0	0.0
B-E6 2b-2-1-2	2.1	10.7	10.2	0.3	2.3	10.5	8.6	0.3
B-E6 2b-2-2-2	0.9	12.8	16.4	0.1	1.4	11.7	12.6	0.2
B-E6 2b-2-3-2	4.5	15.6	3.9	0.0	4.5	16.2	3.6	0.0
B-E6 2b-3-1-2	15.4	20.9	0.0	0.0	12.7	17.9	0.1	0.0
B-E6	14.6	24.7	0.1	0.0	12.2	21.0	0.2	0.0

2b-3-2-2 B-E6 2b-3-3-2	17.5	25.7	0.0	0.0	14.8	23.5	0.1	0.0
B-E6 2b-1-1-3	37.2	to 2-2-1-3	0.0		38.2		0.0	
B-E6 2b-1-2-3	35.8	to 2-2-2-3	0.0		36.8		0.0	
B-E6 2b-1-3-3	37.5	to 2-2-3-3	0.0		38.3		0.0	
B-E6 2b-2-1-3	0.0	11.0	23.5	0.3	**0.0**	10.2	**21.8**	0.4
B-E6 2b-2-2-3	0.0	15.4	23.7	0.0	0.2	15.9	20.5	0.0
B-E6 2b-2-3-3	3.5	15.4	5.7	0.0	3.3	14.1	5.7	0.1
B-E6 2b-3-1-3	12.4	20.6	0.2	0.0	9.7	16.8	0.4	0.0
B-E6 2b-3-2-3	12.6	25.3	0.1	0.0	10.2	23.2	0.4	0.0
B-E6 2b-3-3-3	15.3	23.4	0.1	0.0	12.3	19.2	0.2	0.0
Total	-	-	96.5	3.5	-	-	**96.9**	**3.1**

[**Figure 17.** (Parts 1–3) in the following pages]

Optimization of B-E6 2b-1-1-1 M led to B-E6 2b-2-1-1 M

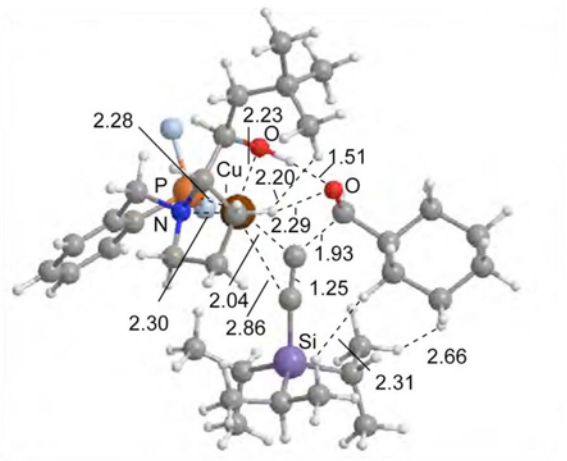

B-E6 2b-1-1-1 m

Optimization of B-E6 2b-1-2-1 M led to B-E6 2b-2-2-1 M

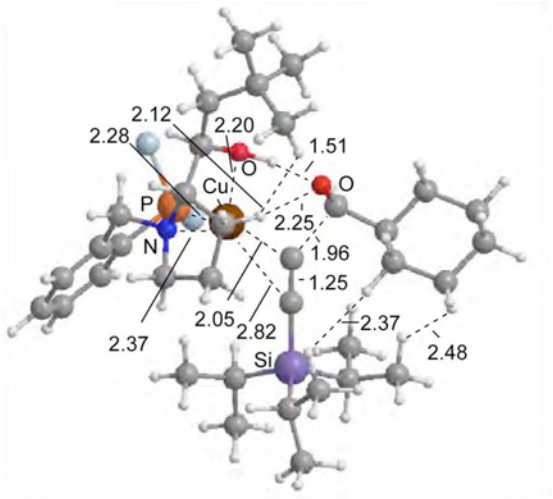

B-E6 2b-1-2-1 m

Optimization of B-E6 2b-1-3-1 M led to B-E6 2b-2-3-1 M

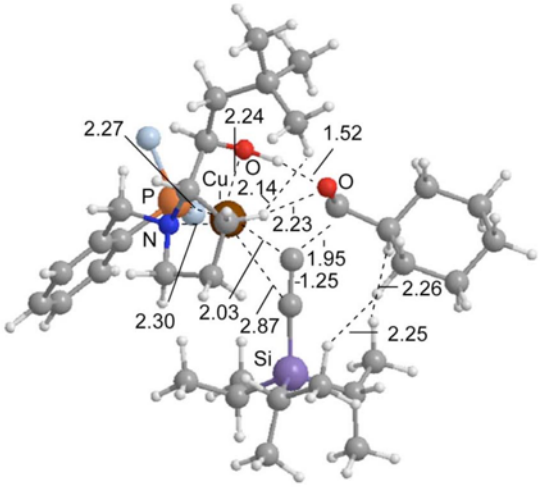

B-E6 2b-1-3-1 m

Figure 17. (Part 1) continued.

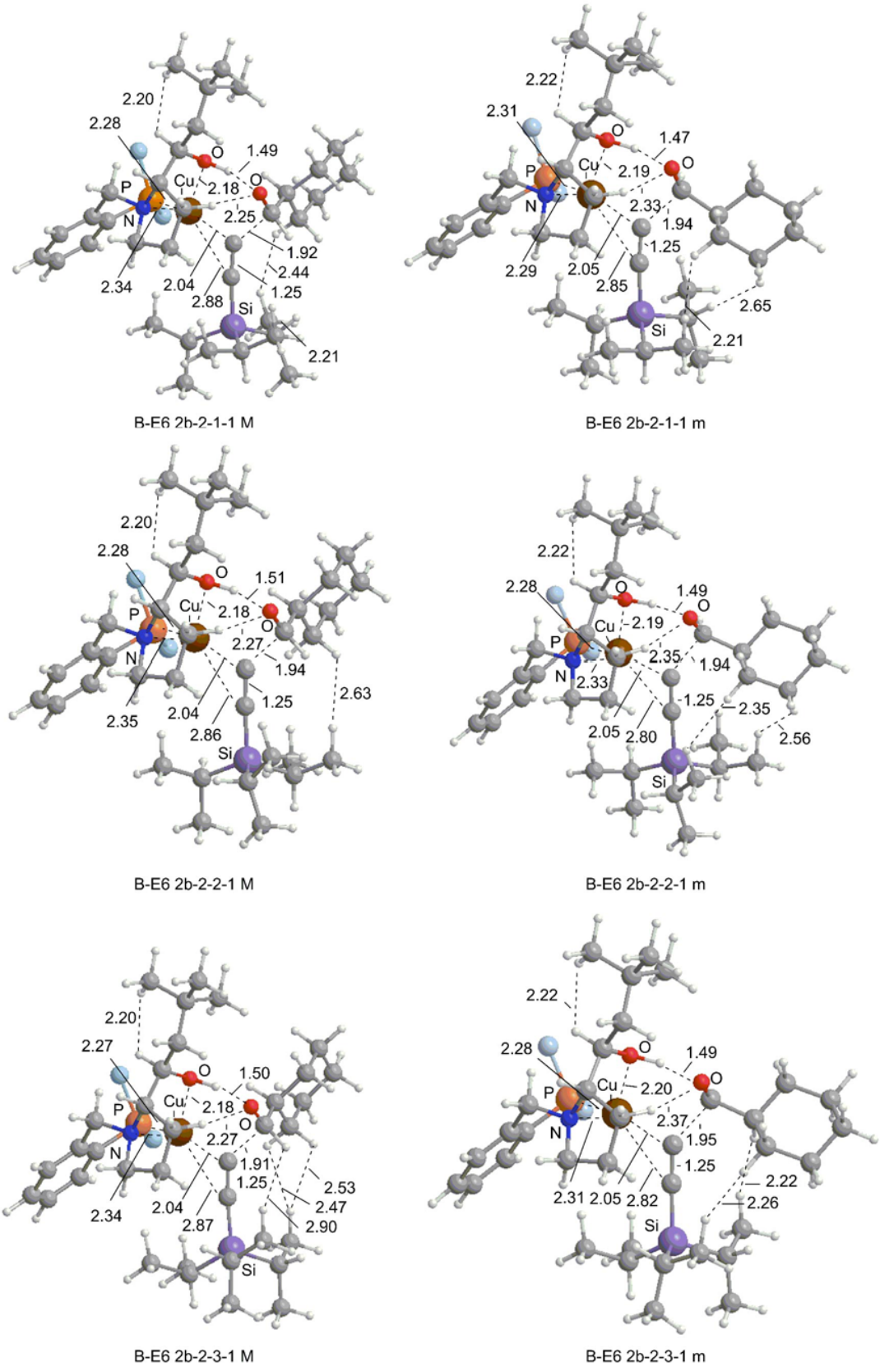

Figure 17. (Part 1) continued.

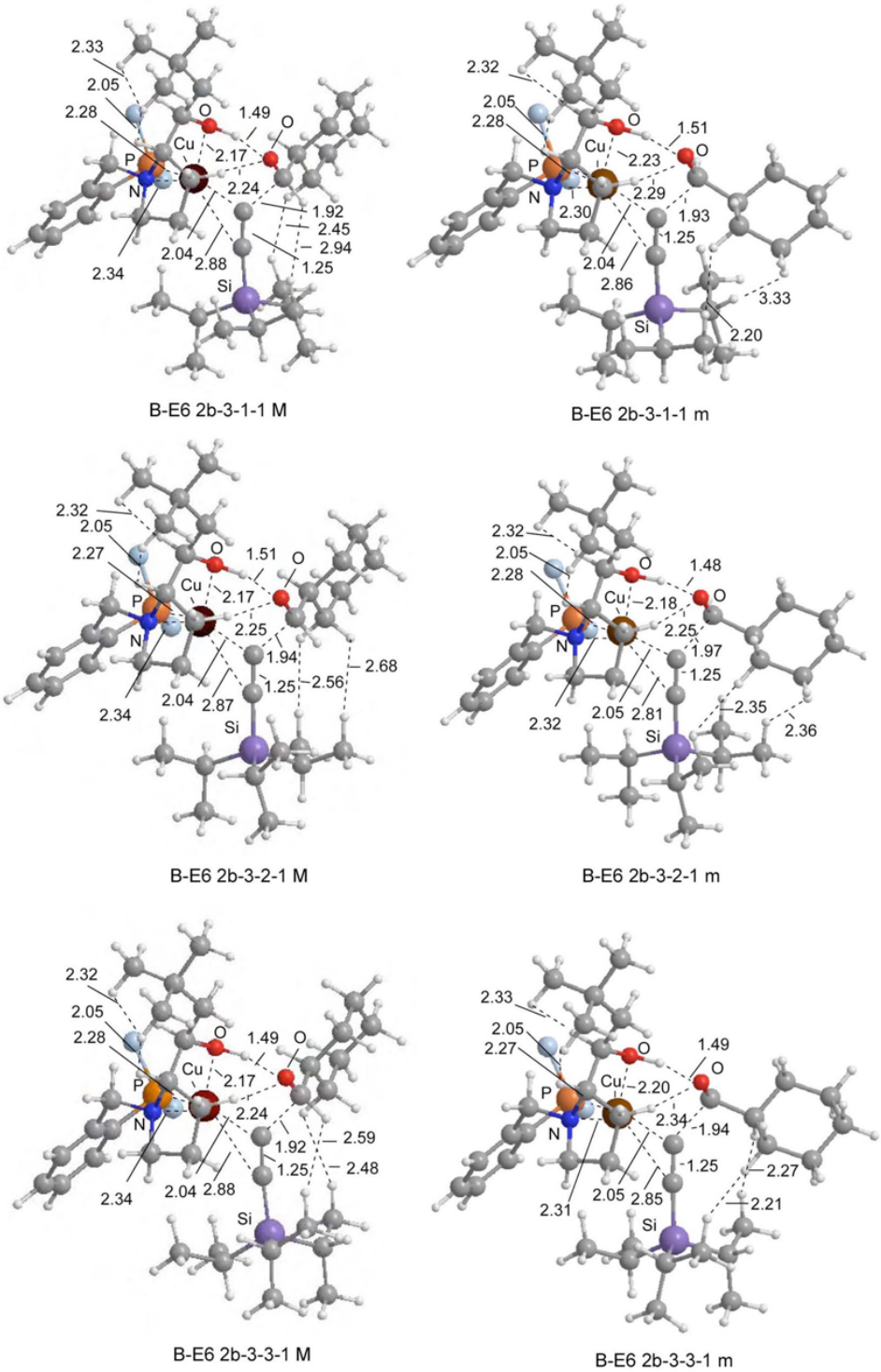

Figure 17. (Part 1) Structures of six-centered TSs for Model-2b with B-E6 2b-x-y-1 conformations (B3LYP/BI). Phenyl groups are shown as right-blue balls for clarity. Cu, P, N, Si atoms are shown in brown, orange, blue, and purple, respectively. Atomic distances are shown in Å.

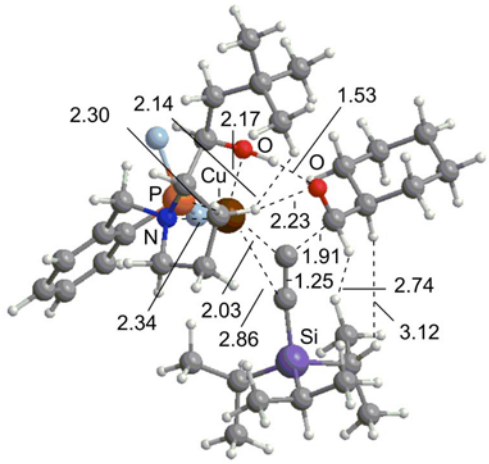

B-E6 2b-1-1-2 M

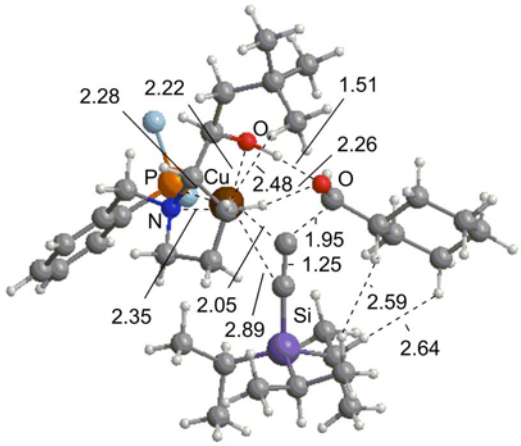

B-E6 2b-1-1-2 m

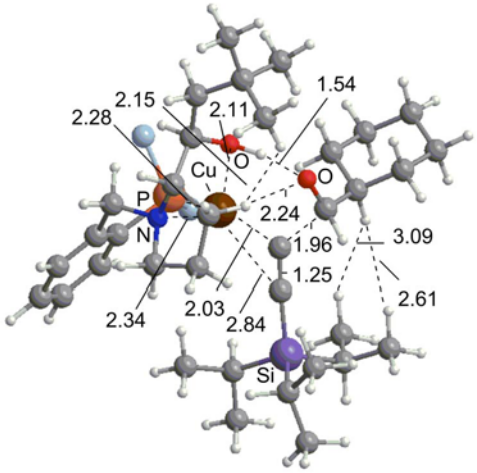

B-E6 2b-1-2-2 M

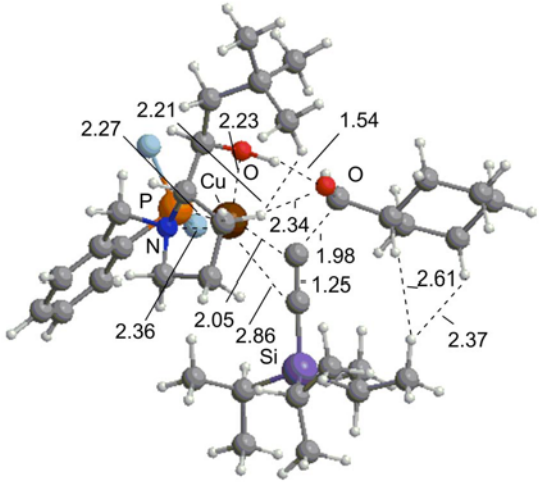

B-E6 2b-1-2-2 m

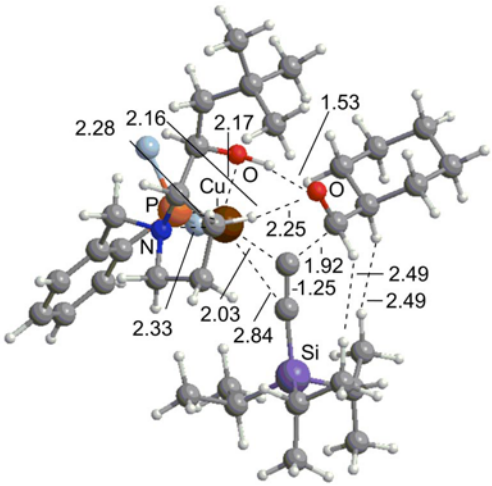

B-E6 2b-1-3-2 M

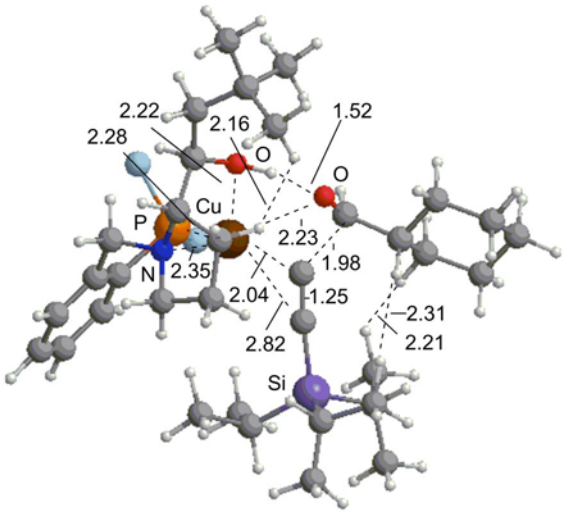

B-E6 2b-1-3-2 m

Figure 17. (Part 2) continued.

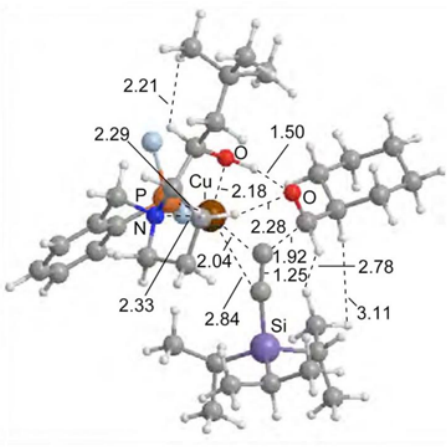

B-E6 2b-2-1-2 M

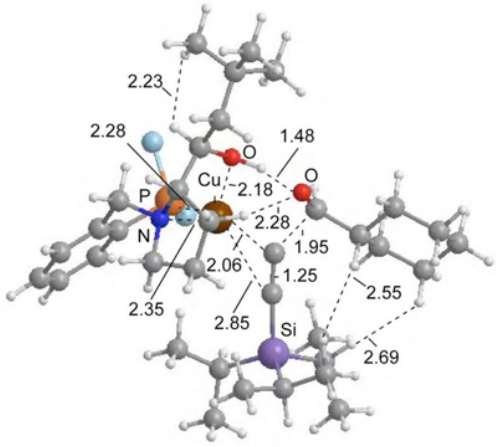

B-E6 2b-2-1-2 m

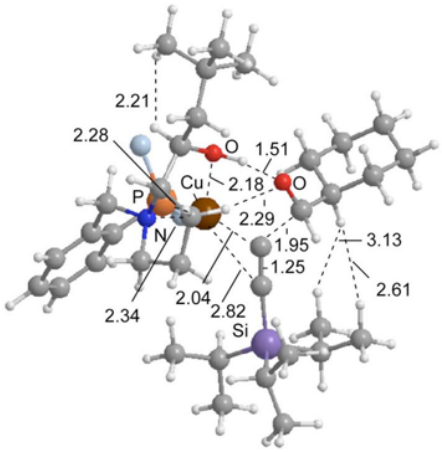

B-E6 2b-2-2-2 M

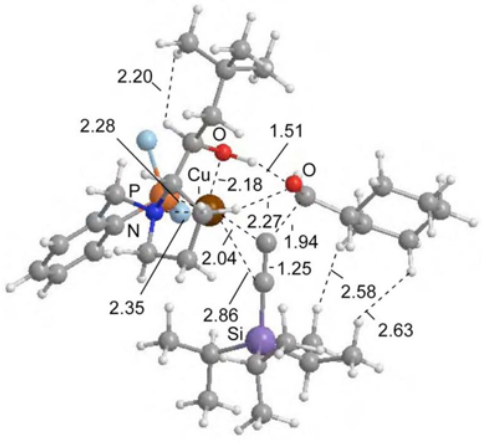

B-E6 2b-2-2-2 m

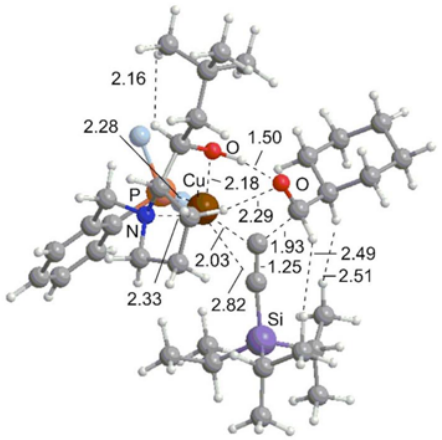

B-E6 2b-2-3-2 M

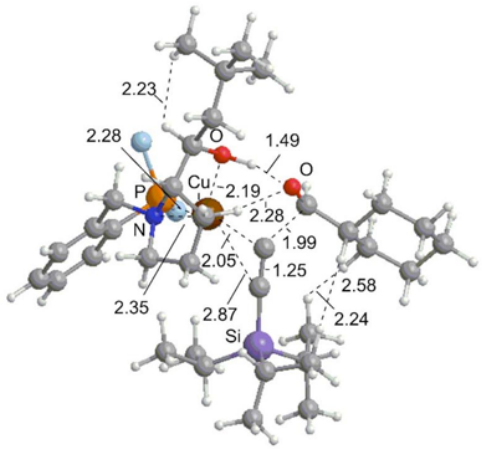

B-E6 2b-2-3-2 m

Figure 17. (Part 2) continued.

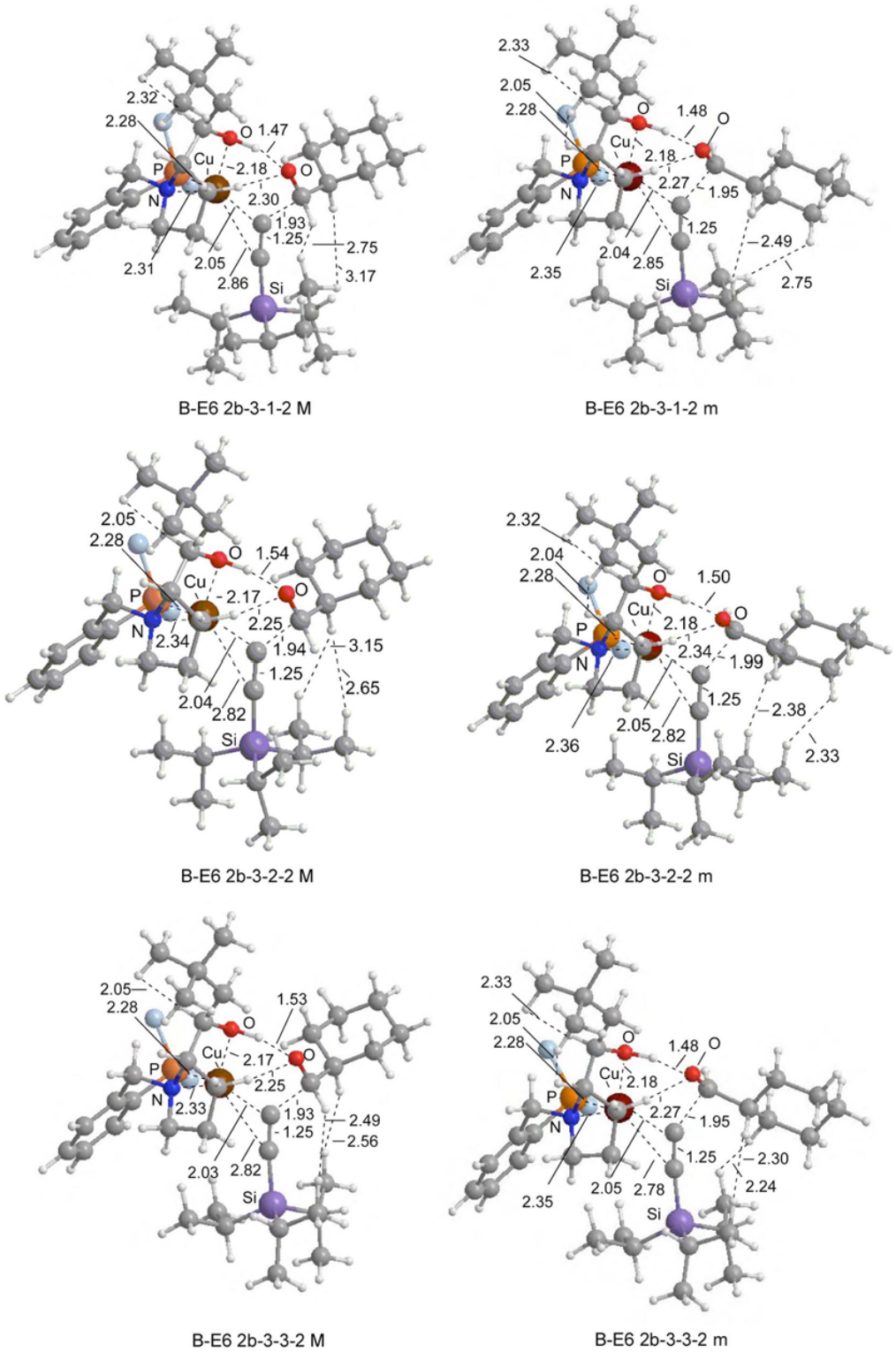

Figure 17 (Part 2). Structures of six-centered TSs for Model-2b with B-E6 2b-x-y-2 conformations (B3LYP/BI). Phenyl groups are shown as right-blue balls for clarity. Cu, P, N, Si atoms are shown in brown, orange, blue, and purple, respectively. Atomic distances are shown in Å.

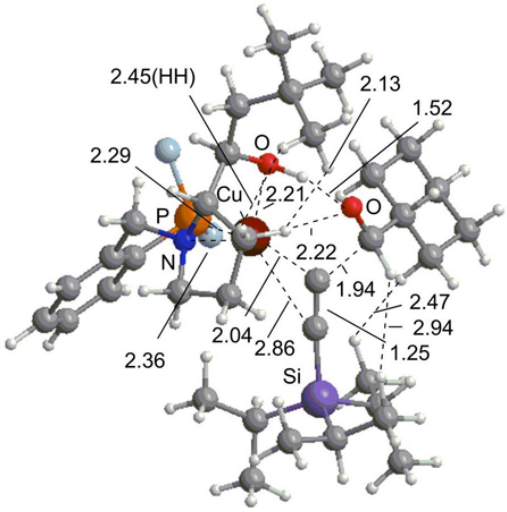

B-E6 2b-1-1-3 M

Optimization of B-E6 2b-1-1-3 m led to B-E6 2b-2-1-3 m

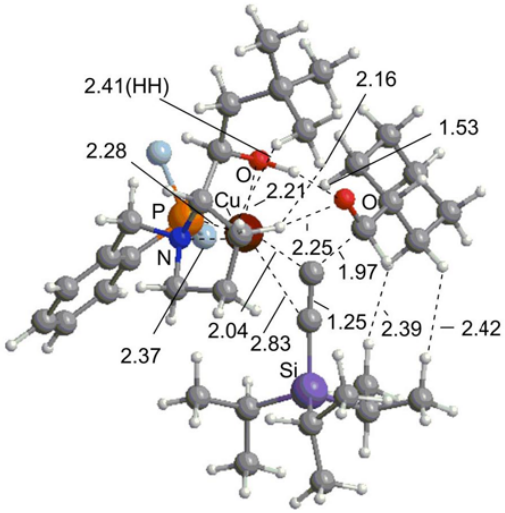

B-E6 2b-1-2-3 M

Optimization of B-E6 2b-1-2-3 m led to B-E6 2b-2-2-3 m

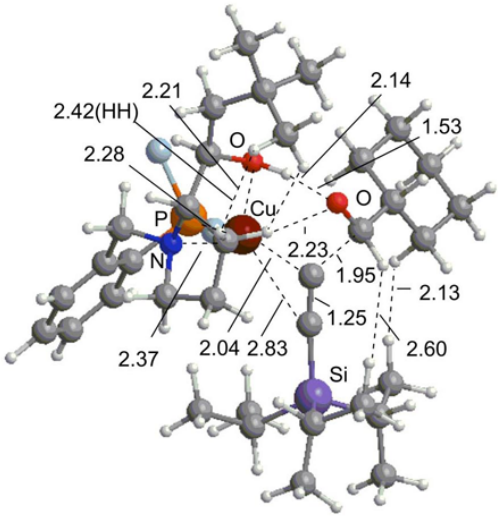

B-E6 2b-1-3-3 M

Optimization of B-E6 2b-1-3-3 m led to B-E6 2b-2-3-3 m

Figure 17. (Part 3) continued.

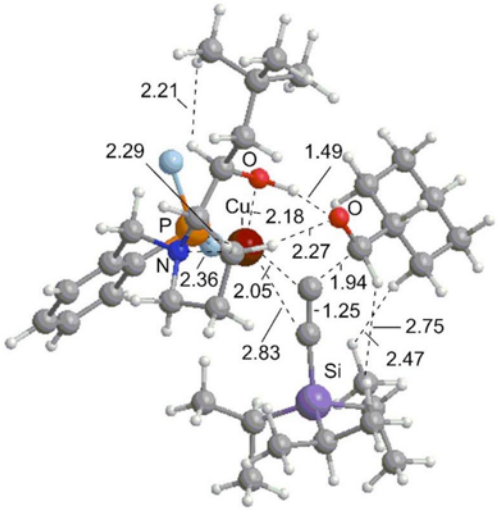

B-E6 2b-2-1-3 M

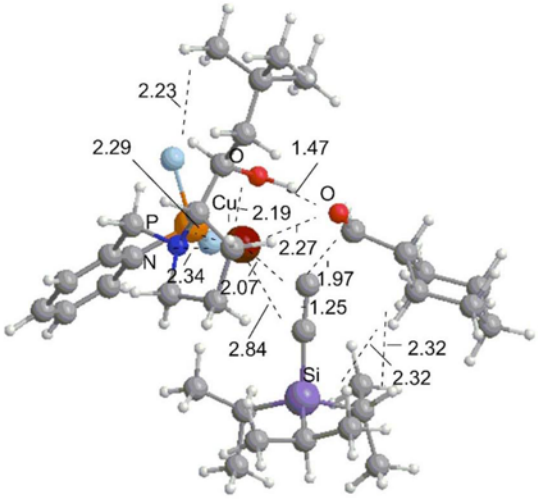

B-E6 2b-2-1-3 m

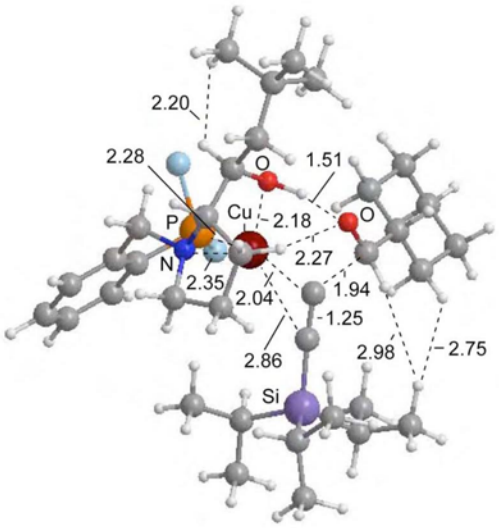

B-E6 2b-2-2-3 M

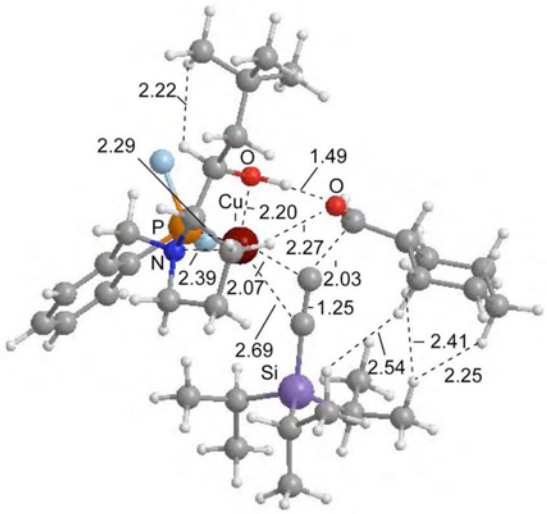

B-E6 2b-2-2-3 m

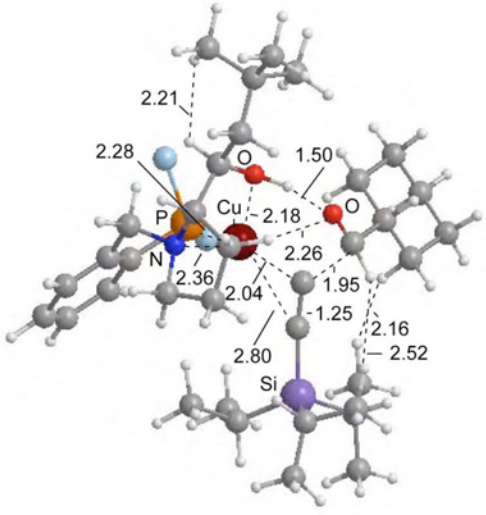

B-E6 2b-2-3-3 M

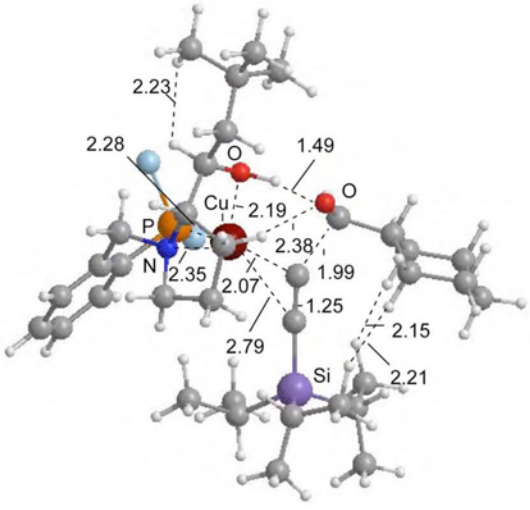

B-E6 2b-2-3-3 m

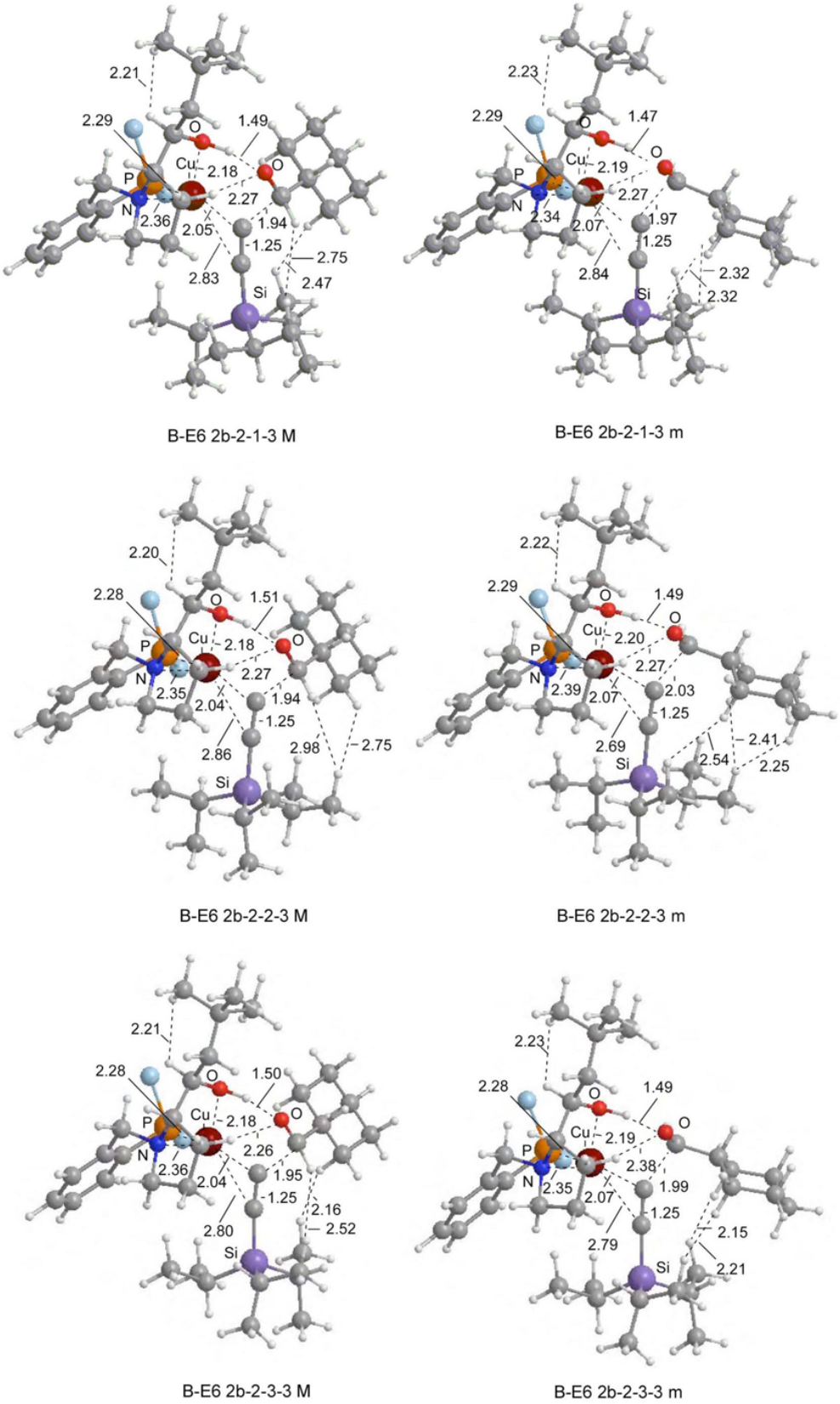

Figure 17. (Part 3) continued.

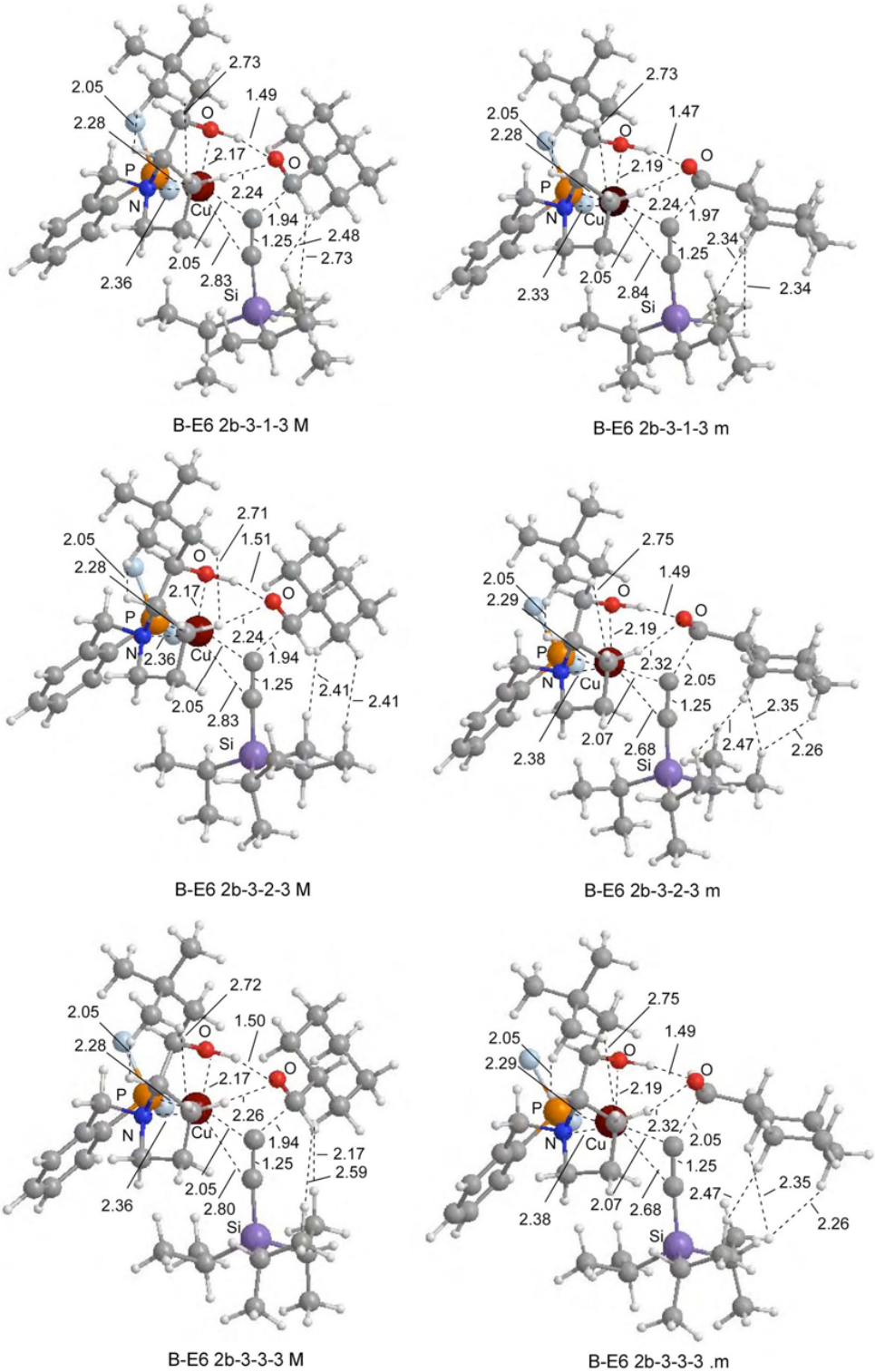

Figure 17. (Part 3) Structures of six-centered TSs for Model-2b with B-E6 2b-x-y-3 conformations (B3LYP/BI). Phenyl groups are shown as right-blue balls for clarity. Cu, P, N, Si atoms are shown in brown, orange, blue, and purple, respectively. Atomic distances are shown in Å.

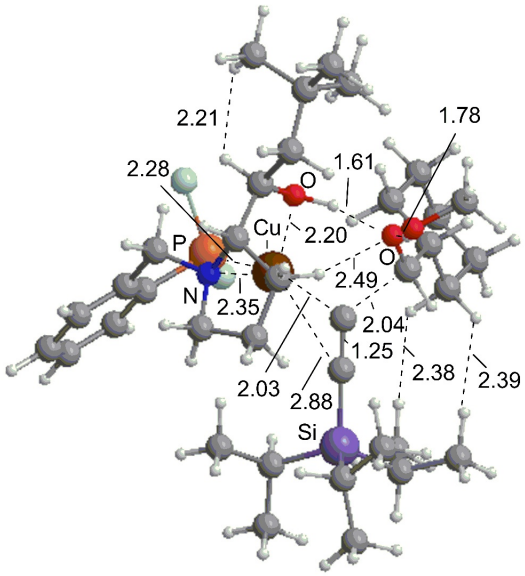

B-E6 2b-2-2-3-3-MeOH M

Figure 18. Structures of six-centered TSs for Model-**2b** with a MeOH molecule with B-E6 2b-2-2-3-3 M conformation (B3LYP/BI). Phenyl groups are shown as right-blue balls for clarity. Cu, P, N, Si atoms are shown in brown, orange, blue, and purple, respectively. Atomic distances are shown in Å.

5. Experimental Section

Instrumentation and Chemicals for Experimental Studies.

NMR spectra were recorded on a Varian Gemini 2000 spectrometer, operating at 300 MHz for ^{1}H NMR and 75.4 MHz for ^{13}C NMR, and 121.4 MHz for ^{31}P NMR, and on a JEOL ECA-600, operating at 600 MHz for ^{1}H NMR. Chemical shift values for ^{1}H and ^{13}C are referenced to Me_4Si and the residual solvent resonances, respectively. Chemical shifts are reported in δ ppm. Mass spectra were obtained with Thermo Fisher Scientific Exactive, JEOL JMS-T100LP or JEOL JMS-700TZ at the Instrumental Analysis Division, Equipment Management Center, Creative Research Institution, Hokkaido University. Elemental analysis was performed at the Instrumental Analysis Division, Equipment Management Center, Creative Research Institution, Hokkaido University. Melting point was measured on a Yanaco MP-500D apparatus. HPLC analyses were conducted on a HITACHI ELITE LaChrom system with a HITACHI L-2455 diode array detector. TLC analyses were performed on commercial glass plates bearing 0.25-mm layer of Merck Silica gel $60F_{254}$. Silica gel (Kanto Chemical Co., Silica gel 60 N, spherical, neutral).

All manipulations were carried out under argon or nitrogen. Unless otherwise noted, materials obtained from commercial suppliers were used without further purification. All solvents for catalytic reactions were degassed *via* three freeze-pump-thaw cycles before use. *t*-BuOH was purchased from Junsei Chem Co., Inc. and other solvents were purchased from Kanto Chem Co., Inc., and used without further purification. Cu(O-*t*-Bu) was prepared according to the reported procedure[45] and was sublimated before use. Aldehydes and alkynes were obtained from commercial suppliers. All aldehydes for catalytic reactions were distilled before use.

Preparation of Hydroxyaminophosphine Derivatives.

(*S*)-1-(2-Diphenylphosphinobenzoyl)-2-pyrrolidinecarboxylate Methyl Ester (4)

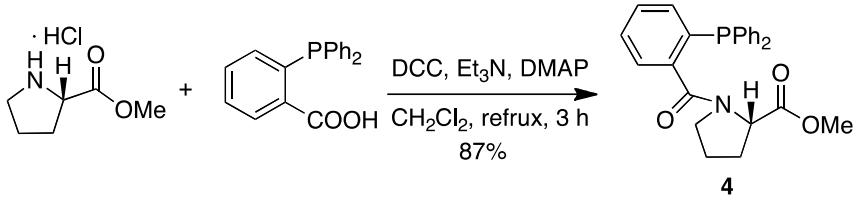

4

Triethylamine (3.58 mL, 25.5 mmol) was added dropwise to a solution of L-proline methyl ester hydrochloride (4.14 g, 25.0 mmol) in CH_2Cl_2 (50 mL) at room temperature. The resulting solution was stirred for 10 min. *o*-(Diphenylphosphino)benzoic acid (9.00 g, 25.0 mmol), DCC (5.16 g, 25.0 mmol) and DMAP (0.305 g, 2.50 mmol) were added, and the mixture was stirred at reflux for 3 h. The mixture was cooled to room temperature and filtered through a pad of celite. The filtrate was concentrated under reduced pressure. The crude product was purified by column chromatography on silica gel (hexane/EtOAc 50:50) to give **4** (9.10 g, 20.75 mmol) in 83% yield.

(*S*)-1-(2-Diphenylphosphinobenzyl)-2-pyrrolidinemethanol (L1)

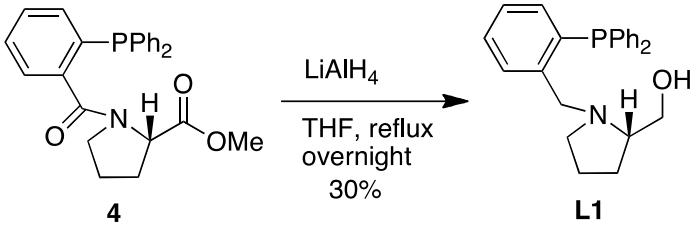

4 L1

A solution of **4** (2.07 g, 5.0 mmol) in THF (20 mL) was added dropwise to a solution of $LiAlH_4$ (0.78 g, 20.5 mmol) in THF (10 mL) at 0 ˚C. After being refluxed at overnight, the mixture was cooled to 0 °C and quenched by H_2O (0.78 mL), 15% NaOH aq (0.78 mL) and H_2O (2.34 mL) in this order. The mixture was filtered through a pad of celite and the solvent was removed under reduced pressure. The crude product was purified with column chromatography on silica gel (hexane/EtOAc = 80:20) to give **L1** (559 mg, 1.49 mmol) in 30% yield. **L1**: Oil. **^{1}H NMR** (300 MHz, C_6D_6) δ 0.78 (m, 1H), 1.17 (m, 1H), 1.49 (m, 1H), 1.65–1.86 (m, 2H), 2.24 (m, 1H), 2.39 (t, 1H, J = 8.1 Hz), 3.07 (d, 1H, J = 12.3 Hz), 3.48 (m, 1H), 3.63 (m, 1H), 3.90 (d, 1H , J = 11.4 Hz), 4.60 (d, 1H, J = 12.3 Hz), 6.92–7.21 (m, 10H), 7.25–7.30 (m, 2H), 7.35–7.41 (m, 2H). **^{13}C**

NMR (75.4 MHz, C_6D_6) δ 22.28, 26.68, 54.21, 59.04 (d, $J_{C\text{-}P}$ = 12.0 Hz), 62.09, 65.79, 128.53 (d, $J_{C\text{-}P}$ = 6.3 Hz), 128.67 (d, $J_{C\text{-}P}$ = 6.3 Hz), 128.68, 128.69, 129.16, 129.97 (d, $J_{C\text{-}P}$ = 6.9 Hz), 133.85 (d, $J_{C\text{-}P}$ = 19.5 Hz), 133.91 (d, $J_{C\text{-}P}$ = 18.9 Hz), 135.77 (d, $J_{C\text{-}P}$ = 1.8 Hz), 136.21 (d, $J_{C\text{-}P}$ = 12.6 Hz), 136.91 (d, $J_{C\text{-}P}$ = 5.1 Hz), 138.88 (d, $J_{C\text{-}P}$ = 9.3 Hz), 145.20 (d, $J_{C\text{-}P}$ = 24.0 Hz). **^{31}P NMR** (121.4 MHz, C_6D_6) δ –16.83. **$[\alpha]_D^{24}$** = –85.0 (c 0.90, $CHCl_3$). **HRMS-ESI** (m/z): $[M+H]^+$ calcd for $C_{24}H_{27}NOP$, 376.18303; found, 376.18215.

(α*R*, 2*S*)-α-(2,2-Dimetylpropynyl)-2-pyrrolidinemethanol (7)

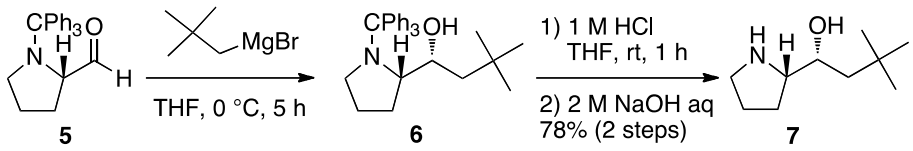

5 6 7

N-Tritylprolinal (**5**) was prepared according to the Chemla's procedure and consistent with the literature data.[13] Then, the stereocontrolled Grignard addition with *N*-tritylprolinal (**5**) (an acyclic Felkin–Anh mode), which was developed by Chemla and co-workers,[13] was applied to the reaction with neopentylmagnesium bromide. Thus, the Grignard reagent (1.0 M in THF, 47.8 mL, 47.8 mmol) was added to a solution of **5** (8.16 g, 23.9 mmol) in THF (50 mL) at 0 °C. After being stirred for 5 h, the mixture was quenched with a saturated aqueous NH_4Cl at 0 °C. The mixture was filtered through a pad of celite and the solvent was removed under reduced pressure. The obtained solid **6** was used for next step without any purification.

1M HCl (20 mL) was added to a solution of **6** (8.81g, 21.3 mmol) in THF (20 mL). After 1 h of vigorous stirring, the two phases were separated. The aqueous phase washed with Et_2O (2 × 20 mL). After 2M NaOH (20 mL) was added to the aqueous solution, the mixture was extracted with $CHCl_3$ (2 × 20 mL). The mixture was dried and concentrated *in vacuo* to afford the **7** (3.18 g, 18.6 mmol) in 78% yield (*vide infra* for determination of the relative configuration).

Determination of the Relative Configuration of 7. The amino alcohol **7** was converted to the cyclic carbamate **8** according to the Chemla's method.[13] The 1,2-*cis* relative configuration of **8** was confirmed by coupling constant and NOESY measurements. **8**: Oil. **^{1}H NMR** (600 MHz, $CDCl_3$) δ 0.99 (s, 9H), 1.43–1.51 (m, 2H), 1.67–1.74 (m, 2H), 1.80–1.88(m, 1H), 2.03–2.09 (m, 1H), 3.17–3.21 (m, 1H), 3.66 (dt,

1H, *J* = 11.7, 5.8 Hz), 3.73 (ddd, 1H, *J* = 11.4, 7.6, 5.1 Hz), 4.75 (ddd, 1H, *J* = 8.7, 7.6, 2.9 Hz). **^{13}C NMR** (75.4 MHz, $CDCl_3$) δ 24.74, 24.98, 29.68, 29.92, 43.91, 45.93, 64.46, 73.54, 162.46.

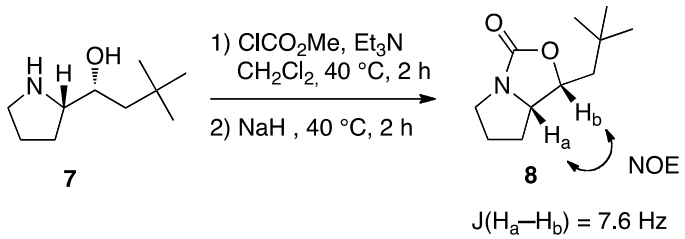

(α*R*,2*S*)-(−)-1-(2-Diphenylphosphinobenzyl)-α-(2,2-dimetylpropynyl)-2-pyrrolidine methanol (L8)

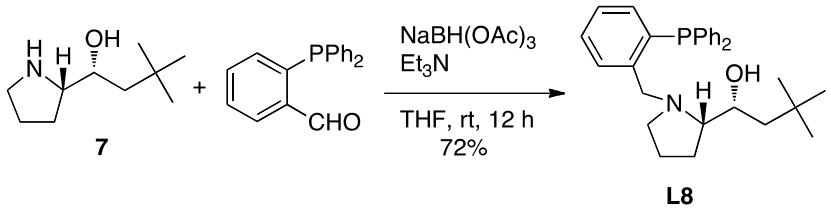

To a solution of **7** (2.50 g, 14.6 mmol) in THF (50 mL) was added 2-diphenylphosphinobenzaldehyde (3.94 g, 14.6 mmol), Et_3N (10.2 mL, 73.0 mmol) and $NaBH(OAc)_3$ (6.19 g, 29.2 mmol) at room temperature. The mixture was stirred at room temperature for 12 h. The mixture was quenched with H_2O. The aqueous layer was extracted with Et_2O several times, and the combined organic layer was dried over $MgSO_4$ and concentrated. The residue was purified by silica gel chromatography (hexane/EtOAc 93:7) to give **L8** (4.70 g, 10.5 mmol) in 72% yield. **L8**: White Solid. **Mp:** 113–114 °C. **^{1}H NMR** (300 MHz, $CDCl_3$) δ 0.75–1.01 (m, 1H), 0.95 (s, 9H), 1.10–1.15 (m, 1H), 1.33–1.42 (m, 2H), 1.51–1.78 (m, 2H), 1.93–2.02 (m, 1H), 2.17–2.22 (m, 1H), 2.49–2.54 (m. 1H), 3.28 (d, 1H, *J* = 3.3 Hz), 3.35 (brs, 1H), 3.94–3.98 (m, 1H), 4.41 (d, 1H, *J* = 3.3 Hz), 6.95–6.99 (m, 1H), 7.13–7.40 (m, 13H). **^{13}C NMR** (75.4 MHz, $CDCl_3$) δ 22.14, 23.03, 29.97, 30.18, 46.84, 54.10, 57.79 (d, $J_{C\text{-}P}$ = 13.7 Hz), 65.33, 70.49, 127.38, 128.38, 128.39 (d, $J_{C\text{-}P}$= 6.3 Hz), 128.46 (d, $J_{C\text{-}P}$= 7.4 Hz), 128.62, 128.92, 129.66 (d, $J_{C\text{-}P}$= 6.3 Hz) 133.59 (d, $J_{C\text{-}P}$ = 19.5 Hz), 133.67 (d, $J_{C\text{-}P}$ = 20.0 Hz), 134.82 (d, $J_{C\text{-}P}$= 1.7 Hz), 135.86 (d, $J_{C\text{-}P}$ = 13.7 Hz), 136.32 (d, $J_{C\text{-}P}$ = 7.4 Hz), 138.02 (d, $J_{C\text{-}P}$ = 7.4 Hz), 144.20 (d, $J_{C\text{-}P}$ = 23.5 Hz). **^{31}P NMR** (121.4 MHz, $CDCl_3$) δ –16.79. **$[\alpha]_D^{26}$** –65.7 (*c* 0.75, $CHCl_3$). **Anal.** Calcd for $C_{29}H_{36}NOP$: C, 78.17; H, 8.14%; N, 3.14. Found: C, 77.80; H, 8.27; N, 3.17%.

(α*R*,2*S*)-(−)-1-(2-Dicyclohexylphosphinobenzyl)-α-(2,2-dimetylpropynyl)-2-pyrrolidinemethanol (L10)

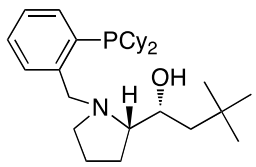

L10

Oil. **^{1}H NMR** (300 MHz, $CDCl_3$) δ 0.98 (s, 9H), 1.07–1.37 (m, 11H), 1.39–1.70 (m, 10H), 1.70–1.95 (m, 7H), 2.07–2.20 (m, 1H), 2.22–2.31 (m, 1H), 2.69 (t, 1H, J = 7.5 Hz), 3.33 (d, 1H, J = 12.3 Hz), 3.85 (brs, 1H), 4.03–4.07 (m, 1H), 4.39 (d, 1H, 12.3 Hz), 7.21–7.35 (m, 3H), 7.44–7.49 (m, 1H). **^{13}C NMR** (75.4 MHz, $CDCl_3$) δ 22.46, 23.16, 26.13 (d, $J_{C\text{-}P}$ = 1.2 Hz), 26.25 (d, $J_{C\text{-}P}$ = 1.2 Hz), 26.73, 26.86 (d, $J_{C\text{-}P}$= 5.8 Hz), 27.02 (d, J = 4.5 Hz), 27.16, 29.03 (d, $J_{C\text{-}P}$ = 2.9 Hz), 29.14 (d, $J_{C\text{-}P}$ = 3.3 Hz), 30.02, 30.24, 30.47, 30.71 34.33 (d, $J_{C\text{-}P}$ = 12.0 Hz), 34.45 (d, $J_{C\text{-}P}$ = 12.0 Hz), 46.75, 53.77, 57.08, 126.47, 128.50, 129.90, (d, $J_{C\text{-}P}$ = 6.3 Hz), 133.05 (d, $J_{C\text{-}P}$ = 4.0 Hz), 134.88 (d, $J_{C\text{-}P}$ = 18.3 Hz), 146.30 (d, $J_{C\text{-}P}$ = 23.5 Hz), **^{31}P NMR** (121.4 MHz, $CDCl_3$) δ –16.82. **$[\alpha]_D^{26}$** –53.3 (*c* 0.54, $CHCl_3$). **HRMS–ESI** (*m/z*): $[M+H]^+$ calcd for $C_{29}H_{48}NOP$, 458.3546; found, 458.3548.

Procedures for Alkynylation of Aldehydes.

Procedure for Alkynylation of Cyclohexanecarboxyaldehyde (1a) with Triisopropyl silylacetylene (2a) (Table 2, entry 13).

In a glove box, Cu(O-*t*-Bu) (2.7 mg, 0.020 mmol) and **L8** (8.9 mg, 0.020 mmol) were placed in a vial tube containing a magnetic stirring bar. A mixture of *t*-BuOH and H_2O (200:1, 0.4 mL) was added to the vial, and then the resulting mixture was stirred at room temperature for 5 min. Triisopropylsilylacetylene (**2a**) (53.8 mL, 0.24 mmol) and cyclohexanecarboxyaldehyde (**1a**) (24.2 mL, 0.20 mmol) were added to the vial. After the test tube was sealed with a screw cap, the vial was removed from the glove box. After being stirred at 25 °C for 48 h, the reaction mixture was concentrated, and then the residue was subjected to column chromatography on silica gel (hexane/EtOAc 95:5) to give **3aa** (57.9 mg, 0.20 mmol) in 98% yield.

Procedure for Alkynylation of Benzaldehyde (1g) with 2a (Table 3, entry 10).

In a glove box, Cu(O-*t*-Bu) (2.7 mg, 0.020 mmol) and **L10** (9.1 mg, 0.020 mmol) were placed in a vial tube containing a magnetic stirring bar. *t*-BuOH (0.4 mL) was added to the vial, and then the resulting mixture was stirred at room temperature for 5 min. Triisopropylsilylacetylene (**2a**) (53.8 mL, 0.24 mmol) and benzaldehyde (**1g**) (20.4 mL, 0.20 mmol) were added to the vial. After the test tube was sealed with a screw cap, the vial was removed from the glove box. After being stirred at 25 °C for 48 h, the reaction mixture was concentrated, and then the residue was subjected to column chromatography on silica gel (hexane/EtOAc 90:10) to give **3ga** (46.2 mg, 0.20 mmol) in 80% yield.

Characterization Data for Propargylic Alcohols (3).

Propargylic alcohols **3ia**[46], **3af**[7] and **3ah**[47] are known compounds.

(*R*)-(–)-1-Cyclohexyl-3-triisopropylsilyl-2-propyn-1-ol (3aa)

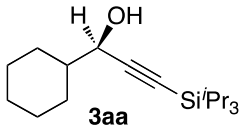

3aa

Oil. **^{1}H NMR** (300 MHz, $CDCl_3$) δ 1.00–1.09 (m, 21H), 1.09–1.33 (m, 5H), 15.2–1.61 (m, 1H), 1.62–1.70 (m, 1H), 1.68 (d, 1H, J = 5.7 Hz), 1.72–1.90 (m, 4H), 4.19 (t, 1H, J = 5.7 Hz). **^{13}C NMR** (75.4 MHz, $CDCl_3$) δ 11.01, 18.47, 25.75, 25.83, 26.37, 27.66, 28.54, 44.06, 67.66, 86.22 107.74. **Anal.** Calcd for $C_{18}H_{34}OSi$: C, 73.40; H, 11.63%. Found: C, 73.22; H, 11.67%. **$[\alpha]_D^{25}$** –5.38 (*c* 0.90, $CHCl_3$). The ee value (94% ee) was determined by chiral HPLC analysis of the *p*-nitrobenzoate derivative obtained by benzoylation of **3aa:** CHIRALCEL® OD-3 column (Daicel Chemical Industries), 4.6 mm × 250 mm, hexane/2-propanol 99.0:1.0, 0.5 mL/min, 40 ˚C, 254 nm UV detector, retention time = 8.7 min (minor), 10.2 min (major).

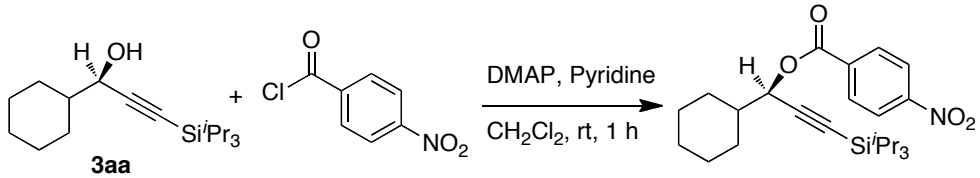

3aa

The absolute configuration of **3aa** was determined by HPLC analysis of (*R*)-(–)-1-cyclohexyl-3-phenyl-2-propyn-1-ol [47], obtained by desilylation followed by Sonogashira coupling reaction from **3aa**.

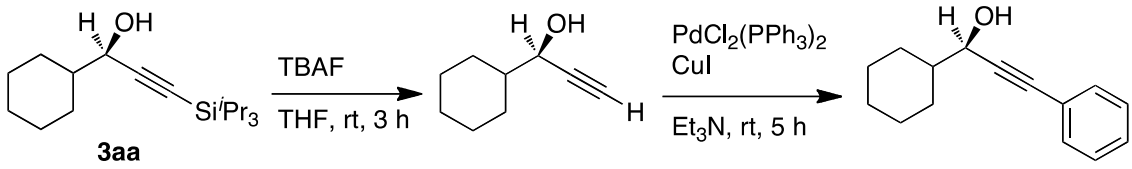

(*R*)-(−)-1-Cyclohexyl-4-triisopropylsilyl-3-butyn-2-ol (3da)

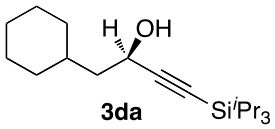

Oil. **^{1}H NMR** (300 MHz, $CDCl_3$) δ 0.80–1.30 (m, 23H), 1.50–1.82 (m, 11H), 4.47 (brq, 1H, J = 6.0 Hz) . ^{13}C NMR (75.4 MHz, $CDCl_3$) δ 11,01, 18.46, 26.14, 26.39, 33.15, 33.21, 34.29, 45.53, 61.16, 85.40, 109.22. **HRMS–ESI** (*m/z*): $[M+Na]^+$ calcd for $C_{19}H_{36}ONaSi$, 331.2428; found, 331.2432. **$[\alpha]_D^{25}$** –1.27 (*c* 0.61, $CHCl_3$). The ee value (90% ee) was determined by chiral HPLC analysis of the *p*-nitrobenzoate derivative obtained by benzoylation of **3da:** CHIRALCEL® OD-3 column (Daicel Chemical Industries), 4.6 mm × 250 mm, hexane/2-propanol 99:1, 0.5 mL/min, 40 ˚C, 254 nm UV detector, retention time = 8.8 min (minor), 9.4 min (major).

(*R*)-(+)-4-Methyl-1-triisopropylsilyl-1-pentyn-3-ol (3ea)

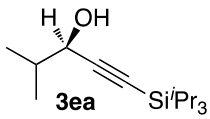

Oil. **^{1}H NMR** (300 MHz, $CDCl_3$) δ 1.01 (d, 3H, J = 6.9 Hz), 10.3 (d, 3H, J = 6.9 Hz), 1.02–1.11 (m, 21H), 1.72 (d, 1H, J = 5.7 Hz), 1.85–1.95 (m, 1H), 4.21 (t, 1H, J = 5.7 Hz). **^{13}C NMR** (75.4 MHz, $CDCl_3$) δ 11.00, 17.04, 18.06, 18.43, 34.37, 62.29, 86.12, 107.39. **Anal.** Calcd for $C_{15}H_{30}OSi$: C, 70.79; H, 11.88%. Found: C, 71.44; H, 11.95%. **$[\alpha]_D^{24}$** +0.48 (*c* 0.60, $CHCl_3$). The ee value (87% ee) was determined by chiral HPLC analysis of the *p*-nitrobenzoate derivative obtained by benzoylation of **3ea:** CHIRALCEL® OD-3 column (Daicel Chemical Industries), 4.6 mm × 250 mm, hexane/2-propanol 99:1, 0.5 mL/min, 40 ˚C, 254 nm UV detector, retention time = 8.8 min (minor), 10.7 min (major).

(*R*)-(−)-1-(*N*-Benzyl-4-piperidinyl)-3-triisopropylsilyl-2-propyn-1-ol (3fa)

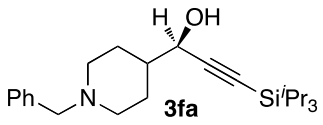

Oil. **^{1}H NMR** (300 MHz, $CDCl_3$) δ 1.03–1.12 (m, 21H), 1.40–1.60 (m, 3H), 1.71 (brs, 1H), 1.77–1.87 (m, 2H), 1.92–2.01 (m, 2H), 2.88–2.97 (m, 2H), 3.50 (d, 2H, J = 1.4 Hz), 4.18 (brs, 1H), 7.20–7.28 (m, 2H), 7.28–3.36 (m, 3H). **^{13}C NMR** (75.4 MHz,

$CDCl_3$) δ 10.98, 18.64, 27.63, 27.95, 29.87, 42.58, 53.21, 53.30, 63.08, 67.00, 86.34, 107.65, 126.93, 128.18, 129.14, 138,72. **Anal.** Calcd for $C_{24}H_{39}NOSi$: C, 74.74; H, 10.19%; N, 3.63. Found: C, 74.86; H, 10.19; N, 3.65%. $[\alpha]_D^{25}$ –2.09 (*c* 0.70, $CHCl_3$). The ee value (94% ee) was determined by chiral HPLC analysis of the *p*-nitrobenzoate derivative obtained by benzoylation of **3fa:** CHIRALCEL® OD-3 column (Daicel Chemical Industries), 4.6 mm × 250 mm, hexane/2-propanol 99:1, 0.5 mL/min, 40 ˚C, 254 nm UV detector, retention time = 23.9 min (major), 32.4 min (minor).

(*R*)-(–)-1-(*N*-Benzyloxycarbonyl-4-piperidinyl)-3-triisopropylsilyl-2-propyn-1-ol (3ga)

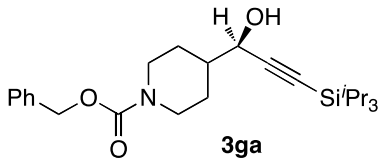

3ga

Oil. **^{1}H NMR** (300 MHz, $CDCl_3$) δ 0.80–1.50 (m, 2H), 1.00–1.10 (m, 21H), 1.68–1.90 (m, 2H), 1.76 (brs, 1H), 2.69–2.85 (m, 2H), 4.20–4.35 (m, 2H), 4.22 (t, 1H, *J* = 5.6 Hz), 5.12 (s, 2H), 7.26–7.37 (m, 5H). **^{13}C NMR** (75.4 MHz, $CDCl_3$) δ 10.91, 18.42, 27.04, 27.68, 42.38, 43.72, 43.75, 66.53, 66.94, 87.07, 106.78, 127.86, 127.97, 128.51, 136.93, 155.33. **Anal.** Calcd for $C_{25}H_{39}NO_3Si$: C, 69.88; H, 9.15%; N, 3.26. Found: C, 70.11; H, 9.17; N, 3.25%. $[\alpha]_D^{24}$ –5.07 (*c* 0.84, $CHCl_3$). The ee value (94% ee) was determined by chiral HPLC analysis of the *p*-nitrobenzoate derivative obtained by benzoylation of **3ga:** CHIRALCEL® OD-3 column (Daicel Chemical Industries), 4.6 mm × 250 mm, hexane/2-propanol 99:1, 0.5 mL/min, 40 ˚C, 254 nm UV detector, retention time = 31.9 min (minor), 36.8 min (major).

(*R*)-(+)-4,4-Dimethyl-1-triisopropylsilyl-1-pentyn-3-ol (3ha)

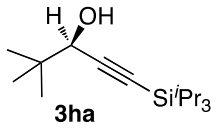

3ha

Oil. **^{1}H NMR** (300 MHz, $CDCl_3$) δ 1.01 (s, 9H), 1.05–1.13 (m, 21H), 1.65 (d, 1H, *J* = 6.3 Hz), 4.02 (d, *J* = 6.3 Hz, 1H), **^{13}C NMR** (75.4 MHz, $CDCl_3$) δ 11.05, 18.47, 25.18, 35.76, 71.85, 86.29, 107.46. **Anal.** Calcd for $C_{16}H_{32}OSi$: C, 71.57; H, 12.01%. Found: C, 71.57; H, 12.11%. $[\alpha]_D^{24}$ +2.59 (*c* 0.67, $CHCl_3$). The ee value (76% ee) was determined by chiral HPLC analysis of the *p*-nitrobenzoate derivative obtained by benzoylation of **3ha:** CHIRALCEL® OD-3 column (Daicel Chemical Industries), 4.6 mm × 250 mm, hexane/2-propanol 99:1, 0.5 mL/min, 40 ˚C, 254 nm UV detector, retention time = 8.4 min (minor), 9.8 min (major).

(*R*)-(+)-Methyl-3-(1-hydroxy-3-triisopropylsiliyl-2-propynyl)benzoate (3ja)

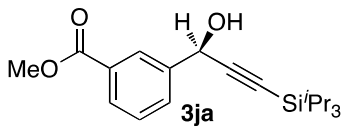

3ja

Oil. **^{1}H NMR** (300 MHz, $CDCl_3$) δ 1.00–1.20 (m, 21H), 2.33 (d ,1H, J = 6.0 Hz), 3.92 (s, 3H), 5.54 (d ,1H, J = 6.0 Hz), 7.47 (t, 1H, J = 7.8 Hz), 7.78 (d, 1H, J = 7.8 Hz), 8.01 (d, 1H, J = 7.8 Hz), 8.30 (s, 1H). **^{13}C NMR** (75.4 MHz, $CDCl_3$) δ 10.58, 18.40, 52.03, 64.46, 88.49, 106.48, 128.01, 128.64, 129.53, 130.35, 131.41, 141.11, 166.96. **HRMS–ESI** (*m/z*): $[M+Na]^+$ calcd for $C_{20}H_{30}O_3NaSi$, 369.1856; found, 369.1855. **$[\alpha]_D^{24}$** +15.80 (*c* 0.70, $CHCl_3$). The ee value (86% ee) was determined by chiral HPLC analysis of the *p*-nitrobenzoate derivative obtained by benzoylation of **3ja:** CHIRALCEL® IC column (Daicel Chemical Industries), 4.6 mm × 250 mm, hexane/2-propanol 99:1, 0.5 mL/min, 40 ˚C, 254 nm UV detector, retention time = 20.1 min (major), 21.5 min (minor).

(*R*)-(+)-1-(4-Fluorophenyl)-3-triisopropylsilyl-2-propyn-1-ol (3ka)

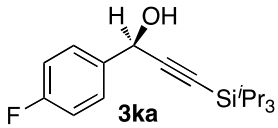

3ka

Oil. **^{1}H NMR** (300 MHz, $CDCl_3$) δ 0.98–1.08 (m, 21H), 2.16 (d, 1H, J = 6.3 Hz), 5.47 (d, 1H, J = 6.3 Hz), 7.06 (t, 2H, J = 8.7 Hz), 7.54–7.58 (m, 2H). **^{13}C NMR** (75.4 MHz, $CDCl_3$) δ 10.99, 18.45, 64.33, 88.30, 106.74, 115.41 (d, 1H, $J_{C\text{-}F}$ = 21.1 Hz), 128.67 (d, 1H, $J_{C\text{-}F}$ = 8.0 Hz), 136.52 (d, 1H, $J_{C\text{-}F}$ = 2.9 Hz), 161.14, 164.41. **Anal.** Calcd for $C_{18}H_{27}FOSi$: C, 70.54; H, 8.88%. Found: C, 70.53; H, 9.04%. **$[\alpha]_D^{26}$** +18.4 (*c* 0.51, $CHCl_3$). After derivation with the *p*-nitrobenzoylchloride the ee value (88% ee) was determined by chiral HPLC analysis of the 4-nitrobenzoate derivative obtained by benzoylation of **3ka:** CHIRALCEL® IC column (Daicel Chemical Industries), 4.6 mm × 250 mm, hexane/2-propanol 99:1, 0.5 mL/min, 40 ˚C, 254 nm UV detector, retention time = 14.6 min (minor), 16.8 min (major).

(*R*)-(+)-1-(4-Chlorophenyl)-3-triisopropylsilyl-2-propyn-1-ol (3ia)

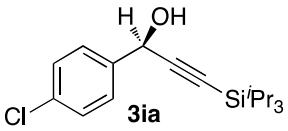

Oil. **^{1}H NMR** (300 MHz, $CDCl_3$) δ 0.90–1.30 (m, 21H), 2.14 (d, 1H, J = 4.5 Hz), 5.46 (d, 1H, J = 4.5 Hz), 7.35 (d, 2H, J = 8.2 Hz), 7.52 (d, 2H, J = 8.2 Hz). **^{13}C NMR** (75.4 MHz, $CDCl_3$) δ 11.01, 18.44, 62.90, 87.77, 106.86, 126.12, 126.62, 128.39, 130.72, 136.20, 138.35. **Anal.** Calcd for $C_{18}H_{27}ClOSi$: C, 66.94; H, 8.43%. Found: C, 77.28; H, 8.49%. **$[\alpha]_D^{24}$** +20.2 (*c* 0.84, $CHCl_3$). The ee value (90% ee) was determined by chiral HPLC analysis of the *p*-nitrobenzoate derivative obtained by benzoylation of **3ia:** CHIRALCEL® IC column (Daicel Chemical Industries), 4.6 mm × 250 mm, hexane/2-propanol 99:1, 0.5 mL/min, 40 °C, 254 nm UV detector, retention time = 14.9 min (minor), 17.2 min (major). The absolute configuration of **3ia** was determined by HPLC analysis of (*R*)-(**+**)-1-(4-chlorophenyl)-3-triisopropylsilyl-2-propyn-1-ol[48,49], obtained by desilylation of **3ia** followed by Sonogashira coupling reaction.

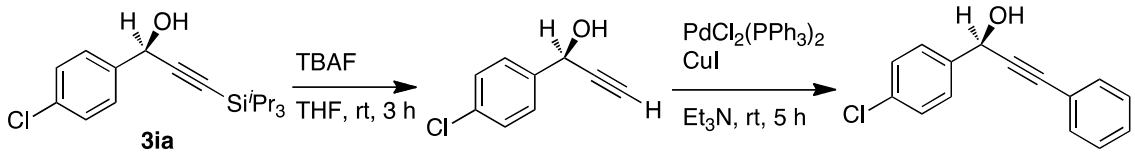

(*R*)-(+)-1-(3-Methoxyphenyl)-3-(triisopropylsilyl)-2-propyn-1-ol (3ma)

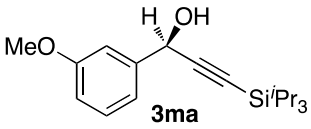

Oil. **^{1}H NMR** (300 MHz, $CDCl_3$) δ 1.03–1.14 (m, 21H), 2.11 (d, 1H, J = 6.6Hz), 3.82 (s, 3H), 5.47 (d, 1H, J = 6.6Hz), 6.85–6.90 (m, 1H), 7.14–7.18 (m, 2H), 7.26–7.32 (m, 1H). **^{13}C NMR** (75.4 MHz, $CDCl_3$) δ 11.03, 18.48, 55.18, 60.02, 87.97, 106.87, 111.77, 114.57, 119.19, 129.64, 142.21, 159.89. **HRMS–ESI** (*m/z*): $[M+Na]^+$ calcd for $C_{23}H_{26}ONaSi$, 341.1876; found, 341.1901. **$[\alpha]_D^{25}$** +21.6 (*c* 0.81, $CHCl_3$). The ee value (91% ee) was determined by chiral HPLC analysis of the *p*-nitrobenzoate derivative obtained by benzoylation of **3ma:** CHIRALCEL® IC column (Daicel Chemical Industries), 4.6 mm × 250 mm, hexane/2-propanol 99.5:0.5, 0.5 mL/min, 40 °C, 254 nm UV detector, retention time = 38.6 min (minor), 42.7 min (major).

(*S*)-(+)-1-(3-Thienyl)-3-triisopropylsilyl-2-propyn-1-ol (3na)

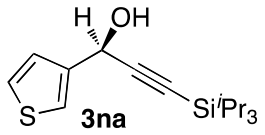

3na

Oil. **^{1}H NMR** (300 MHz, $CDCl_3$) δ 1.05–1.15 (m, 21H), 2.12 (d, 1H, J = 7.2 Hz), 5.51 (d, 1H, J = 7.2 Hz), 7.21–7.23 (m, 1H), 7.31–7.33 (m, 1H), 7.42–7.44 (m, 1H). **^{13}C NMR** (75.4 MHz, $CDCl_3$) δ 10.99, 18.46, 60.93, 86.97, 106.80, 122.75, 126.44, 126.57, 142.16. **Anal.** Calcd for $C_{16}H_{26}OSSi$: C, 65.25; H, 8.90%. Found: C, 65.07; H, 8.97%. **$[\alpha]_D^{25}$** +15.2 (*c* 0.54, $CHCl_3$). The ee value (90% ee) was determined by chiral HPLC analysis of the *p*-nitrobenzoate derivative obtained by benzoylation of **3na:** CHIRALCEL® IC column (Daicel Chemical Industries), 4.6 mm × 250 mm, hexane/2-propanol 99:1, 0.5 mL/min, 40 °C, 254 nm UV detector, retention time = 16.9 min (minor), 18.1 min (major). The absolute configuration of **3na** was determined by HPLC analysis of (*S*)-1-(3-thienyl)-3-triisopropylsilyl-2-propyn-1-ol[48], obtained by desilylation of **3na** followed by Sonogashira coupling reaction.

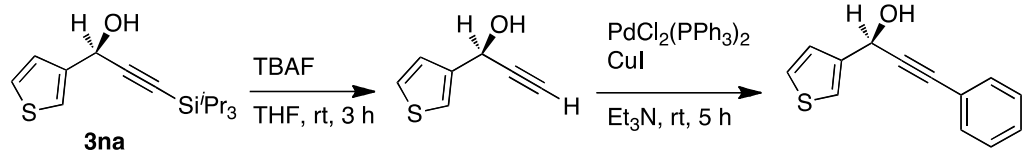

3na

(*R*)-(–)-1-Cyclohexyl-5-methyl-2-hexyn-1-ol (3ac)

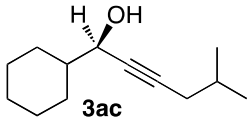

3ac

Oil. **^{1}H NMR** (300 MHz, $CDCl_3$) δ 0.98 (d, 6H, J = 6.6 Hz), 1.01–1.34 (m, 5H), 1.45–1.89 (m, 8H), 2.12 (dd, 2H, J = 1.8 Hz, 6.6 Hz), 4.16 (brs, 1H). **^{13}C NMR** (75.4 MHz, $CDCl_3$) δ 21.86, 25.79, 25.83, 26.34, 27.78, 27.92, 28.51, 44.30, 67.44, 81.01, 85.18. **HRMS–FI** (*m/z*): $[M+H]^+$ calcd for $C_{13}H_{22}O$, 194.1671; found, 196.1678. **$[\alpha]_D^{26}$** –6.31 (*c* 0.80, $CHCl_3$). The ee value (86% ee) was determined by chiral HPLC analysis of the *p*-nitrobenzoate derivative obtained by benzoylation of **3ac:** CHIRALCEL® OD-3 column (Daicel Chemical Industries), 4.6 mm × 250 mm, hexane/2-propanol 99:1, 0.5 mL/min, 40 °C, 254 nm UV detector, retention time = 13.0 (major), 14.0 (minor).

(*R*)-(–)-1-Cyclohexyl-4,4-(dimethyl)-2-pentyn-1-ol (3ad)

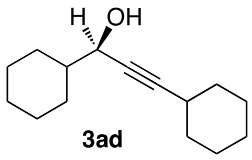

Oil. **^{1}H NMR** (300 MHz, $CDCl_3$) δ 0.98–1.30 (m, 5H), 1.19 (s, 9H), 1.40–1.87 (m, 7H), 4.12 (t, 1H, J = 5.7 Hz). **^{13}C NMR** (75.4 MHz, $CDCl_3$) δ 25.83, 25.86, 26.37, 27.26, 27.91, 28.54, 30.95, 44.33, 67.30, 78.49, 94.60. **HRMS–ESI** (*m/z*): $[M+H]^+$ calcd for $C_{13}H_{22}O$, 194.1671; found, 194.1670. **$[\alpha]_D^{26}$** –4.07 (*c* 0.50, $CHCl_3$). The ee value (85% ee) was determined by chiral HPLC analysis of the *p*-nitrobenzoate derivative obtained by benzoylation of **3ae:** CHIRALCEL® OD-3 column (Daicel Chemical Industries), 4.6 mm × 250 mm, hexane/2-propanol 99.0:1.0, 0.5 mL/min, 40 ˚C, 254 nm UV detector, retention time = 10.0 min (minor), 11.6 min (major).

(*R*)-(–)-1-Cyclohexyl-4-*tert*-butyldimethylsilyoxy-4-methyl-2-pentyn-1-ol (3ag)

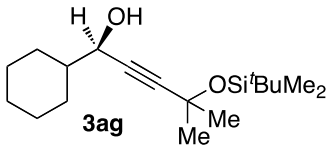

Oil. **^{1}H NMR** (300 MHz, $CDCl_3$) δ 0.16 (m, 6H), 0.86 (s, 9H), 0.98–1.33 (m, 5H), 1.46 (s, 6H), 1.47–1.90 (m, 7H), 4.16 (d, 1H, J = 6.0 Hz) **^{13}C NMR** (75.4 MHz, $CDCl_3$) δ –3.07, 17.77, 25.55, 25.75, 25.77, 26.28, 28.08, 28.43, 32.91, 32.94, 44.07, 66.26, 67.19, 82.22, 91.10. **Anal.** Calcd for $C_{18}H_{34}O_2Si$: C,69.62; H, 11.04%. Found: C, 69.72; H, 11.13%. **$[\alpha]_D^{25}$** –3.68 (*c* 0.70, $CHCl_3$). The ee value (88% ee) was determined by chiral HPLC analysis of the *p*-nitrobenzoate derivative obtained by benzoylation of **3ag:** CHIRALCEL® OD-3 column (Daicel Chemical Industries), 4.6 mm × 250 mm, hexane/2-propanol 99:1, 0.5 mL/min, 40 ˚C, 254 nm UV detector, retention time = 8.2 min (minor), 8.7 min (major).

(*R*)-(–)-1-Cyclohexyl-3-(4-methoxyphenyl)-2-propyn-1-ol (3ai)

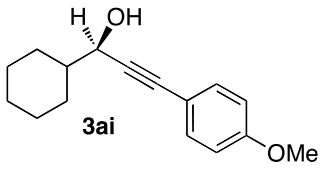

Oil. Racemic product was reported[50]. **$[\alpha]_D^{26}$** –10.2 (*c* 0.50, $CHCl_3$). The ee value (83% ee) was determined by chiral HPLC analysis of the *p*-nitrobenzoate derivative obtained by benzoylation of **3ai:** CHIRALCEL® OD-3 column (Daicel Chemical Industries), 4.6 mm × 250 mm, hexane/2-propanol 90:10, 0.5 mL/min, 40 ˚C, 254 nm UV detector, retention time = 13.7 min (minor), 15.1 min (major).

(*R*)-(–)-1-Cyclohexyl-3-(4-trifluoromethylphenyl)-2-propyn-1-ol (3aj)

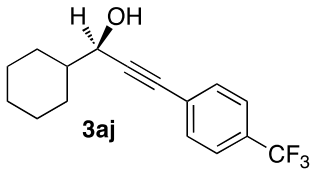

Oil. Racemic product was reported[50]. $[\alpha]_D^{26}$ –5.56 (*c* 0.64, $CHCl_3$). The ee value (72% ee) was determined by chiral HPLC analysis of the *p*-nitrobenzoate derivative obtained by benzoylation of **3aj:** CHIRALCEL® IC-3 column (Daicel Chemical Industries), 4.6 mm × 250 mm, hexane/2-propanol 99:1, 0.5 mL/min, 40 ˚C, 254 nm UV detector, retention time = 17.8 min (minor), 18.6 min (major).

6. References

[1] Park, J.; Hong, S. *Chem. Soc. Rev.* **2012**, *41*, 6931.

[2] Sawamura, M.; Ito, Y. *Chem. Rev.* **1992**, *92*, 857.

[3] Ikariya, T.; Murata, K.; Noyori, R. *Org. Biomol. Chem.* **2006**, *4*, 393.

[4] Doyle, A. G.; Jacobsen, E. N. *Chem. Rev.* **2007**, *107*, 5713.

[5] Akiyama, T. *Chem. Rev.* **2007**, *107*, 5744.

[6] A review on the enantioselective alkynylation of carbonyl carbonyl compounds and imines: Trost, B. M.; Weiss, A. H. *Adv. Synth. Catal.* **2009**, *351*, 963.

[7] Anand, N. K.; Carreira, E. M. *J. Am. Chem. Soc.* **2001**, *123*, 9687.

[8] Takita, R.; Yakura, K.; Ohshima, T.; Shibasaki M. *J. Am. Chem. Soc.* **2005**, *127*, 13760.

[9] (a) Asano, Y.; Hara, K.; Ito, H.; Sawamura, M. *Org. Lett*. **2007**, *9*, 3901. (b) Asano, Y.; Ito, H.; Hara, K.; Sawamura, M. *Organometallics* **2008**, *27*, 5984.

[10] Ito, J.; Asai, R.; Nishiyama, H. *Org. Lett*. **2010**, *12*, 3860.

[11] Bode, J. W.; Carreira E. M. *J. Am. Chem. Soc*. **2001**, *123*, 3611–3612

[12] Marshall, J. A.; Bourbeau, M. P. *Org. Lett.* **2003**, *5*, 3197–3199.

[13] Bejjani, J.; Chemla, F.; Audouin, M. *J. Org. Chem*. **2003**, *68*, 9747.

[14] Becke, A. D. *J. Chem. Phys.* **1993**, *98*, 5648.

[15] Lee, C.; Yang, W.; Parr, R. G. *Phys. Rev. B* **1988**, *37*, 785.

[16] Schaefer, A.; Huber, C.; Ahlrichs, R. *J. Chem. Phys.* **1994**, *100*, 5829.

[17] Hehre, W. J.; Radom, L.; Schleyer, P. v. R.; Pople, J. A. *Ab Initio Molecular Orbital Theory*; Wiley: New York, 1986.

[18] Grimme, S.; *Comput. J. Chem*. **2006**, *27*, 1787.

[19] Miertuš, S.; Scrocco, E.; Tomasi, J. *Chem. Phys.* ***1981***, *55*, 117.

[20] Tomasi, J.; Mennucci, B.; Cammi, R. *Chem. Rev.* **2005**, *105*, 2999.

[21] Carballeira, L.; Pérez-Juste, I.; Alsenoy, C. V. *J. Phys. Chem. A* **2002**, *106*, 3873.

[22] Desiraju, G. R. *Acc. Chem. Res.* ***1996***, *29*, 441.

[23] Chakrabarti, P.; Chakrabarti, S. *J. Mol. Biol*. **1998**, *284*, 867.

[24] For formyl C–H···O hydrogen bonds in enantioselective Lewis-acid catalyzed reactions of aldehydes, see: Corey, E. J.; Lee, T. W. *Chem. Commun*. **2001**, 1321.

[25] TS models involving hydrogen bonds between an N-adjacent sp^3-C–H bond of *N*-acylimidazolinium salts and a carboxylate oxygen atom have been proposed for the enantioselective acyl transfer catalysis. See: Shiina, I.; Nakata, K.; Ono, K.; Onoda, Y.; Itagaki, M. *J. Am. Chem. Soc.* **2010**, *132*, 11629.

[26] Hydrogen bonding interactions between an N-adjacent sp^2-C–H bond and a carboxylate oxygen atom have been proposed for acyl transfer catalysis with 4-(*N*,*N*-dimethylamino)pyridine (DMAP). See: Xu, S.; Held, I.; Kempf, B.; Mayr, H.; Steglich, W.; Zipse, H. *Chem. Eur. J.* **2005**, *11*, 4751.

[27] List proposed the occurrence of sp^3-C–H···O=P interactions in the transition state of the Brønsted acid catalyzed enantioselective S_N2-type O-alkylations. The C–H bond is located at the pentagonal carbon center with a partial positive charge. See: Čorić, I.; Kim, J. H.; Vlaar, T.; Patil, M.; Thiel, W.; List, B. *Angew. Chem. Int. Ed.* **2013**, *52*, 3490.

[28] For X-ray crystal structures involving $(2\text{-pyridyl})_3C$–H···Cl^- interactions in Pd(IV) complexes coordinated with a tridentate pyridine ligand, see: Maleckis, A.; Kampf, J. W.; Sanford, M. S. *J. Am. Chem. Soc*. **2013**, *135*, 6618.

[29] Spartan '08. Wavefunction, Inc; Irvine, CA, USA , **2008**.

[30] Gaussian 09, Revision C.01, Frisch, M. J., Trucks, G. W., Schlegel, H. B., Scuseria, G. E., Robb, M. A., Cheeseman, J. R., Scalmani, G., Barone, V., Mennucci, B., Petersson, G. A., Nakatsuji, H., Caricato, M., Li, X., Hratchian, H. P., Izmaylov, A. F., Bloino, J., Zheng, G., Sonnenberg, J. L., Hada, M., Ehara, M., Toyota, K., Fukuda, R., Hasegawa, J., Ishida, M., Nakajima, T., Honda, Y., Kitao, O., Nakai, H., Vreven, T., Montgomery, Jr., J. A., Peralta, J. E., Ogliaro, F., Bearpark, M., Heyd, J. J., Brothers, E., Kudin, K. N., Staroverov, V. N., Kobayashi, R., Normand, J., Raghavachari, K., Rendell, A., Burant, J. C., Iyengar, S. S., Tomasi, J., Cossi, M., Rega, N., Millam, N. J., Klene, M., Knox, J. E., Cross, J. B., Bakken, V.,

Adamo, C., Jaramillo, J., Gomperts, R., Stratmann, R. E., Yazyev, O., Austin, A. J., Cammi, R., Pomelli, C., Ochterski, J. W., Martin, R. L., Morokuma, K., Zakrzewski, V. G., Voth, G. A., Salvador, P., Dannenberg, J. J., Dapprich, S., Daniels, A. D., Farkas, Ö., Foresman, J. B., Ortiz, J. V., Cioslowski, J., Fox, D. J. Gaussian, Inc., Wallingford CT, **2009**.

[31] Nakamura, E., Mori, S., Nakamura, M.& Morokuma, K. *J. Am. Chem. Soc.* **1997**, *119*, 4887.

[32] Glendening, E. D., Badenhoop, J, K., Reed, A. E., Carpenter, J. E., Bohmann, J. A., Morales, C. M., Weinhold, F. *NBO 5.9*. Theoretical Chemistry Institute, University of Wisconsin, Madison, USA , **2001**.

[33] Cheong, P. H.-Y., Houk, K. N., Warrier, J. S., Hanessian, S. *Adv. Synth. Catal.* **2004**, *346*, 1111.

[34] Pfafferott, G., Oberhammer, H., Boggs, J. E., Caminati, W. *J. Am. Chem. Soc.* **1985**, *107*, 2305.

[35] El-Gogary, T. M., Soliman, M. S. *Spectrochim. Acta, Part A*. **2001**, *57*, 2647.

[36] Carballeira, L., Pérez-Juste, I. *J. Chem. Soc., Perkin Trans.* **1998**, *2*, 1339.

[37] Pipek, J., Mezey, P. G. *J. Chem. Phys.* **1989**, *90*, 4916.

[38] Fukui, K. *J. Phys. Chem.* **1970**, *74*, 4161.

[39] Fukui, K. *Acc. Chem. Res.* **1981**, *14*, 363.

[40] Gonzalez, C., Schlegel, H.B. *J. Chem. Phys.* **1989**, *90*, 2154.

[41] Gonzalez, C., Schlegel, H.B. *J. Phys. Chem.* **1990**, *94*, 5523.

[42] Hratchian, H.P., Schlegel, H. B. *J. Chem. Phys.* **2004**, *120*, 9918.

[43] Hratchian, H.P., Frisch, M. J. *J. Chem. Phys.* **2011**, *134*, 204103 (9 pages).

[44] Spartan '08 for Windows. Wavefunction, Inc; Irvine, CA, USA, **2008**.

[45] Tsuda, T., Hashimoto, T., Saegusa, T. *J. Am. Chem. Soc.* **1972**, *94*, 658.

[46] Moore, D., Pu, L. *Org. Lett.* **2002**, *4*, 1855.

[47] Corey, E. J., Cimprich K. A. *J. Am. Chem. Soc.* **1994**. *116*, 3151.

[48] Blay, G., Cardona, L., Fernández, I., Aleixandre, A. M., Muñoz M. C., Pedro, J. R. *Org. Biomol. Chem.* **2009**, *7*, 4301.

[49] Xu, Z., Chen, C., Xu, J., Miao, M., Yan, W. Wang, R. *Org. Lett.* **2004**, *6*, 1193.

[50] Wadhwa, K., Chintareddy V. R., and Verkade, J. G. *J. Org. Chem.* **2009**, *74*, 6681.

Chapter 2

Enantioselective Alkynylation of α-Keto Ester Derivatives Catalyzed by Chiral Hydroxy Amino Phosphine Copper Complexes

1. Introduction

Chiral propargylic alcohols are versatile synthetic intermediates in organic synthesis.[1] In particular, chiral tertiary propargylic alcohols are found in many important pharmaceuticals and bioactive natural products. Catalytic enantioselective alkynylation of ketone derivatives with terminal alkynes appears to be the efficient and useful method for the preparation of chiral tertiary propargylic alcohols.[2] However, it is challenging because of the steric repulsion that occurs in the carbon–carbon bond-formation step and the difficulty in the discrimination of the enantiotopic faces. To date, this has been achieved by using various ketone derivatives such as α-keto esters,[3] trifluoromethyl ketones[4] and α-diketones[5] under the influence of chiral transition metal catalysts.

Earlier, the author reported the enatioselective alkynylation of aldehydes with terminal alkynes catalyzed by copper(I) complexes with prolinol-based hydroxy amino phosphine chiral ligand **L1** in alcoholic solvents (Chapter 1).[6] In this chapter, the author reports that the same class of chiral hydroxyl amino phosphine ligands are applicable to copper(I)-catalyzed enantioselective alkynylations of α-keto esters with terminal alkynes. This copper catalysis provides an efficient method for accessing a wide range of enantioenriched chiral tertiary propargylic alcohols with high enantioselectivities. The hydrogen-bonding interactions between chiral catalysts and substrates in alcoholic solvents are proposed.

2. Results and Discussion

The author's earlier investigation on the copper-catalyzed enantioselective alkynylation of aldehydes with terminal alkynes indicated that the use of prolinol-based hydoroxy amino phosphine chiral ligands in alcoholic solvents was important for promotion of the reaction. On the basis of this consideration, the author examined copper complexes (10 mol%) with prolinol-based hydroxy amino phosphine for catalytic activity and enantioselectivity in the reaction of α-keto ester **1a** and phenylacetylene (**2a**) in the presence of K_2CO_3 (30 mol%) in *t*-BuOH at 25 °C over 24 h (Table 1). Specifically, the use of the prototype hydroxy amino phosphine chiral ligand **L1** imparted high product yield, but the enatioselectivity was moderate (entry 1). The effect of the ligand modification at the alcoholic site of the chiral P,N,OH-ligand was examined (entries 2–4). The use of the secondary (**L2**) or tertiary (**L3**) alcohol type

ligands caused slight improvement of the stereocontrol, but decreased product yields (entries 2 and 3). The ligand (**L4**) with a neopentyl group in the alcoholic site, which exhibited high performance in the previously reported reaction with aldehydes[6] did not lead to the improvement of the enantioselectivity (entry 4).

Next, the effect of the *P*-substituents in the chiral P,N,OH-ligand was examined. Introduction of electro-donating MeO group (**L5**) to para-position of the aromatic ring increased the product yield (96%) and enantioselectivity (70% ee) (entry 5). On the other hand, the electro-withdrawing F substituent (**L6**) at the para-position of the aromatic ring was less effective (entry 6). The use of Cy_2P (**L7**) as a P-substituent led to a significant improvement in the enantioselectivity (87% ee) (entry 7). These results imply that the electro-donating nature of the P-substituent in the chiral P,N,OH-ligand favored the copper catalysis.

Notably, the protection of the hydroxy group in **L4** as a methyl ether (**L8**) completely inhibited the reaction (entry 8). This result strongly indicated a critical role for the alcoholic site.

The nature of the solvent had a strong impact on the yield and enantioselection, as in the case for the copper-catalyzed alkynylation of aldehydes (Table 2).[6] In the case of the investigation, the author used **L7** as a chiral P,N,OH-ligand for the reaction between **1a** and **2a**. Replacing *t*-BuOH with THF, dioxane or CH_3CN caused a decrease in enantioselectivities (74%, 77% and 78% ees) with lower yields (26%, 31% and 35%) (entries 2–4).

Table 1. Copper-catalyzed enantioselective alkynylation of **1a** and **2a**.

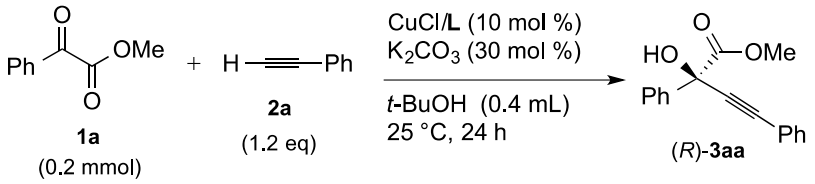

entry	ligand	solvent	yield, % [a]	ee, % [b]
1	**L1**	*t*-BuOH	92	56
2	**L2**	*t*-BuOH	67	58
3	**L3**	*t*-BuOH	68	67
4	**L4**	*t*-BuOH	71	67
5	**L5**	*t*-BuOH	96	70
6	**L6**	*t*-BuOH	57	57
7	**L7**	*t*-BuOH	97	88
8	**L8**	*t*-BuOH	0	–

[a] Yield of the isolated product (silica gel chromatography). [b] Determined by HPLC analysis.

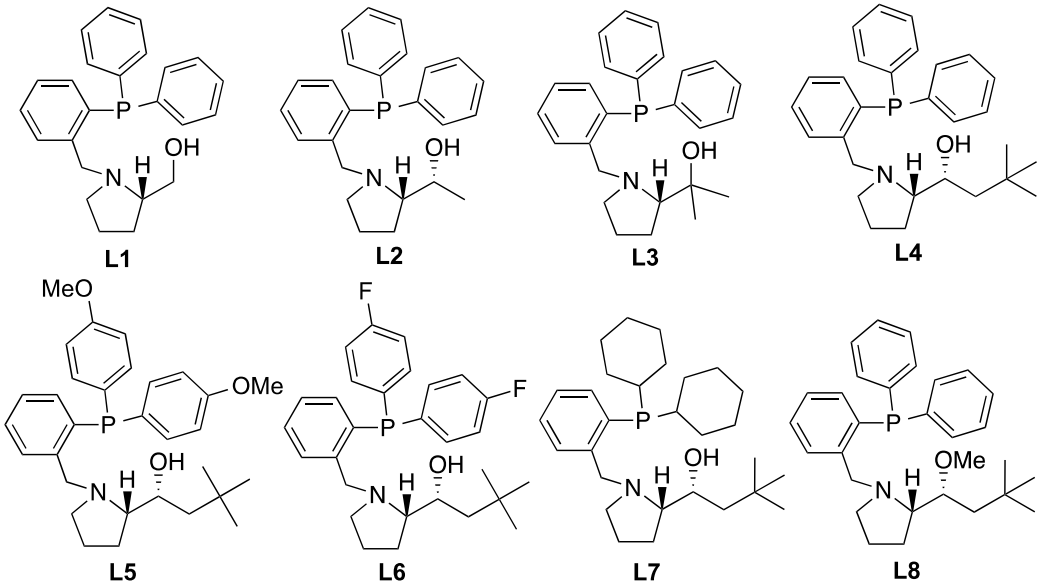

Table 2. Solvent effect.

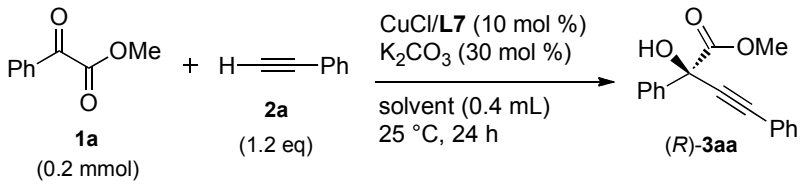

entry	solvent	yield, % [a]	ee, % [b]
1	*t*-BuOH	97	88 (Table 1, entry 7)
2	THF	26	74
3	dioxane	31	77
4	CH_3CN	35	78

[a] Yield of the isolated product (silica gel chromatography).

[b] Determined by HPLC analysis.

Various α-keto ester derivatives were subjected to the alkynylation with phenylacetylene (**2a**) with the Cu–**L7** catalyst system (Table 3). In some cases, *i*-PrOH was used as a solvent because *i*-PrOH was better than *t*-BuOH in terms of the enantioselectivity. The α-keto esters (**1b** and **1c**) with ester groups other than the methyl ester group also served as substrates (entries 1 and 2). The reactions produced the corresponding tertiary propargylic alcohols in high yields, with a tendency toward increased enantioselectivities with the increasing steric demands of the ester moieties (see Table 1, entry 10). The functional groups such as chloro, fluoro or methoxy groups were tolerated as a substituent on the aromatic ring of α-keto esters (entries 3–5). The keto ester bearing a 2-naphthyl group also underwent the alkynylation with 94% ee (entry 6).

The aliphatic α-keto esters are also suitable substrates (entries 7 and 8). The reactions of aliphatic aldehydes (**1h** and **1i**) with a branch at the α- or β-position proceeded with high enantioselectivities, but the yields were moderate due to self-condensation of the keto ester. The cyclic keto ester such as α-keto pantolactone (**1j**) reacted with a high enantioselectivity at –20 °C (entry 9).

Table 3. Scope of copper-catalyzed enantioselective alkynylation of **2a**.

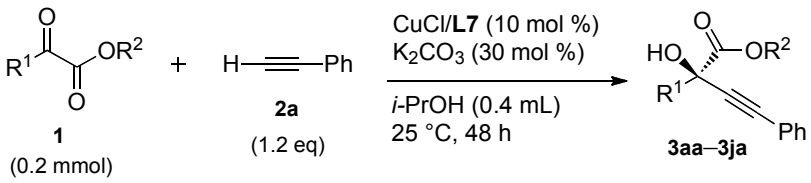

entry	keto ester **1**	propargylic alcohol **3**	yield,%[a]	ee, %[b]
1 [c]	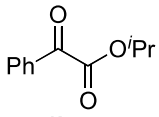 **1b**	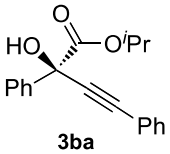 **3ba**	99	90
2 [c]	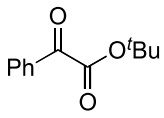 **1c**	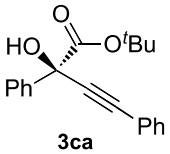 **3ca**	78	91
3	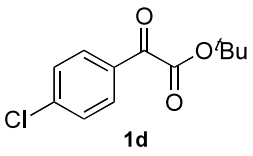 **1d**	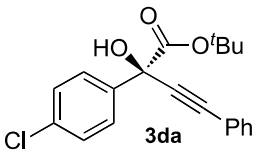 **3da**	97	92
4	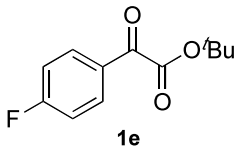 **1e**	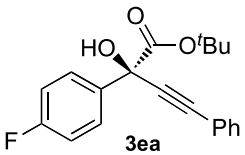 **3ea**	98	90
5	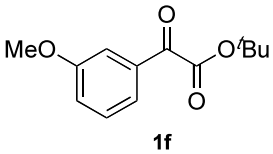 **1f**	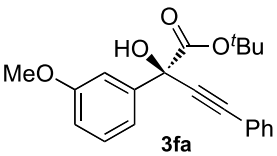 **3fa**	97	93
6	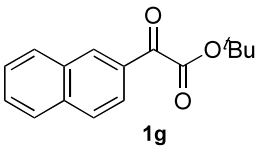 **1g**	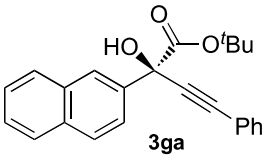 **3ga**	92	94

7	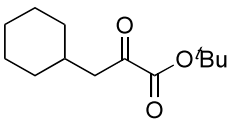 1h	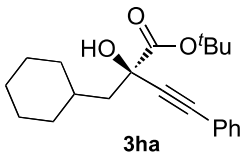 3ha	55	90
8	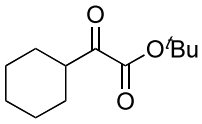 1i	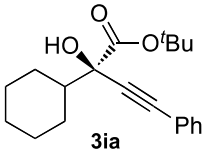 3ia	73	86
9[d]	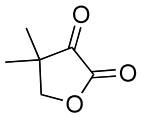 1j	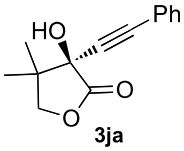 3ja	99	90

[a] Yield of the isolated product (silica gel chromatography). [b] Determined by HPLC analysis. [c] The reaction was carried out in *t*-BuOH. [d] The reaction was carried out at –20 °C.

Various enantioenriched tertiary propargylic alcohols (**1c, 1d** and **1k**) with different substituents at the alkyne terminus were obtained through copper-catalyzed protocols (Table 4). The aromatic alkyne **2b** with an electron-donating MeO substituent reacted with high product yield and enantioselectivity (entry 1). On the other hand, the substitution of the aromatic ring with the electron-withdrawing CF_3 group resulted in a decrease in the yield and enantioselectivity (entry 2). The 1,3-enyne derivative **2d** afforded dienyne **3cd** with high enantiocontrol (91% ee) (entry 3). Aliphatic alkynes served as a substrate (entries 4 and 5). The reaction of linear aliphatic alkyne **2e** with **1d** proceeded with reasonably high enantioselectivity (entry 4). The α-branched aliphatic alkyne **2f** reacted with high yield and enantioselectivity (entry 5). The silylacetylene **2g** reacted with **1k** in somewhat lower enantioselectivity than the aromatic and aliphatic alkynes (entry 6).

Table 4. Copper-catalyzed enantioselective alkynylation of various alkynes.

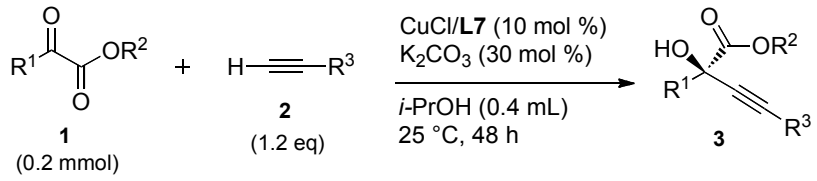

entry	keto ester **1**	alkyne **2**	propargylic alcohol **3**	yield, %[a]	ee, %[b]
1	**1c**	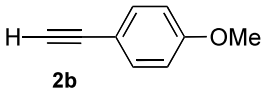 **2b**	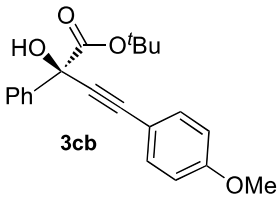 **3cb**	97	93
2	**1c**	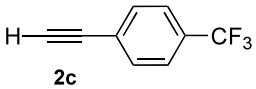 **2c**	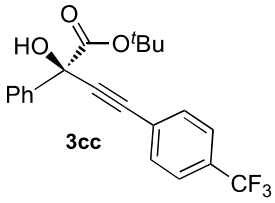 **3cc**	70	88
3	**1c**	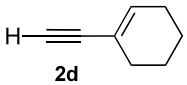 **2d**	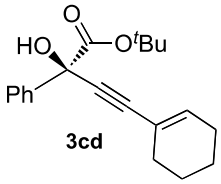 **3cd**	84	91
4	**1d**	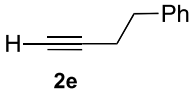 **2e**	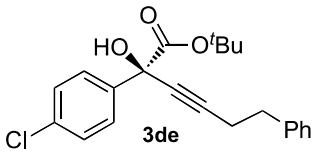 **3de**	87	88
5	**1d**	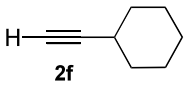 **2f**	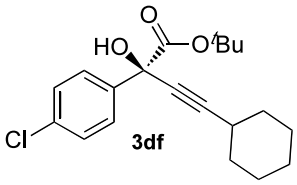 **3df**	98	90
6[c]	**1k**	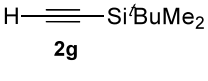 **2g**	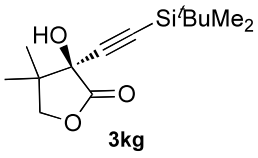 **3kg**	95	76

[a] Yield of the isolated product (silica gel chromatography). [b] Determined by HPLC analysis. [c] The reaction was carried out at 0 °C.

3. Enantioselection Model

In this enantioselective catalysis, a hydroxyl group of the chiral ligand played a critical role in promoting the reaction, and protic solvents promoted a favorable reaction rate and enantioselectivity. These observations are common with the copper-catalyzed enantioselective alkynylation of aldehydes described in the preceding chapter. This strongly suggests that the ligand–substrate hydrogen bonding interactions would also occur in the enantioselective alkynylation of keto esters. The enatioselection models that account for the stereochemical outcome are given in Figure 1. Highly directional catalyst–substrate two-point hydrogen bonding consisting of the O–H···O and sp^3-C–H···O hydrogen bonds allows a well-defined arrangement of the keto ester. In the transition state (**TS1**) leading to the major enantiomer, the R^1 substituent of the keto ester locates perpendicularly to the axis of the copper acetylide, while the R^1 substituent and the acetylide substituent R^3 are nearly eclipsed to each other in the transition state (**TS2**) leading to the minor enantiomer. The catalyst recognizes the R^1 group larger than the CO_2R^2 group. Accordingly, steric repulsion between the R^1 and R^3 group in **TS2** would be a major factor to increase an energy barrier for the reaction pathway for the minor enantiomer.

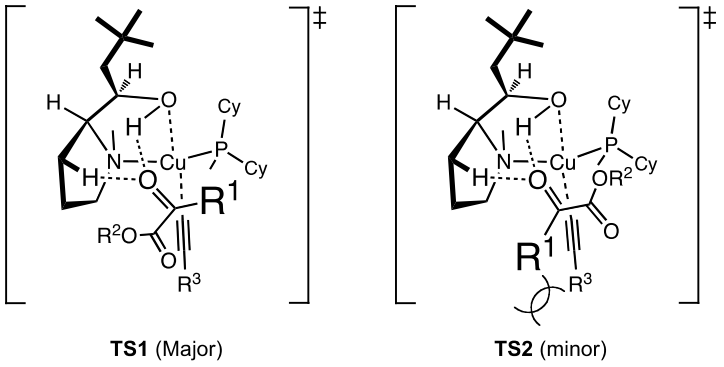

Figure 1. Model for enantiodiscrimination.

4. Summary

The author has developed the enatioselective direct alkynylation of α-keto esters with terminal alkynes catalyzed by a copper(I) complex with prolinol-based hydroxy amino phosphine chiral ligand in alcoholic solvents. The enantioselective catalysis is applicable for various α-keto ester derivatives in combination with various alkynes with different terminal substituents, thus providing a useful method for preparing

enantioenriched chiral tertiary propargylic alcohols. The ligand–substrate hydrogen bonding interactions in the enantiodifferentiating transition state are proposed.

5. Experimental Section

Instrumentation and Chemicals for Experimental Studies.

NMR spectra were recorded on a Varian Gemini 2000 spectrometer, operating at 300 MHz for ^{1}H NMR and 75.4 MHz for ^{13}C NMR, and 121.4 MHz for ^{31}P NMR. Chemical shift values for ^{1}H and ^{13}C are referenced to Me_4Si and the residual solvent resonances, respectively. Chemical shifts are reported in δ ppm. Mass spectra were obtained with Thermo Fisher Scientific Exactive, JEOL JMS-T100LP or JEOL JMS-700TZ at the Instrumental Analysis Division, Equipment Management Center, Creative Research Institution, Hokkaido University. Elemental analysis was performed at the Instrumental Analysis Division, Equipment Management Center, Creative Research Institution, Hokkaido University. HPLC analyses were conducted on a HITACHI ELITE LaChrom system with a HITACHI L-2455 diode array detector. TLC analyses were performed on commercial glass plates bearing 0.25-mm layer of Merck Silica gel $60F_{254}$. Silica gel (Kanto Chemical Co., Silica gel 60 N, spherical, neutral).

All manipulations were carried out under argon or nitrogen. Unless otherwise noted, materials obtained from commercial suppliers were used without further purification. All solvents for catalytic reactions were degassed *via* three freeze-pump-thaw cycles before use. *t*-BuOH was purchased from Junsei Chem Co., Inc. and other solvents were purchased from Kanto Chem Co., Inc., and used without further purification.

Preparation of Hydroxyaminophosphine Derivatives.

Ligands **L1**, **L4**, **L7** are known compounds.[6]

(α*R*,2*S*)-(−)-1-(2-Diphenylphosphinobenzyl)-α-methyl-2-pyrrolidinemethanol (L2)

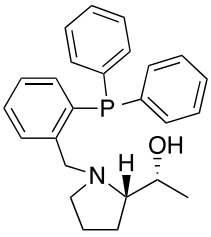

L2

Oil. **^{1}H NMR** (300 MHz, $CDCl_3$) δ 0.60–0.80 (m, 1H), 1.12 (d, J = 6.6 Hz, 3H), 1.22–1.40 (m, 1H), 1.41–1.70 (m, 2H), 1.88-2.00 (m, 1H), 2.18-2.26 (m, 1H), 2.36–2.44 (m, 1H), 3.18 (d, J = 12.3 Hz, 1H), 3.54 (brs, 1H), 4.15–4.22 (m, 1H), 4.54 (d, J = 12.3 Hz, 1H), 6.97–7.02 (m, 1H), 7.12–7.39 (m, 14H). **^{13}C NMR** (75.4 MHz, $CDCl_3$) δ 18.45, 21.52, 22.55, 50.04, 57.85, 57.93 (d, $J_{C\text{-}P}$ = 20.1 Hz), 63.62, 69.70, 127.29, 128.15 (d, $J_{C\text{-}P}$ = 6.3 Hz), 128.33 (d, $J_{C\text{-}P}$ = 4.5 Hz), 128.81, 129.59 (d, $J_{C\text{-}P}$ = 6.9 Hz), 133.15 (d, $J_{C\text{-}P}$ = 19.6 Hz), 133.22 (d, $J_{C\text{-}P}$ = 18.9 Hz), 135.12 (d, $J_{C\text{-}P}$ = 2.4 Hz), 135.40 (d, $J_{C\text{-}P}$ = 13.2 Hz), 136.19 (d, $J_{C\text{-}P}$ = 6.3 Hz), 138.08 (d, $J_{C\text{-}P}$ = 9.7 Hz), 144.22 (d, $J_{C\text{-}P}$ = 24.0 Hz). **^{31}P NMR** (121.4 MHz, $CDCl_3$) δ –17.64. **HRMS-ESI** (m/z): $[M+H]^+$ calcd for $C_{26}H_{29}NOP$, 390.1981 ; found, 390.1979. **$[\alpha]_D^{24}$** = –42.5 (c 1.07, $CHCl_3$).

(*S*)-(−)-1-(2-Diphenylphosphinobenzyl)-α,α-dimethyl-2-pyrrolidinemethanol (L3)

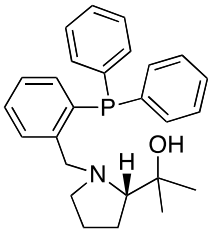

L3

Oil. **^{1}H NMR** (300 MHz, $CDCl_3$) d 0.86 (s, 3H), 1.13 (s, 3H), 1.30–1.59 (m, 3H), 1.77–1.90 (m, 1H), 2.25–2.36 (m, 1H), 2.42–2.51 (m, 1H), 2.65–2.73 (m, 1H), 3.70 (d, J = 13.2 Hz, 1H), 3.88 (brs, 1H), 4,51 (d, J = 13.2 Hz, 1H), 6.96–7.04 (m, 1H), 7.16–7.34 (m 12H), 7.40–7.48(m, 1H). **^{13}C NMR** (75.4 MHz, $CDCl_3$) δ 23.86, 24.65, 27.59, 28.00, 54.36, 62.84 (d, $J_{C\text{-}P}$ = 15.6 Hz), 73.48, 73.56, 127.38, 128.29 (d, $J_{C\text{-}P}$ = 6.9 Hz), 128.36, 128.42 (d, $J_{C\text{-}P}$ = 6.9 Hz), 128.61, 129.08, 129.71 (d, $J_{C\text{-}P}$ = 7.5 Hz), 133.29 (d, $J_{C\text{-}P}$ = 17.7 Hz), 133.88 (d, $J_{C\text{-}P}$ = 20.1 Hz), 135.07 (d, $J_{C\text{-}P}$ = 1.7 Hz), 135.27 (d, $J_{C\text{-}P}$ = 11.4 Hz), 136.37 (d, $J_{C\text{-}P}$ = 5.7 Hz), 137.73 (d, $J_{C\text{-}P}$ = 8.6 Hz), 145.44 (d, $J_{C\text{-}P}$ = 25.2 Hz). **^{31}P NMR** (161.8 MHz, $CDCl_3$) δ –16.42. **HRMS-ESI** (m/z): $[M+H]^+$ calcd for $C_{26}H_{31}NOP$, 404.21433; found, 404.21473. **$[\alpha]_D^{26}$** = –47.4 (c 0.96, $CHCl_3$).

(α*R*,2*S*)-(−)-1-(2-bis(4-fluorophenyl)phosphinobenzyl)-α-(2,2-dimetylpropynyl)-2-pyrrolidinemethanol (L4)

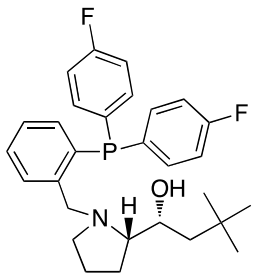

L5

Solid. **^{1}H NMR** (300 MHz, $CDCl_3$) δ 0.96 (s, 9H), 1.10–1.18 (m, 1H), 1.33–1.45 (m, 2H), 1.48–1.63 (m, 2H), 1.63–1.77 (m, 1H), 1.90–2.01 (m, 1H), 2.15–2.23 (m, 1H), 2.40–2.48 (m, 1H), 3.21 (d, J = 12.6 Hz, 1H), 3.38 (brs, 1H), 3.95–4.00 (m, 1H), 4.40 (d, J = 12.6 Hz, 1H), 6.89–7.10 (m, 5H), 7.11–7.40 (m, 7H). **^{13}C NMR** (75.4 MHz, $CDCl_3$) 22.09, 23.06, 30.04, 30.27, 46.89, 54.09, 57.88 (d, $J_{C\text{-}P}$ = 12.6 Hz), 65.34, 70.56, 115.56 (dd, $J_{C\text{-}P}$= 20.7 Hz, $J_{C\text{-}F}$= 6.9 Hz) 115.68 (dd, $J_{C\text{-}P}$= 20.7 Hz, $J_{C\text{-}F}$= 8.4 Hz), 127.47, 129.10, 129.78 (d, $J_{C\text{-}P}$ = 6.3 Hz), 131.69 (dd, $J_{C\text{-}P}$ = 7.5 Hz, $J_{C\text{-}F}$ = 3.3 Hz), 133.28 (dd, $J_{C\text{-}P}$ = 9.9 Hz, $J_{C\text{-}F}$ = 3.3 Hz), 134.40, 135.21 (dd, $J_{C\text{-}P}$ = 9.6 Hz, $J_{C\text{-}F}$ = 8.4 Hz), 135.48 (dd, $J_{C\text{-}P}$ = 10.2 Hz, $J_{C\text{-}F}$ = 7.5 Hz), 135.56, 143.99 (d, $J_{C\text{-}P}$ = 24.0 Hz), 163.11 (d, $J_{C\text{-}F}$ = 249.0 Hz), 163.23 (d, $J_{C\text{-}F}$ = 249.0 Hz), **HRMS-ESI** (m/z): $[M+H]^+$ calcd for $C_{29}H_{35}NOFP$, 482.2416 ; found, 482.2419. **^{31}P NMR** (121.4 MHz, $CDCl_3$) δ –19.15.

(α*R*,2*S*)-(−)-1-(2-Bis(4-methoxyphenyl)phosphinobenzyl)-α-(2,2-dimetylpropynyl)-2-pyrrolidinemethanol (L5)

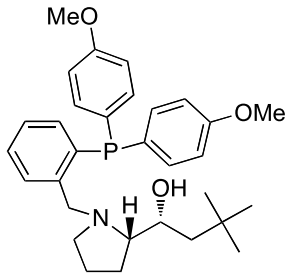

L6

Oil. **^{1}H NMR** (300 MHz, $CDCl_3$) δ 0.95 (s, 9H), 1.08–1.18 (m, 2H), 1.24–1.52 (m, 2H), 1.53–1.64 (m, 1H), 1.69–1.81 (m, 1H), 1.95–2.05 (m, 1H), 2.18–2.25 (m, 1H), 2.56–2.63 (m, 1H), 3.29 (d, J = 12.6 Hz, 1H), 3.79 (s, 6H), 3.86-3.91 (m, 1H), 4.29 (d, J = 12.6 Hz, 1H), 6.83–6.88 (m, 4H), 6.88–6.97 (m, 1H), 7.12–7.39 (m, 7H). **^{13}C NMR** (75.4 MHz, $CDCl_3$) δ 22.46, 23.15, 29.99, 30.23, 46.90, 54.21, 55.21, 55.07, 55.08, 57.54 (d, $J_{C\text{-}P}$ = 14.4 Hz), 65.43, 70.35, 114.10, 114.21, 127.22, 127.54 (d, $J_{C\text{-}P}$ = 5.1 Hz), 128.61, 128.87 (d, $J_{C\text{-}P}$ = 8.1 Hz), 129.46 (d, $J_{C\text{-}P}$ = 5.7 Hz), 134.08, 135.07 (d, $J_{C\text{-}P}$ = 2.1 Hz), 135.35 (d, $J_{C\text{-}P}$ = 2.1 Hz), 137.01 (d, $J_{C\text{-}P}$ = 14.4 Hz), 143.69 (d, $J_{C\text{-}P}$ = 22.4 Hz), 160.17 (d, $J_{C\text{-}P}$ = 5.1 Hz). **^{31}P NMR** (161.8 MHz, $CDCl_3$) δ -19.45. **HRMS-ESI** (m/z): $[M+H]^+$ calcd for $C_{31}H_{41}NO_3P$, 506.2817 ; found, 506.2819 **$[\alpha]_D^{23}$** = –49.4 (c 1.23, $CHCl_3$).

Procedure for Alkynylation of α-Ketoesters.

Procedure for Alkynylation of Benzoylformate (1a) with Phenylacetylene (2a).

In a glove box, CuCl (2.0 mg, 0.020 mmol) , K_2CO_3 (8.3 mg, 0.020 mmol) and **L7** (9.1 mg, 0.020 mmol) were placed in a vial containing a magnetic stirring bar. *t*-BuOH (0.4 mL) was added to the vial, and then the resulting mixture was stirred at room temperature for 5 min. Phenylacetylene (**2a**) (26.4 mL, 0.24 mmol) and benzoylformate **1a** (28.3 mL, 0.20 mmol) were added to the vial. After the vial was sealed with a screw cap, the vial was removed from the glove box. After being stirred at 25 °C for 24 h, the reaction mixture was concentrated, and then the residue was subjected to column chromatography on silica gel (hexane/EtOAc 95:5) to give **3aa** (51.0 mg, 0.19 mmol) in 97% yield.

Characterization Data.

Methyl (*R*)-(+)-2-Hydroxyl-2,4-diphenyl-3-yn-butyrate (3aa)

Known compound.

$[\alpha]_D^{21}$+16.1 (*c* 0.98, $CHCl_3$), (lit.[3a] $[\alpha]_D^{24}$+19.56, c 4.04, $CHCl_3$, *R*).

***iso*-Propyl (*R*)-(+)-2-Hydroxyl-2,4-diphenyl-3-yn-butyrate (3ba)**

(*S*)-compound was reported.

$[\alpha]_D^{22}$+29.9 (*c* 1.07, $CHCl_3$), (lit.[2m] $[\alpha]_D^{20}$–27.9, c 0.50, $CHCl_3$, *S*).

***tert*-Butyl (+)-2-Hydroxyl-2,4-diphenyl-3-yn-butyrate (3ca)**

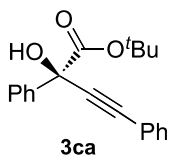

3ca

Oil. **^{1}H NMR** (300 MHz, $CDCl_3$) δ 1.43 (s, 9H), 4.39 (s, 1H), 7.30–7.42 (m, 5H), 7.48–7.54 (m, 2H), 7.69–7.75 (m, 2H). **^{13}C NMR** (75.4 MHz, $CDCl_3$) δ 27.55, 63.32, 84.32, 85.42, 87.69, 122.24, 126.16, 128.14, 128.29, 128.35 128.73, 131.85, 139.85, 170.82. **HRMS–ESI** (*m/z*): $[M+Na]^+$ calcd for $C_{20}H_{20}O_3Na$, 331.1315; found, 331.1315. $[\alpha]_D^{24}$ +22.8 (*c* 1.30, $CHCl_3$). The ee value (92% ee) was determined by chiral HPLC analysis: CHIRALCEL® IC column (Daicel Chemical Industries), 4.6 mm × 250 mm, hexane/2-propanol 99.5:0.5, 0.5 mL/min, 40 °C, 254 nm UV detector, retention time = 13.9 min (major), 15.4 min (minor).

***tert*-Butyl (+)-2-(4-Chlorophenyl)-2-hydroxy-4-phenyl-3-yn-butyrate (3da)**

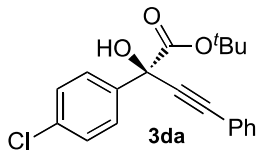

3da

Oil. **^{1}H NMR** (300 MHz, $CDCl_3$) δ 1.43 (s, 9H), 4.40 (s, 1H), 7.30–7.38 (m, 5H), 7.46–7.53 (m, 2H), 7.63–7.69 (m, 2H). **^{13}C NMR** (75.4 MHz, $CDCl_3$) δ 27.53, 62.82, 84.66, 85.61, 87.30, 121.96, 127.72, 128.29, 128.33, 128.90, 131.85, 134.33, 138.44, 170.41. **HRMS–ESI** (*m*/*z*): $[M+Na]^+$ calcd for $C_{20}H_{19}O_3ClNa$, 365.0915 ; found, 365.0915. **$[\alpha]_D^{24}$** +27.89 (*c* 1.46, $CHCl_3$). The ee value (92% ee) was determined by chiral HPLC analysis: CHIRALCEL® IC column (Daicel Chemical Industries), 4.6 mm × 250 mm, hexane/2-propanol 97:3, 0.5 mL/min, 40 ˚C, 254 nm UV detector, retention time = 15.6 min (major), 16.7 min (minor).

***tert*-Butyl (+)-2-Hydroxyl-2-(4-fluorophenyl)-4-phenyl-3-yn-butyrate (3ea)**

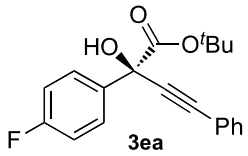

3ea

Oil. **^{1}H NMR** (300 MHz, $CDCl_3$) δ 1.43 (s, 9H), 4.40 (s, 1H), 7.02–7.10 (m, 2H), 7.31-7.38 (m, 3H), 7.46–7.53 (m, 2H), 7.66–7.74 (m, 2H) . **^{13}C NMR** (75.4 MHz, $CDCl_3$) δ 27.55, 72.82, 84.53, 85.56, 87.49, 115.01 (d, $J_{C\text{-}F}$ = 21.75 Hz), 122.04, 128.11 (d, $J_{C\text{-}F}$ = 8.59 Hz), 128.33, 128.88, 131.85, 135.70, 162.77 (d, $J_{C\text{-}F}$ = 246.70 Hz), 170.63. **HRMS–ESI** (*m*/*z*): $[M+Na]^+$ calcd for $C_{20}H_{19}O_3FNa$, 349.1210; found, 349.1209. **$[\alpha]_D^{24}$** +26.35 (*c* 1.40, $CHCl_3$). The ee value (90% ee) was determined by chiral HPLC analysis: CHIRALCEL® IC column (Daicel Chemical Industries), 4.6 mm × 250 mm, hexane/2-propanol 97:3, 0.5 mL/min, 40 ˚C, 254 nm UV detector, retention time = 15.7 min (major), 17.1 min (minor).

***tert*-Butyl (+)-2-Hydroxyl-2-(3-methoxyphenyl)-4-phenyl-3-yn-butyrate (3fa)**

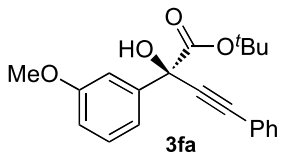

3fa

Oil. **^{1}H NMR** (300 MHz, $CDCl_3$) δ 1.44 (s, 9H), 3.83 (s, 3H), 4.37 (s, 1H), 6.85–6.91 (m, 1H), 7.27–7.37 (m, 6H), 7.47–7.53 (m, 2H). **^{13}C NMR** (75.4 MHz, $CDCl_3$) δ 27.56, 55.27, 84.37, 85.37, 87.62, 86.34, 111.77, 114.01, 118.66, 122.25, 128.30, 138.74, 129.16, 131.86, 141.41, 159.44, 170.72. **HRMS–ESI** (*m*/*z*): $[M+Na]^+$ calcd for $C_{21}H_{22}O_4Na$, 361.1410 ; found, 361.1412. **$[\alpha]_D^{24}$** +20.48 (*c* 1.48, $CHCl_3$). The ee value (93% ee) was determined by chiral HPLC analysis: CHIRALCEL® OD-3 column (Daicel Chemical Industries), 4.6 mm × 250 mm, hexane/2-propanol 97:3, 0.5 mL/min,

40 ˚C, 254 nm UV detector, retention time = 16.9 min (major), 18.6 min (minor).

***tert*-Butyl (+)-2-Hydroxyl-2-(naphtharen-2-yl)-4-phenyl-3-yn-butyrate (3ga)**

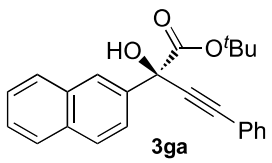

3ga

Oil. **^{1}H NMR** (300 MHz, $CDCl_3$) δ 1.43 (s, 9H), 4.50 (s, 1H), 7.33–7.41 (m, 3H), 7.47–7.58 (m, 4H), 7.67–7.80 (m, 1H) 7.81–7.92 (m, 3H), 8.20–8.25 (m, 1H). **^{13}C NMR** (75.4 MHz, $CDCl_3$) δ 27.58, 73.44, 84.50, 85.64, 87.71, 122.25, 123.12, 125.34, 126.17, 126.39, 127.54, 127.97, 128.33, 128.50, 128.80, 131.91, 132.90, 133.20, 137.16, 170.79. **Anal.** Calcd for $C_{24}H_{22}O_2$: C, 80.42; H, 6.19%. Found: C, 80.04; H, 6.18%. **$[\alpha]_D^{24}$** +40.19 (*c* 1.46, $CHCl_3$). The ee value (94% ee) was determined by chiral HPLC analysis: CHIRALCEL® IC column (Daicel Chemical Industries), 4.6 mm × 250 mm, hexane/2-propanol 97:3, 0.5 mL/min, 40 ˚C, 254 nm UV detector, retention time = 32.05 min (major), 36.41 min (minor).

***tert*-Butyl (–)-2-(Cyclohexylmethyl)-2-hydroxy-4-phenyl-3-butyn-btyrate (3ha)**

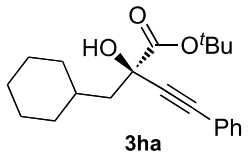

3ha

Oil. **^{1}H NMR** (300 MHz, $CDCl_3$) δ 0.93–2.02 (m, 13H), 1.55 (s, 9H), 3.63 (s, 1H), 7.26–7.35 (m, 3H), 7.38–7.44 (m, 2H). **^{13}C NMR** (75.4 MHz, $CDCl_3$) δ 26.26, 26.29, 27.71, 27.77, 34.04, 34.47, 46.39, 71.37, 83.60, 89.01, 122.49, 128.21, 128.43, 131.69, 172.13. **HRMS–ESI** (*m/z*): $[M+Na]^+$ calcd for $C_{21}H_{28}O_3Na$, 359.1931; found, 351.1930. **$[\alpha]_D^{25}$** –16.65 (*c* 0.92, $CHCl_3$). The ee value (90% ee) was determined by chiral HPLC analysis: CHIRALCEL® IC column (Daicel Chemical Industries), 4.6 mm × 250 mm, hexane/2-propanol 99:1, 0.5 mL/min, 40 ˚C, 254 nm UV detector, retention time = 17.99 min (major), 20.03 min (minor).

***tert*-Butyl (–)-2-Hydroxyl-2-cyclohexyl-4-phenyl-3-yn-butyrate (3ia)**

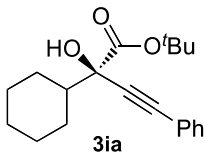

3ia

Oil. **^{1}H NMR** (300 MHz, $CDCl_3$) δ 1.08–1.19 (m, 6H), 1.54 (s, 9H), 1.61–1.71 (m, 1H), 1.75–1.98 (m, 3H), 2.10–2.20 (m, 1H), 3.59 (s, 1H), 7.25–7.36 (m, 3H), 7.40–7.45 (m, 2H). **^{13}C NMR** (75.4 MHz, $CDCl_3$) δ 26.12, 26.14, 26.31, 26.40, 26.72, 27.86, 46.25, 74.63, 83.63, 84.19, 88.12, 122.58, 128.20, 128.39, 131.77, 171.76. **HRMS–ESI** (*m/z*): $[M+Na]^+$ calcd for $C_{20}H_{26}O_3Na$, 337.1774; found, 337.1773. **$[\alpha]_D^{24}$** –16.66 (*c* 1.00, $CHCl_3$). The ee value (86% ee) was determined by chiral HPLC analysis:

CHIRALCEL® IC column (Daicel Chemical Industries), 4.6 mm × 250 mm, hexane/2-propanol 97:3, 0.5 mL/min, 40 °C, 254 nm UV detector, retention time = 27.9 min (major), 33.2 min (minor).

(+)-2-Hydroxyl-2-(4-phenyl-1-butynyl)-3,3-dimethyl-pentalactone (3ja)

(–)-compound was reported.

$[\alpha]_D^{23}$ +1.3 (*c* 0.73, $CHCl_3$), (lit.[3a] $[\alpha]_D^{20}$, –17.5, c 0.45, $CHCl_3$).

***tert*-Butyl (–)-2-Hydroxyl-2-phenyl-4-(4-methoxyphenyl)-3-yn-butyrate (3cb)**

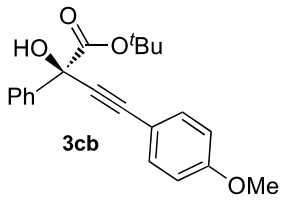

Oil. **^{1}H NMR** (300 MHz, $CDCl_3$) δ 1.43 (s, 9H) 3.82 (s, 3H), 4.37 (s, 1H), 6.86 (d, 2H, *J* = 9.0 Hz), 7.27–7.42 (m, 3H), 7.45 (d, 2H, *J* = 9.0 Hz) 7.67–7.75 (m, 2H). **^{13}C NMR** (75.4 MHz, $CDCl_3$) δ 27.56, 55.29, 73.37, 84.18, 85.46, 86.34, 113.92, 114.31, 126.21, 128.11, 128.30, 133.34, 140.025, 159.92, 170.96. **Anal.** Calcd for $C_{21}H_{22}O_4$: C, 74.54; H, 6.55%. Found: C, 74.32; H, 6.56%. $[\alpha]_D^{24}$ +33.08 (*c* 1.29, $CHCl_3$). The ee value (93% ee) was determined by chiral HPLC analysis: CHIRALCEL® IC column (Daicel Chemical Industries), 4.6 mm × 250 mm, hexane/2-propanol 97:3, 0.5 mL/min, 40 °C, 254 nm UV detector, retention time = 43.8 min (major), 51.1 min (minor).

***tert*-Butyl (–)-2-Hydroxyl-2-phenyl-4-(4-trifluoromethylphenyl)-3-yn-butyrate (3cc)**

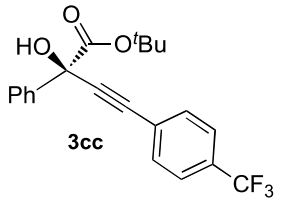

Oil. **^{1}H NMR** (300 MHz, $CDCl_3$) δ 1.44 (s, 9H) 4.42 (s, 1H), 7.30–7.44 (m, 3H), 7.57–7.66 (m, 4H), 7.66–7.74 (m, 2H). **^{13}C NMR** (75.4 MHz, $CDCl_3$) δ 27.53, 73.27, 83.88, 84.64, 90.19, 123.80 (q, $J_{C\text{-}F}$ = 272.27 Hz), 125.25 (q, $J_{C\text{-}F}$ = 3.9 Hz), 126.03, 126.32, 128.25, 128.54, 130.01 (q, $J_{C\text{-}F}$ = 37.40 Hz), 132.12, 139.52, 170.48. **HRMS–ESI** (*m/z*): $[M+Na]^+$ calcd for $C_{21}H_{19}O_3FNa$, 399.1179 ; found, 399.1178. $[\alpha]_D^{23}$ +8.76 (*c* 2.00, $CHCl_3$). The ee value (88% ee) was determined by chiral HPLC analysis: CHIRALCEL® IC column (Daicel Chemical Industries), 4.6 mm × 250 mm, hexane/2-propanol 97:3, 0.5 mL/min, 40 °C, 254 nm UV detector, retention time = 13.8 min (major), 16.0 min (minor).

***tert*-Butyl (+)-2-Hydroxyl-2-phenyl-4-(1-Cyclohexenyl)-3-yn-butyrate (3cd)**

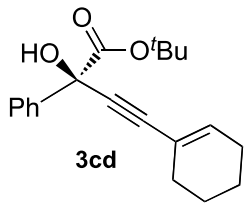

Oil. **^{1}H NMR** (300 MHz, $CDCl_3$) δ 1.40 (m, 9H), 1.54–1.70 (m, 4H), 2.07–2.21 (m, 4H), 4.28 (s, 1H), 6.18–6.22 (m, 1H), 7.26–7.38 (m, 3H), 7.62–7.67 (m, 2H). **^{13}C NMR** (75.4 MHz, $CDCl_3$) δ 21.41, 22.19, 25.62, 27.54, 28.93, 73.27, 83.98, 84.97, 87.39, 119.89, 126.20. 128.04. 128.19. 136.06. 140.12. 171.07. **HRMS–ESI** (*m*/*z*): $[M+Na]^+$ calcd for $C_{20}H_{24}O_3Na$, 335.1618 ; found, 335.1618. **$[\alpha]_D^{22}$** +23.23 (*c* 1.03, $CHCl_3$). The ee value (91% ee) was determined by chiral HPLC analysis: CHIRALCEL® IC column (Daicel Chemical Industries), 4.6 mm × 250 mm, hexane/2-propanol 95:5, 0.5 mL/min, 40 ˚C, 254 nm UV detector, retention time = 18.9 min (major), 22.6 min (minor).

***tert*-Butyl (+)-2-(4-Chlorophenyl)-2-hydroxy-6-phenyl-3-yn-hexyrate (3de)**

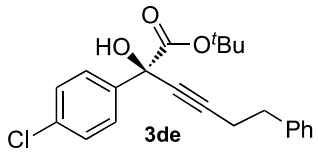

Oil. **^{1}H NMR** (300 MHz, $CDCl_3$) δ 1.37 (s, 9H), 2.62 (d, 2H, *J* = 7.2 Hz), 2.88 (d, 2H, *J* = 7.2 Hz), 4.26 (s, 1H), 7.20–7.35 (m, 7H), 7.43–7.48 (m, 2H). **^{13}C NMR** (75.4 MHz, $CDCl_3$) δ 20.75, 27.46, 34.55, 72.41, 79.32, 84.28, 85.88, 126.36, 127.70, 128.08, 128.41, 128.47, 134.05, 138.69, 140.27, 170.64. **HRMS–ESI** (*m*/*z*): $[M+Na]^+$ calcd for $C_{22}H_{33}O_3Na$, 393.1228; found, 393.1229. **$[\alpha]_D^{24}$** +27.4 (*c* 1.12, $CHCl_3$). The ee value (88% ee) was determined by chiral HPLC analysis: CHIRALCEL® IC column (Daicel Chemical Industries), 4.6 mm × 250 mm, hexane/2-propanol 97:3, 0.5 mL/min, 40 ˚C, 254 nm UV detector, retention time = 21.5 min (minor), 23.6 min (major).

***tert*-Butyl (+)-2-(4-Chlorophenyl)-2-hydroxy-4-cyclohexyl-3-yn-butyrate (3df)**

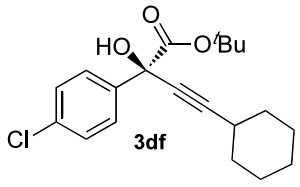

Oil. **^{1}H NMR** (300 MHz, $CDCl_3$) δ 1.31–1.43 (m, 2H), 1.40 (s, 9H) 1.43–1.62 (m, 3H), 1.65–1.86 (m, 5H), 2.49–2.60 (m, 1H), 4.25 (s, 1H), 7.31 (d, 2H, *J* = 8.7 Hz), 7.59 (d, 2H, *J* = 8.7 Hz). **^{13}C NMR** (75.4 MHz, $CDCl_3$) δ 24.06, 25.43, 27.07, 28.35, 31.75, 31.76, 71.98, 76.15, 83.67, 90.34, 127.32, 127.71, 133.65, 138.50, 170.50. **Anal.** Calcd for $C_{20}H_{25}ClO$: C, 68.86; H, 7.22%. Found: C, 68.72; H, 7.28%. **$[\alpha]_D^{24}$** +31.80 (*c* 1.70, $CHCl_3$). The ee value (90% ee) was determined by chiral HPLC analysis: CHIRALCEL® IC column (Daicel Chemical Industries), 4.6 mm × 250 mm,

hexane/2-propanol 99:1, 0.5 mL/min, 40 ˚C, 254 nm UV detector, retention time = 24.5 min (major), 26.1 min (minor).

(*S*)-2-((*tert*-butyldimethylsilyl)ethynyl)-2-hydroxy-3,3-dimethyl-pentalactone (3kg)

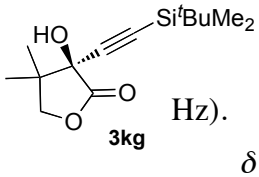

3kg

Oil. **^{1}H NMR** (300 MHz, $CDCl_3$) δ 0.12 (s, 2H), 0.93 (s, 9H), 1.12 (s, 3H), 1.26 (s, 3H), 2.89 (s, 1H), 4.02 (dd, 1H, J = 8.4, 21.3 Hz). **^{13}C NMR** (75.4 MHz, $CDCl_3$) δ 16.47, 19.52, 20.25, 25.93, 44.24, 74.56, 76.62, 93.88, 99.33. **Anal.** Calcd for $C_{14}H_{24}O_3Si$: C, 62.64; H, 9.01%. Found: C, 62.44; H, 8.76%. **$[\alpha]_D^{25}$** –2.71 (*c* 1.02, $CHCl_3$). The ee value (76% ee) was determined by chiral HPLC analysis: CHIRALCEL® IC column (Daicel Chemical Industries), 4.6 mm × 250 mm, hexane/2-propanol 97:3, 0.5 mL/min, 40 ˚C, 254 nm UV detector, retention time = 14.0 min (major), 16.2 min (minor).

6. References

[1] (a) Roush, W. R.; Sciotti, R. J. *J. Am. Chem. Soc.* **1994**, *116*, 6457. (b) Roethle, P. A.; Trauner, D. *Org. Lett.* **2006**, *8*, 345. (c) Chen, Q.; Schwitzer, D.; Kane, J.; Davisson, V. J.; Helquist, P. *J. Org. Chem.* **2011**. *76*, 5157.

[2] (a) Jiang, B.; Feng, Y. *Tetrahedron Lett.* **2002**, *43*, 2975. (b) Cozzi, P. G. *Angew. Chem. Int. Ed.* **2003**, 42, 2895. (c) Lu, G.; Li, X. S.; Jia, X.; Chan, W. L.; Chan, A. S. C. *Angew. Chem. Int. Ed.* **2003**, *42*, 5057. (d) Cozzi, P. G; Alesi, S. *Chem. Commun.* **2004**, 2448. (e) Ramón, D. J.; Yus, M. *Angew. Chem. Int. Ed.* **2004**, *43*, 284. (f) Saito, B.; Katsuki, T. *Synlett* **2004**, 1557. (g) Zhou, Y.; Wang, R.; Xu, Z.; Yan, W.; Liu, L.; Kang, Y.; Han, Z. *Org. Lett.* **2004**, *6*, 4147. (h) Forrat, V. J.; Ramón, D. J.; Yus, M. *Tetrahedron: Asymmetry* **2005**, *16*, 3341. (i) Mao, J. C.; Wan, B. S.; Wu, F.; Lu, S. W. *J. Mol. Catal. A* **2005**, *237*, 126. (j) Chen, C.; Hong, L.; Xu, Z.-Q.; Liu, L.; Wang, R. *Org. Lett.* **2006**, *8*, 2277. (k) Lu, G.; Li, X.; Li, Y. M.; Kwong, F. Y.; Chan, A. S. C. *Adv. Synth. Catal.* **2006**, *348*, 1926. (l) Cai, H. Q.; Chen, C.; Liu, L.; Ni, J. M.; Wang, R. *J. Mol. Catal. A* **2006**, *253*, 86. (m) Infante, R.; Gago, A.; Nieto, J.; Andrés, C. *Adv. Synth. Catal.* **2012**, *354*, 2797.

[3] (a) Jiang, B.; Chen, Z.; Tang, X. *Org. Lett.* **2002**, *4*, 3451. (b) Aikawa, K.; Hioki,Y.; Mikami, K. *Org. Lett.* **2010**, *12*, 5716. (c) Ohshima, T.; Kawabata, T.; Takeuchi, Y.; Kakinuma, T.; Iwasaki, T.; Yonezawa, T.; Murakami, H.; Nishiyama, H.; Mashima,

K. *Angew. Chem. Int. Ed.* **2011**, *50*, 6296. (d) Wang, T.; Niu, J.-L.; Liu, S.-L.; Huang, J.-J.; Gong, J-F.; Song, M.-P. *Adv. Synth. Catal.* **2013**. *355*. 927.

[4] Motoki, R.; Kanai, M.; Shibasaki, M. *Org. Lett.* **2007**, *9*, 2997.

[5] Dhondi, P. K.; Carberry, P.; Choi, L. B.; Chisholm, J. D. *J. Org. Chem.* **2007**, *72*, 9590.

[6] Ishii, T.; Watanabe, R.; Moriya, T.; Ohmiya, H.; Mori, S.; Sawamura, M. *Chem. Eur. J.* **2013**, *19*, 13547.

Publication List

Chapter 1

"Cooperative Catalysis of Metal and O–H···O/sp^3-C–H···O Two-point Hydrogen Bonds in Alcoholic Solvents: Copper-catalyzed Enantioselective Direct Alkynylation of Aldehydes with Terminal Alkynes"

Takaoki Ishii, Ryo Watanabe, Toshimitsu Moriya, Hirohisa Ohmiya, Seiji Mori, Masaya Sawamura, *Chem. Eur. J.* **2013**, *19*, 13547.

Acknowledgment

The studies described in this thesis have been carried out under the direction of Professor Masaya Sawamura at Graduate School of Chemical Sciences and Engineering, Hokkaido University. These are concerned with enantioselective alkynylation of carbonyl compounds based on cooperative copper catalyst.

I respect and gratitude to Professor Masaya Sawamura for giving me an opportunity to do the project work in organometallic chemistry and providing me all support and guidance throughout this work. I am extremely grateful to Associate Professor Hirohisa Ohmiya for his dedicated guidance and considerate suggestions. He inspired me greatly to work in this study.

I deeply indebted to Professor Seiji Mori and Mr. Ryo Watanabe of Ibaraki University for their significant assistance with computer calculations in Chapter 1. Their cooperation was essential for understanding of reaction mechanism.

I would like to acknowledge Professor Hajime Ito and Assistant Professor Tomohiro Iwai for giving thoughts, advice and ideas for improvement of the study.

I would like to express my appreciation to Dr. Toshimitsu Moriya, Dr. Hideto Ito, Dr. Soichiro Kawamorita, Dr. Yusuke Makida and all the other members in Prof. Sawamura's group for their invaluable supports and warm encouragements.

A part of this work was supported by the Global COE Program from the Ministry of Eduaction, Culture, Sports, Science and Technology, Japan.

Financial support from Hokkaido University (Frontier Scholarship) was indispensable and I sincerely appreciate the support.

Finally, I express my gratefulness to my parents, Mr. Hideki Ishii and Mrs. Sumi Ishii, and my younger sister, Ms. Chihiro Ishii, for their hearty encouragement and continuous assistance.

Takaoki Ishii
Graduate School of Chemical Sciences
and Engineering, Hokkaido University
March 2013